



UNIVERSITÉ DU
LUXEMBOURG

PhD-FSTC-2017-26

The Faculty of Sciences, Technology and Communication

DISSERTATION

Presented on 12/05/2017 in Luxembourg

to obtain the degree of

DOCTEUR DE L'UNIVERSITÉ DU LUXEMBOURG
EN BIOLOGIE

by

MAHSA MOEIN

Born on 1 May 1985 in Esfahan (Iran)

DISSECTING THE CROSSTALK BETWEEN
INTRACELLULAR CALCIUM SIGNALING AND
MITOCHONDRIAL METABOLISM

DISSERTATION DEFENSE COMMITTEE

PROF. DR. RUDI BALLING, Dissertation Supervisor
University of Luxembourg

DR. ALEXANDER SKUPIN, Co-supervisor
University of Luxembourg

PROF. DR. JORGE GONCALVES, Chairman
University of Luxembourg

PROF. DR. GENEVIÉVE DUPONT, Member
Université Libre de Bruxelles

DR. ALESSANDRO PRIGIONE, Member
Max Delbrück Center for Molecular Medicine

Abstract

Cells must signal in order to adapt to environmental changes. They typically detect extracellular signals by the receptors on the cellular plasma membrane. Such a signal is transferred to the cellular processes through the second messengers which leads to activating a cellular response. To enable information transferring and information processing, cells need energy which is mainly provided by mitochondria in eukaryotic cells. Thus, the crosstalk between cellular signaling and energy metabolism is essential for proper cellular function.

Ca^{2+} is a versatile and universal intracellular second messenger that regulates many diverse cellular processes and is therefore under very tight spatiotemporal homeostatic control. Ca^{2+} homeostasis is performed through a set of components from the Ca^{2+} -signaling toolkit to create signals with different spatial and temporal properties. Mitochondria are not only the main energy providers in eukaryotic cells, but represent an essential component of the Ca^{2+} -signaling toolkit having a significant impact on the spatiotemporal features of Ca^{2+} signals. In addition to the role of Ca^{2+} buffering, mitochondria also play a vital function in Ca^{2+} homeostasis by providing ATP. The released Ca^{2+} from internal and external Ca^{2+} stores should be sequestered or pumped back across the large concentration gradient. This process is performed by Ca^{2+} -ATPase pumps or by ion gradients which are kept by consuming ATP. Furthermore, Ca^{2+} plays an important role in energy metabolism by enhancing the activity of rate limiting enzymes in the mitochondrial matrix. Rising the Ca^{2+} concentration in the mitochondrial matrix leads to an increasing activity of mitochondrial dehydrogenases, oxidative phosphorylation and ATP production. Recent studies revealed that altered Ca^{2+} homeostasis and mitochondrial metabolism contribute to the development of neurodegenerative diseases like Parkinson's and Alzheimer's diseases.

The present thesis investigates the crosstalk between Ca^{2+} signaling and mitochondrial metabolism by combining mathematical modeling with Ca^{2+} imaging and metabolic flux analysis in electrically non-excitable cells. First, we showed by modeling and experiments that glucose deprivation results in decreasing cellular ATP, increasing frequency of Ca^{2+} signals and rising glutamine uptake rate. Second, we investigated the effect of different Ca^{2+} oscillation frequencies on the cellular metabolic activity. For this purpose, we stimulated cells by extracellular agonists that stimulate IP_3 -mediated Ca^{2+} signaling and measured the period of Ca^{2+} signals and glucose/glutamine uptake rates. The analysis showed a well-defined relation between the frequency of Ca^{2+} spiking and glucose/glutamine uptake rates indicating a metabolic decoding of Ca^{2+} signaling. Third, we simulated the effect of PINK1 deficiency on the Ca^{2+} dynamics and mitochondrial metabolism using our proposed Ca^{2+} -mitochondrial metabolism model. We showed by modeling that down regulation of the mitochondrial Ca^{2+} uniporter (MCU) restores Ca^{2+} homeostasis and respiration in the cells

with PINK1 deficiency. This result was in agreement with experiments on dopaminergic (DA) neurons in the zebrafish larvae. Finally, to analyze Ca^{2+} signals captured during Ca^{2+} imaging experiments, we developed a user-friendly software which can precisely compute the signal's features of diverse Ca^{2+} signals.

We conclude that compromising cellular metabolism modifies the profile of Ca^{2+} signals and Ca^{2+} spikes in turn can change the metabolic profile of the cell. We also showed that the information of extracellular stimuli encoded in the frequency of Ca^{2+} signals is decoded by the energy metabolism through increasing glucose and glutamine uptake rates. We speculate that the encoded information of the extracellular stimuli in the frequency of Ca^{2+} signals is transferred into mitochondria and subsequently decoded by the mitochondrial Ca^{2+} - sensitive enzymes leading to an increase in the TCA cycle activity and rising oxidative phosphorylation. We also showed that stimulating cells with extracellular stimuli leads to increasing ATP production. Therefore, dysregulation of the crosstalk between Ca^{2+} signaling and mitochondrial metabolism compromises the information transfer and decoding mechanism which may lead to energy deficit, Ca^{2+} dysregulation and subsequently may cause neurodegeneration.

Acknowledgements

Over the last years, a great many people contributed to the success of my PhD project. I would like to express my gratitude to all those who helped me succeed with my work.

I would like to thank my official supervisor and the director of LCSB, Prof. Rudi Balling, for all his encouragement throughout my PhD project and his advice on how to conduct good research. His support was undoubtedly crucial for the success of my PhD project.

I would like to thank my supervisor, Dr. Alexander Skupin, for his significant effort to make my research work match the highest academic standards. I am grateful to have had the opportunity to work with and learn from one of the best researchers in the field.

I would like to thank Dr. Andre Wegner, for giving me insights into the cellular metabolism and metabolomics fields.

I would like to express my gratitude for all the friendships I have formed with my colleagues in the Integrating Cell Signaling (ICS) Lab. My colleagues not only provided me with helpful advice along the way but also contributed to a warm work environment.

Last but not the least, I would like to thank my husband for his patience, support and encouragement that motivated me to keep up the hard work during my PhD. I would also like to thank my parents for their lifelong support and for enabling me to pursue my dreams.

Contents

Contents	v
List of Figures	ix
Acronyms	xi
1 Introduction	1
1.1 Motivation	1
1.2 Our Systems Biology Approach	5
1.3 Aims	7
1.4 Organization of the Dissertation	7
2 The Calcium-Energy Metabolism System	9
2.1 The Calcium Signaling Toolkit	9
2.1.1 Plasma Membrane Calcium Proteins	11
2.1.2 Sarco/Endoplasmic Reticulum	16
2.1.3 Mitochondria	19
2.1.4 Calcium-Regulated Enzymes	21
2.1.5 Calcium Signaling in Electrically Non-Excitable Cells	22
2.2 Energy Metabolism	23
2.2.1 Glycolysis	24
2.2.2 Tricarboxylic Acid (TCA) Cycle and Electron Transport Chain (ETC)	25
2.2.3 Glycogenesis and Glycogenolysis	27
2.2.4 Glutaminolysis	28
2.2.5 Regulation of Cellular Metabolism	29
2.3 Crosstalk Between Intracellular Ca^{2+} Signaling and Mitochondrial Metabolism	30
2.4 Medical Relevance in the Neurodegenerative Diseases	33
2.4.1 Parkinson's Disease	33
2.4.2 Alzheimer's Disease	34
2.5 Describing Biological Systems by Mathematical Models	37
2.5.1 General Biochemical Models	37

2.5.2	Modeling Calcium Oscillations with ODEs	39
2.6	Summary	40
3	Material and Methods	41
3.1	Developed Model for the Crosstalk of Ca^{2+} Signaling and Mitochondrial Metabolism	41
3.1.1	Model Implementation	42
3.1.2	Model Parameter Scan	50
3.2	Cell Lines	50
3.2.1	Human embryonic kidney (HEK) 293 cells	50
3.2.2	C8-D1A: Astrocyte type I clone	53
3.3	Experimental Protocols	53
3.3.1	Media Used for Experiments	53
3.3.2	Single-Cell Imaging of Calcium in C8-D1A cells	54
3.3.3	Single-Cell Imaging of Calcium in HEK293 cells	55
3.3.4	Measuring Extracellular Metabolites	55
3.3.5	ADP/ATP Ratio Measurement	56
3.3.6	Statistics	56
3.4	Summary	57
4	Results	59
4.1	Model Implications	61
4.1.1	ATP-Dependent Model versus ATP-Independent Model	61
4.1.2	Impact of Mitochondrial Substrates on Ca^{2+} Signaling	62
4.2	Experimental Results	67
4.2.1	Astrocytic Calcium-Energy Metabolism System	67
4.2.2	Astrocytes Nutrients Utilization	68
4.2.3	Frequency of Ca^{2+} Spikes is High in the Cells with no Glucose Accessibility	68
4.2.4	Glutamine Uptake Rate is High in the Cells with no Glucose Accessibility	71
4.2.5	Stimulation of GPCRs Increases Frequency of Ca^{2+} Spikes	73
4.2.6	Stimulation of GPCRs Increases Glucose and Glutamine Uptake Rate	74
4.2.7	Metabolic Decoding of Ca^{2+} Signals in Astrocytes and HEK293	74
4.2.8	Effect of Ca^{2+} on Regulation of ATP Production	74
4.3	Simulation of PINK1 Deficiency Using Ca^{2+} -mitochondrial Model	76
4.4	CaSiAn: Calcium Signaling Analysis Software	80
4.5	Summary	83

5 Discussion	85
6 Conclusion and Future Perspectives	91
6.1 Conclusion	91
6.2 Future Perspectives	92
A CaSiAn: Calcium Signal Analysis Software	95
A.1 Peak and Nadir Detection	95
A.2 Background Removal and Normalization	96
A.3 Feature Extraction	98
A.4 Tool Overview	104
A.4.1 Setup	105
A.4.2 Preprocessing	106
A.4.3 Feature Extraction	107
A.5 Case Study	107
Bibliography	113

List of Figures

1.1	Systems biology approach	2
1.2	Our approach for dissecting the crosstalk between Ca^{2+} signaling and mitochondrial metabolism	6
2.1	Overview of the calcium signaling toolkit	12
2.2	Sequence of reactions in the glycolysis process	26
2.3	Overview of the tricarboxylic acid (TCA) cycle and electron transport chain (ETC) in mitochondria	28
2.4	Calcium oscillation in cytosol and ER, simulated by the Goldbeter model.	40
3.1	Illustration of the two model components	43
3.2	Schematic representation of the calcium-mitochondrial metabolism model	43
3.3	Calcium dynamics in relation to other variables	51
3.4	Model parameter scan	52
3.5	C8-D1A astrocytic cell line.	53
4.1	Components and interactions in the calcium-mitochondrial system	60
4.2	Calcium and ATP dynamics in ATP-dependent model versus ATP-independent model	62
4.3	Dynamic of Ca^{2+} and ATP with respect to varying the rate of intracellular ATP hydrolysis	63
4.4	Ca^{2+} homeostasis is an energy demanding process	64
4.5	Dynamics of calcium and ATP fluxes in cytosol and mitochondria while decreasing FBP exponentially.	65
4.6	Effect of mitochondrial substrates on Ca^{2+} signaling is independent of IP_3 concentration and MCU expression level	66
4.7	Effect of mitochondrial substrate on the intracellular ATP and Ca^{2+}	66
4.8	Schematic representation of astrocytic calcium-energy metabolism system	69
4.9	Astrocytes utilize nutrients	70
4.10	Effect of glucose availability on the intracellular ATP and period of Ca^{2+} signals	71

4.11 Schematic representation of the effect of Ca^{2+} and ADP/ATP ratio on the TCA cycle enzymes	72
4.12 Effect of glucose deprivation on the ADP/ATP ratio and glutamine uptake rate	72
4.13 Period of Ca^{2+} spikes evoked by stimulation of GPCRs	73
4.14 Glutamine and glucose uptake rates in dependence on the stimulation of GPCRs in C8-D1A and HEK293 cells	75
4.15 Glucose and glutamine uptake rates decrease with increasing periods of Ca^{2+} signals in C8-D1A cells	76
4.16 Metabolic decoding of Ca^{2+} signals in astrocytes and HEK293 cells	77
4.17 Increasing ATP supply upon stimulation of GPCRs.	77
4.18 Effect of PINK1 deficiency on the zebrafish larvae DA neural cells and the rescue mechanism	78
4.19 Simulation of PINK1 deficiency and the rescue mechanism	79
4.20 Graphical user interface of CaSiAn software	81
4.21 Workflow of CaSiAn	82
5.1 Metabolic decoding of Ca^{2+} signals.	89
A.1 Detecting and removing false positive peaks	97
A.2 Overview of Ca^{2+} spike descriptors	101
A.3 Spike amplitude	101
A.4 Spike width	102
A.5 Effective area under spike	103
A.6 Increasing rate and Decreasing rate	105
A.7 An overview of CaSiAn	105
A.8 CaSiAn fits different curves to the signal baseline	106
A.9 An analyzed Ca^{2+} signal in CaSiAn	108
A.10 Statistical analysis of Ca^{2+} signal descriptors	109

Acronyms

AD Alzheimer's Disease.

ANT Adenine Nucleotide Translocases.

ATP Adenosine Triphosphate.

Ca²⁺ Calcium.

DA Dopamine.

ER Endoplasmic Reticulum.

ETC Electron Transport Chain.

FBP Fructose 1,6-bisphosphatase.

GLC Glucose.

GLN Glutamine.

GLU Glutamate.

GPCR G Protein-Coupled Receptors.

ICDH NAD-Isocitrate Dehydrogenase.

IP₃ Inositol triphosphate.

IP₃R Inositol 1,4,5-trisphosphate receptors.

ISI Interspike Interval.

KGDH α -Ketoglutarate/Oxoglutarate Dehydrogenase.

MCU Mitochondrial Calcium Uniporter.

NAD Nicotinamide Adenine Dinucleotide.

NCX Sodium-Calcium Exchanger.

OXPHOS Oxidative Phosphorylation.

PD Parkinson's Disease.

PDH Pyruvate Dehydrogenase.

Acronyms

PMCA Plasma Membrane Ca^{2+} -ATPase pump.

ROS Reactive Oxygen Species.

RYR Ryanodine receptors.

SEM Standard Error of Mean.

SERCA Sarco/Endoplasmic Reticulum Ca^{2+} -ATPase pump.

SR Sarcoplasmic Reticulum.

T_{av} Average of Interspike Intervals.

TCA Tricarboxylic Acid.

VGCC Voltage-Gated Calcium Channels.

Chapter 1

Introduction

1.1 Motivation

Life is made of cells. Individual cells perform biochemical processes needed to maintain their structure and functionality. For this purpose, cells permanently turn over energy and communicate with the environment and each other to orchestrate the chemical reactions sustaining life. This thesis analyzes the crosstalk between Ca^{2+} , a versatile second messenger, and mitochondrial metabolism as the power plant of the cells. Calcium signaling is composed of several components like cell membrane Ca^{2+} channels, the endoplasmic reticulum, Ca^{2+} buffers and mitochondria to create the intracellular Ca^{2+} signaling toolkit. Energy metabolism is formed by all metabolic pathways that transform energy which is required for multiple cellular functions where mitochondria play a predominant role in eukaryotic cells. To analyze the crosstalk between these two essential cellular systems, the present interdisciplinary thesis combines mathematical modeling, Ca^{2+} imaging and metabolic flux analysis.

Due to the complexity of the calcium and energy metabolism system, we used a systems biology approach to study the interaction between Ca^{2+} regulation and energy metabolism system. This systems biology approach takes into account the complexity of the underlying mechanisms by integrating computational and experimental techniques to understand the system as a whole and not the role of a particular gene or protein. A systems biology approach aims at understanding how the dynamics of a cellular system originates from the underlying structure and is organized in a cycle with four steps shown in Figure 1.1. The loop starts with defining a biological problem. Then the problem is modeled using mathematics and statistics in order to acquire, store and analyze the current biological information. Using the model simulations a set of hypotheses are tested and a number of predictions are made. These predictions are subsequently tested by the wet lab experiments which lead to

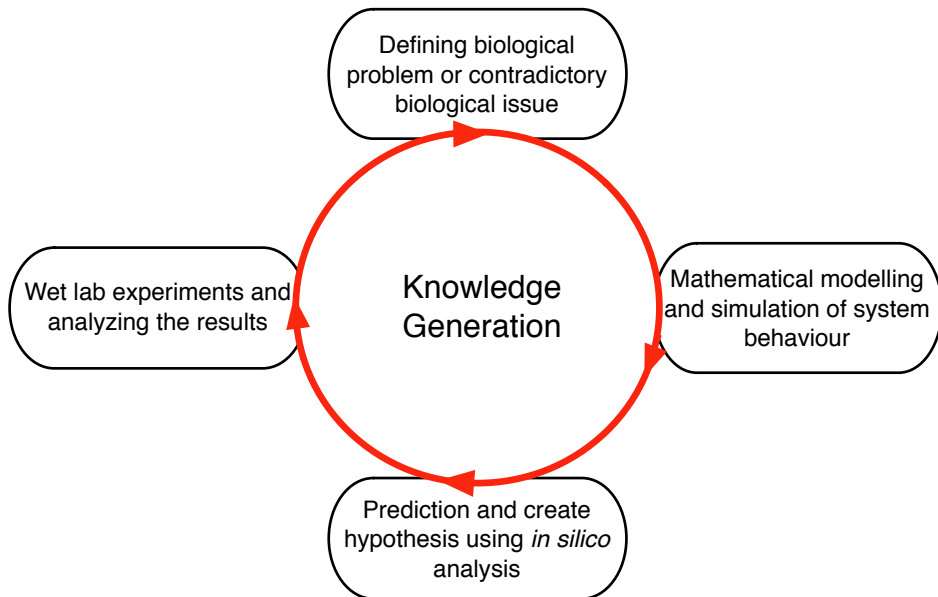


Figure 1.1. Steps for creating knowledge of a biological system by a systems biology approach. The loop starts with identifying biological problem. The problem is subsequently modeled by mathematical equations and solved by computer simulations. In the next step, new predictions are done by the *in silico* model. The model predictions are examined by wet lab experiments and new biological data are provided which can be used for improving the mathematical model.

model acceptance or rejection, or the model has to be improved in order to capture the experimental observations successfully. The newly generated experimental data for the biological question should subsequently be integrated in the model. By repeating the cycle and refining the *in silico* model and performing new *in vivo* and *in vitro* experiments, we obtain a deeper understanding of the biological system. This thesis performs all steps of the systems biology approach to develop a mechanistic understanding of the crosstalk between Ca^{2+} signaling and mitochondrial metabolism.

Ca^{2+} is a versatile and universal intracellular messenger and operates as a critical signal within the cells from conception to death [Berridge et al., 1998]. Cells utilize different sources of Ca^{2+} for signaling. The concentration of Ca^{2+} within the cytoplasm is maintained at a low level in a non-stimulated cell, typically around 100 nM. Ca^{2+} concentration increases inside the cytoplasm by a wide variety of external stimuli, including binding of hormones or growth factors, electrical depolarization or mechanical stimulation. The stimulus is detected by a specific transduction machinery and leads to increasing cytoplasmic Ca^{2+} concentration, with typically cytoplasmic Ca^{2+} concentration of 1 μM , but it depends on the cell type, stimulus and exactly where the Ca^{2+} concentration is measured [Clapham, 2007]. Changing the cytosolic Ca^{2+} concentration generates calcium signals inside the cytosol which can be measured by Ca^{2+} indicator dyes. Cells have access to multiple sources of Ca^{2+} . The extracellular space is generally believed to have the largest concentration of Ca^{2+} ,

around 1.5 mM. In addition to the extracellular space, cells also can access Ca^{2+} stores from intracellular organelles. Some intracellular Ca^{2+} sources are the sarcoplasmic/endoplasmic reticulum, golgi apparatus and mitochondria. Ca^{2+} signals exhibit complex spatiotemporal properties which allow them to control many different cellular processes such as cell growth, secretion, contraction and metabolism [Berridge et al., 2003].

The interplay between Ca^{2+} regulation and energy metabolism was initially described by Vasington and Murphy [Vasington and Murphy, 1961] and Deluca and Engstrom [DeLuca and Engstrom, 1961] in 1961 who discovered that isolated kidney mitochondria could accumulate large amounts of Ca^{2+} in an energy driven process [Carafoli, 2012]. Ca^{2+} can transfer the information content of extracellular stimuli downstream to the intracellular events in a reliable way. Binding a signal molecule (agonist) to the cell membrane receptors stimulates formation of inositol 1,4,5-trisphosphate (IP_3) that leads to releasing Ca^{2+} from intracellular Ca^{2+} stores. Upon Ca^{2+} release from these stores, mitochondria take up the large amount of Ca^{2+} that activates several dehydrogenases within the tricarboxylic acid (TCA) cycle and thus increases ATP production [Griffiths and Rutter, 2009]. Ca^{2+} is then extruded from mitochondria by different Ca^{2+} exchangers. The existence of these Ca^{2+} channels allows mitochondria to operate as a Ca^{2+} buffer which makes a significant impact on the spatiotemporal features of Ca^{2+} signals. In addition to the mitochondrial role in Ca^{2+} buffering, energy metabolism also plays a vital function in Ca^{2+} homeostasis by providing ATP. The released Ca^{2+} from internal and external Ca^{2+} stores should be sequestered or pumped back across the large plasma membrane concentration gradient. This process is performed by Ca^{2+} -ATPase pumps or by ion gradients which are kept by consuming ATP and rendering Ca^{2+} homeostasis to an energy demanding process that has metabolic cost for cells [Chan et al., 2009]. Thus, on one hand calcium ions regulate mitochondrial activity which leads to ATP production and on the other hand the produced ATP by mitochondria is consumed by ATPase pumps for Ca^{2+} regulation inside the cell (see Figure 1.2).

The Ca^{2+} signals are created by variation of the 'on' reactions that introduce Ca^{2+} into cytoplasm and the 'off' reactions through which this Ca^{2+} is removed [Berridge et al., 2003]. Thus, cells can use frequency or amplitude of Ca^{2+} signals to encode information. Several studies have shown that the encoded information in the frequency of Ca^{2+} signals then can be decoded by proteins with multiple Ca^{2+} binding sites that can regulate the proteins activity and thereby cellular program. To date, NFAT (nuclear factor of activated T-cells) [Dolmetsch et al., 1998, Tomida et al., 2003], NF- κ B (nuclear factor kappa-light-chain-enhancer of activated B cell) [Dolmetsch et al., 1998, Frantz et al., 1994, Hu et al., 1999], CaMKII (Ca^{2+} /calmodulin-dependent protein kinase II) [De Koninck and Schulman, 1998, Dupont and Goldbeter, 1998], MAPK (mitogen- activated protein kinase) [Kupzig et al., 2005] and calpain [Tompa et al., 2001] have been reported to have frequency decoding

properties. In 1980, a study by Denton and McCormack showed that Ca^{2+} enhances the activity of three key intramitochondrial dehydrogenases: pyruvate dehydrogenase (PDH), NAD-isocitrate dehydrogenase (ICDH) and oxoglutarate dehydrogenase (KGDH) [Denton et al., 1980]. In 1995 Hajnoczky et al. studied the control of Ca^{2+} -sensitive mitochondrial enzymes by monitoring mitochondrial Ca^{2+} and the redox state of flavoproteins and pyridine nucleotides simultaneously with cytosolic Ca^{2+} in single hepatocytes. They showed a dependency between Ca^{2+} spikes and mitochondrial NADH concentration and concluded that the hormone-induced Ca^{2+} oscillation activates Ca^{2+} -sensitive mitochondrial enzymes in a frequency dependent manner [Hajnóczky et al., 1995]. Although they could show that cytosolic Ca^{2+} signals can be decoded by mitochondrial enzymes, they could not describe the decoding relation between frequency of Ca^{2+} signals and the mitochondrial enzyme activity.

In order to have a mechanistic understanding of the intracellular calcium pathways and Ca^{2+} downstream effects, accurate analysis of Ca^{2+} signals is crucial. Real time single cell fluorescence imaging of Ca^{2+} concentration is one of the common techniques for capturing Ca^{2+} transients. Ca^{2+} signals are extracted from image frames by averaging the light intensities in the regions of interest. Computing features of Ca^{2+} signals like frequency, amplitude and spike width precisely needs setting parameters that are fitted to each signal and can overcome the issues resulting from noise in the Ca^{2+} signals. While there are widely available implementations of the peak detection and signal analysis methods in software packages like Matlab, R, octave and python, using them for Ca^{2+} signal analysis needs specific modifications for each signal that requires typically a lot of efforts while at the end there is a high possibility to have high rate of false positives in detected signal's peaks. Thus, there is high demand for a software which can easily and precisely analyze Ca^{2+} signals.

In the present thesis, we investigate the crosstalk between Ca^{2+} signaling and mitochondrial metabolism. Recent studies have revealed that the disruption of this interplay contribute to neurodegeneration diseases. Dysregulation in the cellular Ca^{2+} signaling may lead to mitochondrial Ca^{2+} overload, decreasing respiration and result in increased mitochondrial autophagy [Soman et al., 2016]. In addition, It is hypothesized that repetitive stimulation of oxidative phosphorylation by Ca^{2+} signals leads to increased production of reactive oxygen species (ROS) which damage mitochondrial proteins such as complex I and mtDNA, reducing the efficiency of oxidative phosphorylation. ROS also can damage ER proteins and increase the concentration of misfolded proteins. This model has been particularly popular to explain the increased vulnerability of SNc DA neurons [Surmeier et al., 2010].

The present thesis uses an interdisciplinary approach to understand the underlying mechanism of the interplay between Ca^{2+} signaling and mitochondrial metabolism by:

- Developing a *in silico* model of the crosstalk between Ca^{2+} signaling and mitochondrial metabolism.
- Exploring the effect of mitochondrial carbon inputs on the intracellular ATP level and frequency of Ca^{2+} signals by model simulations and wet lab experiments.
- Identifying the impact of Ca^{2+} signaling on the mitochondrial substrate uptake and ATP production by experiments.
- Establishing the metabolic decoding relation of intracellular Ca^{2+} signals.
- Simulating the PINK1 deficiency and the rescue mechanism using the *in silico* model.
- Developing a user-friendly tool for characterizing Ca^{2+} signals for a large amount of observations, fast, easily and precisely.

1.2 Our Systems Biology Approach

To address the open questions on calcium-energy metabolism crosstalk, we rely on a systems biology approach. In the modeling part, we use ordinary differential equations (ODEs). Several models have been proposed for modeling Ca^{2+} dynamics, but most of them neglect mitochondria, although it is an effective organelle which can shape spatio-temporal properties of Ca^{2+} signals [Goldbeter et al., 1990, Li et al., 1994, De Young and Keizer, 1992]. They also do not consider Ca^{2+} signaling as an energy demanding process since they don't take into account the ATP consumption of the Ca^{2+} ATPase-pumps [Fall and Keizer, 2001, Bertram and Arceo II, 2008]. Thus, most of the existing Ca^{2+} and mitochondrial models do not focus on the crosstalk between Ca^{2+} signaling and mitochondrial metabolism. In this thesis, we extend the previous studies to propose a mathematical model which can simulate the crosstalk between calcium signaling and mitochondrial metabolism in electrically non-excitable cells. Thus we integrate a well-established model of IP_3 -mediated Ca^{2+} signaling with the simplified model of mitochondrial Ca^{2+} handling and metabolic function. With the model, we investigate the effect of Ca^{2+} on the mitochondrial metabolism as well as the impact of mitochondrial substrates on the Ca^{2+} signaling. We also explore how varying the expression levels of different Ca^{2+} channels affects the period of cytosolic Ca^{2+} signals.

In the experimental part, we use live cell Ca^{2+} imaging, extracellular metabolic flux analysis and ADP/ATP ratio assays. We perform Ca^{2+} imaging of individual cells while exposing them to extracellular agonists that stimulate IP_3 production and Ca^{2+} release from endoplasmic reticulum. We measure Ca^{2+} signals in two cell lines, human embryonic kidney (HEK) 293 and C8-D1A astrocytic cells while exposing them to carbachol (CCh) and adenosine triphosphate (ATP). Then we extract Ca^{2+} signals from individual cells and measure interspike intervals (ISI) using our developed Calcium Signaling Analysis (CaSiAn)

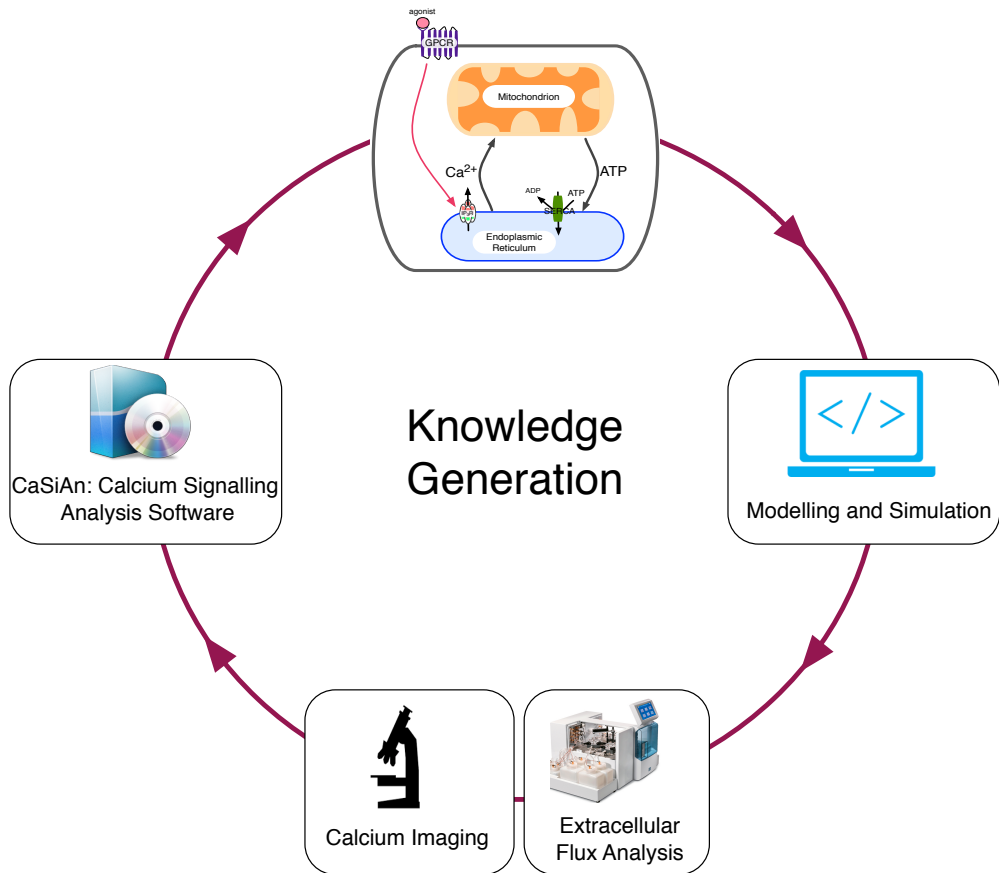


Figure 1.2. Our approach for dissecting the crosstalk between Ca^{2+} signaling and mitochondrial metabolism. The crosstalk between IP_3 -mediated Ca^{2+} signaling and mitochondrial metabolism is mathematically modeled and the predicted scenarios are tested by Ca^{2+} imaging and metabolic flux analyses. The extracted Ca^{2+} signals are analyzed by the developed software and the results are used for validation and improvement of the model. We also used the outcome of Ca^{2+} imaging experiments for designing the experiments of flux analysis and vice versa. Thus, we performed all steps of a system's biology approach (Figure 1.1) to have a mechanistic understanding of the biological problem.

software. CaSiAn is an open source software implemented with java language that provides a full-fledged user interface allowing biologists to easily analyze a large amount of Ca^{2+} signals, tune peak detection parameters for each signal, examine detected peaks/nadirs of Ca^{2+} signals and access the quantified descriptors of Ca^{2+} spikes in the form of an excel or text file.

To know the effect of IP_3 -mediated Ca^{2+} signaling on the mitochondrial metabolism, we measure glucose and glutamine uptake rate for different agonist concentrations. To quantify glucose and glutamine uptake rate, we measure the remaining metabolites within the medium and then compute the consumed amount of glucose and glutamine over the time. By normalizing the total glucose or glutamine uptake rate to the cell number, we obtain the glucose or glutamine uptake rates per cell. Together with the measured periods of Ca^{2+} sig-

nals for different agonist concentration, these uptake rates can be expressed as a metabolic decoding relation of Ca^{2+} signaling. Finally, we investigate the effect of IP_3 -mediated Ca^{2+} signaling on the intracellular ATP by measuring the ADP/ATP ratio of the cells to explore how exposing cells to extracellular stimuli affects mitochondrial metabolism.

1.3 Aims

In this dissertation, we characterize the crosstalk between Ca^{2+} signaling and mitochondrial metabolism by an interdisciplinary approach (Figure 1.2). Specifically, we have the following aims:

1. Developing a computational *in silico* model, dedicated to simulate the interplay between Ca^{2+} signaling and mitochondrial metabolism. This model integrates a well-established model of IP_3 -mediated Ca^{2+} signaling with the simplified model of mitochondrial Ca^{2+} handling and metabolic function. This model is discussed in Section 3.1.
2. Predicting the effect of mitochondrial carbon inputs and cellular ATP level on the Ca^{2+} homeostasis using *in silico* simulations. The results of simulations are validated by *in vitro* experiments where periods of Ca^{2+} signals are measured in the glucose deprived cells. These results are discussed in Sections 4.1.2 and 4.2.3.
3. Exploring the effect of different Ca^{2+} profiles on the cellular metabolic activity by measuring the glucose/glutamine uptake rate and cellular ATP level. For this purpose, we measured the glucose/glutamine uptake rate while exposing cells to the different concentrations of extracellular stimulus which induce Ca^{2+} releasing from IP_3Rs channels. The results of these experiments are discussed in Sections 4.2.6 and 4.2.8.
4. Establishing the metabolic decoding relation of Ca^{2+} signals by measuring the periods of Ca^{2+} signals as well as glucose/glutamine uptake rate while cells are stimulated with different concentrations of extracellular stimuli. The results of these experiments are discussed in Section 4.2.7.
5. Simulating the PINK1 deficiency and the rescue mechanism using *in silico* model. The model could reveal the experimental results which are discussed in Section 4.3.
6. Developing an open source software implemented with java language that provides a full-fledged user interface allowing biologists to analyze a large amount of Ca^{2+} signals fast and precisely. This software is explained in Section 4.4.

1.4 Organization of the Dissertation

Chapter 2 contains a description of the Ca^{2+} signaling components, energy metabolism system and the crosstalk between Ca^{2+} signaling and mitochondrial metabolism. Then we provide the medical relevance of the Ca^{2+} -mitochondrial crosstalk in the neurodegenerative diseases like Parkinson's and Alzheimer's diseases. We also describe a background information about modeling biological reactions using ordinary differential equations (ODEs).

Chapter 3 describes our developed mathematical model for the crosstalk between intracellular Ca^{2+} signaling and mitochondrial metabolism. The parameter scan is performed to validate the applicability of our proposed model. The results of simulations are compared with the experimental observations and also published data. Then we describe the applied experimental methods for answering the biological questions.

Chapter 4 describes the simulations and experiments which are performed for dissecting the crosstalk between Ca^{2+} signaling and mitochondrial metabolism. The robustness of the ATP-dependent model versus ATP-independent model is discussed. Then the ATP-dependent model is used for simulating the impact of mitochondrial carbon inputs on the Ca^{2+} signaling and cellular ATP level. The model predictions are validated by our experiments. The effect of extracellular stimuli and frequency of Ca^{2+} signals on the glucose and glutamine fluxes is investigated by performing a set of *in vitro* experiments and the results show metabolic decoding of Ca^{2+} signals by the energy metabolism. The application of our developed Ca^{2+} -mitochondrial model in predicting the effect of PINK1 deficiency is discussed. At the end, a description of the implemented software for analyzing Ca^{2+} signals is provided.

Chapter 5 discusses the results.

Chapter 6 summaries the thesis contributions and discusses perspectives on future work.

Chapter 2

The Calcium-Energy Metabolism System

The calcium-energy metabolism system, formed by spatiotemporal interaction between calcium regulation and energy metabolism components, plays a pivotal role in cell survival or death. Ca^{2+} is known as signal of life and death and Ca^{2+} signaling is highly controlled by different proteins and organelles. Metabolism is also highly regulated and any dysregulation of metabolism leads to disease.

To get more insights into the calcium-energy metabolism system and its important roles in diseases, we provide some background information in this chapter. The chapter is designed as follows:

- We review the components of Ca^{2+} signaling toolkit (Section 2.1).
- We explain the glycolysis pathway and mitochondrial functioning as the main sources of ATP production in the eukaryotic cells (from Section 2.2).
- We discuss the role of Ca^{2+} dyshomeostasis and mitochondrial dysfunction in Parkinson's and Alzheimer's diseases (Sections 2.4)
- We explain the crosstalk between Ca^{2+} regulation and mitochondrial metabolism (Section 2.3).
- We illustrate the description of biological systems by mathematical models (Section 2.5).

2.1 The Calcium Signaling Toolkit

Calcium is the fifth most abundant element in the earth's crust. Ca^{2+} is a ubiquitous intracellular messenger which plays an important role in signal transduction pathways and biochemistry of cells [Berridge et al., 2003]. The level of intracellular Ca^{2+} is determined by a balance between the reactions that introduce Ca^{2+} into the cytoplasm and the reactions

through which the Ca^{2+} is removed. Releasing Ca^{2+} from internal or external stores in response to stimuli, and then removing it from the cytosol cause to the creation of Ca^{2+} signals inside the cell.

Calcium is involved in many cellular processes ranging from the regulation of enzyme activity to programmed cell death. Ca^{2+} operates over a wide temporal and spatial scale to control many different cellular processes as fertilization, proliferation, learning and memory, muscle contraction, gene regulation and metabolism [Berridge et al., 1998]. Synaptic plasticity which is one of the important neurochemical foundations of learning and memory is strongly affected by the level of Ca^{2+} ions. Neurons communicate with each other primarily through fast chemical synapses. At such synapses an action potential generated near the cell body propagates down the axon where it opens voltage-gated Ca^{2+} channels. Ca^{2+} ions entering nerve terminals trigger the rapid release of vesicles containing neurotransmitter, which is ultimately detected by receptors on the postsynaptic cell [Zucker and Regehr, 2002]. Synaptic plasticity is often dependent on Ca^{2+} influx through the N-Methyl-D-aspartic acid (NMDA) receptor (NMDAR) which then leads to the release of Ca^{2+} from intracellular stores [Colbran and Brown, 2004]. A large Ca^{2+} influx to the neurons through NMDARs is called long-term potentiation and small Ca^{2+} influx to the neurons through NMDARs is called long-term depression [Abraham and Bear, 1996]. Very high Ca^{2+} concentration around nerve cells leads to neural over-excitation and the resulting brain damage can cause progressive memory loss [Berridge, 2010].

In fertilization, Ca^{2+} signal might occur via several routes which leads to increasing Ca^{2+} concentration inside the egg and initiate cell proliferation and gene regulation [Santella et al., 2004]. Muscle contraction happens by releasing Ca^{2+} from intracellular stores and binding to troponin. Binding Ca^{2+} to troponin leads to binding myosin to actin which cause pulling actin filaments. As an example of Ca^{2+} involvement in gene expression, we can point to the NFAT transcription factor which is activated by Ca^{2+} and the Ca^{2+} /calmodulin-dependent serine phosphatase calcineurin [Hogan et al., 2003]. NFAT proteins are phosphorylated and reside in the cytoplasm in resting cells. Upon stimulation, they are dephosphorylated by calcineurin, translocate to the nucleus, and become transcriptionally active providing a direct link between intracellular Ca^{2+} signaling and gene expression [Hogan et al., 2003]. In metabolism Ca^{2+} acts as a driving force for ATP production in mitochondria by activating TCA cycle enzymes. Calcium is also signal of death. Very high cytosolic Ca^{2+} concentration can lead to apoptosis by overloading mitochondrial Ca^{2+} which leads to abnormal mitochondrial metabolism, releasing more cytochrome c, which may activate caspases (a family of protease enzymes playing essential roles in programmed cell death) [Berridge et al., 1998]. Because of involvement of Ca^{2+} in variety cellular functions, it is under very tight homeostatic control to ensure that the resting level of intracellular Ca^{2+} is maintained low (between

20-100 nM) [Berridge, 1997].

Intracellular Ca^{2+} concentration have spatiotemporal properties. At the spacial domain, they can either activate highly localized cellular processes like mitochondrial metabolism or can activate processes in global scale like insulin secretion. In the temporal domain, information of certain cellular processes are encoded in the frequency of calcium signals. Regulation of widely different Ca^{2+} profiles needs involvement of different cellular channels and organelles in Ca^{2+} homeostasis [Berridge et al., 2003]. Intracellular Ca^{2+} levels increase either from sources outside of the cell or from Ca^{2+} stores inside the cells like endoplasmic reticulum (ER). In the electrically excitable cells like dopaminergic (DA) neurons, opening of voltage gated channels on the cell membrane leads to increasing intracellular Ca^{2+} level, while in the electrically non-excitatory cells like astrocytes cellular Ca^{2+} levels increase due to releasing Ca^{2+} from ER. So in each cell type, different components of the Ca^{2+} signaling system are expressed to create different Ca^{2+} signal profiles based on their functionality. Figure 2.1 shows different components of Ca^{2+} signaling toolkit. In the following, we will describe each component and their roles in the Ca^{2+} homeostasis.

2.1.1 Plasma Membrane Calcium Proteins

Voltage-gated calcium channels: Voltage-gated calcium channels (VGCC) or voltage-operated channels (VOC) are key transducers of membrane potential variations into intracellular Ca^{2+} transients that initiate many physiological events [Catterall, 2011]. These channels transfer the information content of an action potential in the cell surface membrane into the cell through an intracellular Ca^{2+} transient. Among the many types of voltage-gated Ca^{2+} channel, L-type Ca^{2+} channels exhibit slow voltage-dependent inactivation, therefore are long (L) lasting [Zuehlke et al., 1999]. This channel has four subunits: $\text{Ca}_v1.1$, $\text{Ca}_v1.2$, $\text{Ca}_v1.3$, $\text{Ca}_v1.4$.

In cardiac and smooth muscle cells, activation of L-type Ca^{2+} channels initiates contraction directly by increasing cytosolic Ca^{2+} concentration and indirectly by activating calcium induced calcium release (CICR) process by ryanodine-sensitive Ca^{2+} release channels (RyR) in the sarcoplasmic reticulum (SR) [Catterall, 2011]. Neuronal L-type calcium channels, $\text{Ca}_v1.2$ and $\text{Ca}_v1.3$ which localize to soma and dendrites of neurons, open with fast kinetics and carry substantial calcium entry in response to individual action potential waveforms [Helton et al., 2005]. Dihydropyridine antagonist blockade demonstrates that L-type calcium channels are critical for activity-dependent gene expression and for regulating plasticity at certain synapses [Hell et al., 1993].

Dopaminergic (DA) neurons in the substantia nigra pars compacta express L-, N-, P/Q- and R-type Ca^{2+} channels, but it is indicated that L-type channels have lower threshold

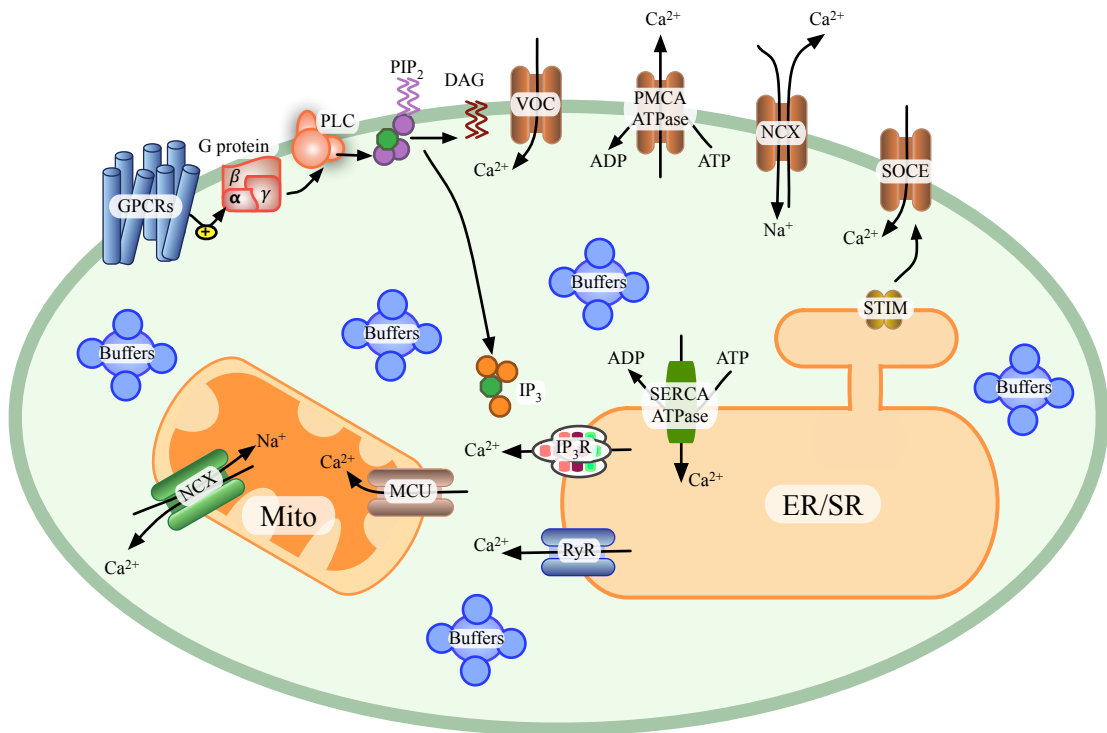


Figure 2.1. Overview of the calcium signaling toolkit. Binding a stimuli to a G protein-coupled receptor (GPCR) activates phospholipase C (PLC) through G protein and leads to cleaving phosphatidylinositol bisphosphate (PIP₂) and forming diacylglycerol (DAG) and inositol 1,4,5-trisphosphate (IP₃). DAG stays on the plasma membrane whereas IP₃ diffuses into cytosol and binds to IP₃ channels that leads to opening them and induce Ca²⁺ release from ER into cytosol. Ca²⁺ can also release from ER through ryanodine receptors (RyR). Ca²⁺ concentration inside the cytosol can also increase via other sources: Ca²⁺ release through store-operated Ca²⁺ channels (SOC), Ca²⁺ release through voltage-operated channels (VOC) and Ca²⁺ entry through mitochondrial Na⁺/Ca²⁺ exchanger (NCX). Ca²⁺ can be removed from the cytoplasm by SERCA and PMCA pumps, through the plasma membrane Na⁺/Ca²⁺ exchanger (NCX) or by mitochondrial uniporter Ca²⁺ channel (MCU). Different proteins and organelles can buffer Ca²⁺. Calmodulin (CaM) is one of the main Ca²⁺ binding proteins which has capacity of the binding four Ca²⁺. STIM: stromal interaction molecule

activation and conduct the large portion of whole cellular calcium. This finding supports the previous studies suggesting that rhythmic firing in DA neurons is blocked by L-type Ca²⁺ channels [Durante et al., 2004]. Ca_v1.2 and Ca_v1.3 channels respond well to brief action potential-like stimuli and deactivate slowly and permit calcium influx for several milliseconds after the membrane potential returns to -80 mV [Helton et al., 2005]. Elevated intracellular Ca²⁺ triggers inactivation of L-type calcium channels [Peterson et al., 1999]. It has been shown that calmodulin is a critical Ca²⁺ sensor for both inactivation and facilitation of L-type Ca²⁺ channels [Zuehlke et al., 1999].

Store-operated channels: Store-operated Ca²⁺ channels (SOC), store-operated Ca²⁺ entry (SOCE) or Ca²⁺ release-activated Ca²⁺ current (I_{CRAC}) is a Ca²⁺ influx pathway in electri-

cally non-excitable cells that is controlled by the Ca^{2+} content of the intracellular stores. These channels are activated by emptying of intracellular Ca^{2+} stores, but the mechanism that translate the fall in Ca^{2+} content of SR/ER to plasma membrane Ca^{2+} channels is not completely understood [Venkatachalam et al., 2002]. Recently it was shown that stromal interaction molecule-1 (STIM1) which is a single spanning transmembrane protein located mainly on the ER membrane and Orai1 (calcium release-activated calcium channel protein 1) which is a plasma membrane protein, are two key players in activating SOCE in response to diminished luminal Ca^{2+} levels [Stathopoulos et al., 2008]. The current view is that the ER Ca^{2+} sensor STIM1 re-localizes and forms puncta at the junction of the ER and the cell plasma membrane (PM) upon store depletion. By a mechanism that is unknown, STIM1 interacts with Orai1, leading to its activation. Such a spatial arrangement implies a very close association between the superficial part of the ER and the PM, estimated to be around 10-20 nm [Prakriya et al., 2006, Demaurex et al., 2009].

Due to binding of a Ca^{2+} -mobilizing signal such as IP_3 , Ca^{2+} is released from the ER. Emptying the intracellular stores is detected by a protein, most probably an inositol-1,4,5-triphosphate receptor (IP_3R) or a rynodine receptor (RYR), which leads to a conformational change that is transported to SOC to induce Ca^{2+} entry across plasma membrane [Berridge et al., 2003]. Emptying the internal Ca^{2+} stores and activating I_{CRAC} can be induced by inhibition sarcoplasmic/endoplasmic reticulum Ca^{2+} -ATPase (SERCA) pumps or by Ca^{2+} buffers which passively uptake Ca^{2+} or by mitochondria that can effectively compete with SERCA pumps and reduce the rate of store refilling. Mitochondrial Ca^{2+} uptake decreases the opening threshold of SOC and increase their sensitivity to inositol-1,4,5-triphosphate (IP_3) [Parekh, 2003]. SOCE can be deactivated by Ca^{2+} -dependent inactivation process, which results from a negative feedback of Ca^{2+} entering through the SOCE that can be partially prevented by the use of fast Ca^{2+} chelators like BAPTA or the slow one like EGTA.

Plasma membrane Ca^{2+} -ATPase pump: The plasma membrane Ca^{2+} -ATPase (PMCA) pumps export one Ca^{2+} ion to the extracellular space by hydrolysis one molecule ATP in all eukaryotic cells. Ca^{2+} pumps are important for the precise maintenance of the cellular Ca^{2+} homeostasis and their malfunction cause numerous disease phenotypes [Brini and Carafoli, 2009]. PMCA types 1 and 4 are distributed ubiquitously while PMCA types 2 and 3 are restricted to some tissues, the most important being the nervous system. The transcripts of all four PMCA genes undergo alternative splicing, which greatly increases the number of PMCA variants [Brini et al., 2013].

All PMCA types except type 2 are activated in the presence of calmodulin (CaM) that increases their affinity by one or even two orders of magnitude. The kinetics of interplay with calmodulin differ in the four basic isoform, PMCA type 1 and 4 have lower affinity

than two tissue restricted isoforms. PMCA_s are inhibited in the absence of CaM (calcium-modulated protein) by a mechanism that involves binding of their C-terminal tail to the two major intracellular loops [Strehler et al., 2007]. For activation, Ca²⁺-CaM should bind to the C-terminal and make a conformational change that displaces the auto-inhibitory tail from the major catalytic domain. PMCA_s type 2 which are highly expressed in the central nervous system and its related tissues are highly active in absence of CaM. The PMCA2 pump is widely distributed in the brain and is expressed in high levels in the cerebellum.

Sodium-calcium exchanger: The sodium-calcium exchanger (NCX) is an ion transport protein on the plasma membrane that extrudes Ca²⁺ in parallel with PMCA. It also can work in the reverse mode and mediates Ca²⁺ entry in parallel with various ion channels. The amount of Ca²⁺ movement and its direction depend on the net electrochemical driving force on the exchanger like the Na⁺, Ca²⁺ and K⁺ gradients across plasma membrane or membrane potential which varies during action potential. The rate of Ca²⁺ transport by NCX increases or decreases as Ca²⁺ concentration is raised or lowered, respectively in order to meet cellular demands for rapid transport of Ca²⁺ and Ca²⁺ regulation [Blaustein and Lederer, 1999].

G protein coupled receptors: G protein-coupled receptors (GPCRs) are the fourth largest protein superfamily in mammalian genomes [Marinissen and Gutkind, 2001]. They have a seven-transmembrane topology coupled with heterotrimeric G protein and mediate cellular response to a variety of extracellular signals ranging from photons and small molecules to peptides and proteins, and thus have great potential as therapeutic targets for a broad spectrum of diseases.

The heterotrimeric G protein is composed of three subunits: α , β and γ . Binding of agonist to GPCRs leads to the exchange of GDP for GTP bound to the α subunit and separate G α and G $\beta\gamma$ subunits. These activated subunits affect their target proteins and activate or inhibit the production of variety second messengers such as cAMP (cyclic-adenosine monophosphate), cGMP, diacylglycerol (DAG), inositol (1,4,5)-trisphosphate (IP₃), arachidonic acid and phosphatidic acid. G α is inactivated when a GTPase enzyme binds to it and hydrolyzes the GTP, causing it to re-associate with G $\beta\gamma$.

Among all second messengers that are activated by G α subunit, the cAMP and the phosphatidylinositol signal pathways are two canonical ones. G $s\alpha$ and G $i\alpha$ activate adenylyl cyclase (AC). The specific isoforms of AC catalyse the conversion of intracellular ATP to cAMP. Due to binding of two cAMP molecules to each cAMP-dependent protein kinase or protein kinase A (PKA) regulatory subunit, they become active. Thus cAMP is considered a second messenger and PKA a secondary effector. In human airway smooth muscle cells, PKA phosphorylates cAMP response element binding (CREB) transcription factor, phos-

pholipase C (PLC), the inositol trisphosphate receptor (IP₃R) and myosin light chain kinase (MLCK) [Billington and Hall, 2012].

An important second messenger stimulated by GPCRs is Ca²⁺. Many hormones and neurotransmitters transmit their information by increasing cytosolic Ca²⁺ concentration. Gq α or Gi (activated by released G β γ) activate phospholipase C- β (PLC β) that catalyzes formation of IP₃ and diacylglycerol (DAG) from phosphatidylinositol 4,5-biphosphate (PIP2). IP₃ binds to IP₃R on the membrane of ER and open these channels that leads to leaking Ca²⁺ to cytoplasm. The released Ca²⁺ from ER then can activate SOCE channels on the plasma membrane and lead to a global rise in cytosolic Ca²⁺ concentration.

Metabotropic Glutamate Receptors: The metabotropic glutamate receptors (mGluRs) are member of the GPCRs family and are activated by binding glutamate. Many studies have shown improved learning and memory by drugs that target mGluRs activation [Rickard and Ng, 1995]. The mGluRs have many subtypes that can be categorized into three groups based on their functions in the central nervous system: group I includes mGluR1 and mGluR5, group II includes mGluR2 and mGluR3, and group III includes mGluR4, mGluR6, mGluR7, and mGluR8. Activation of group I of mGluRs increase neuronal excitation whereas activation of group II and group III mGluRs tends to decrease excitation [Hölscher et al., 1999].

Stimulation of group I by glutamate leads to forming IP₃ that cause to Ca²⁺ release from ER, and making diacylglycerol (DAG) that increase protein kinase C (PKC) activity which is needed for upregulating N-methyl-D-aspartate (NMDA) receptors. NMDA receptor gated Ca²⁺ channels are the ionotropic family (ligand-gated ion channels) of glutamate receptors that are activated when glutamate is bound to NMDA and the postsynaptic neuron is largely depolarized by Na⁺. This leads to opening the channel and Ca²⁺ enter to the neurons. Opening NMDA leads to entering Ca²⁺ to the cell which then activate many cellular processes. Increasing neural Ca²⁺ concentration either through NMDA receptors or IP₃ -induced Ca²⁺ release from internal stores is required for long term potentiation (LTP) induction. Neurological disorders like Alzheimer's disease displaying memory loss have shown abnormalities in glutamate receptors and Ca²⁺ regulation [Rickard and Ng, 1995, Hölscher et al., 1999].

Purinergic receptors: ATP and related purine nucleotide act as an extracellular signaling molecule that stimulates a large family of purinergic receptors found on the cell surface of virtually all mammalian cells. There are three class of purinergic receptors: P1 and P2Y receptors that are GPCRs and P2X receptors that are ligand-gated ion channels. P1 receptors are stimulated by binding adenosine, P2Y receptors are activated by nucleotides like, ATP, ADP, UTP, UTD and P2X receptors are activated just by binding ATP. Thus, ATP not only act as a key source of the cellular energy, it also functions as a potent extracellular messenger

producing its effects via the P2 receptor family (P2X and P2Y).

Binding three ATP molecules to each subunit of P2X receptors evokes a conformational change in the structure of the ion channel that results in the opening of the ion-permeable pore, allowing cations such as Na^+ and Ca^{2+} enter the cell, depolarize cell membrane and activate various Ca^{2+} sensitive intracellular processes. P2X receptors are expressed in nerve and glial cells and have been shown to modulate synaptic transmission. They are also able to initiate contraction in cells of the heart muscle, skeletal muscle, and various smooth muscle tissues. Binding ATP to P2Y receptors leads to forming IP_3 second messenger and releasing Ca^{2+} from internal stores. ATP can release from cells in physiological conditions with a number of neurotransmitters like acetylcholine, norepinephrine, glutamate. Released ATP can be degraded to ADP, AMP and adenosine by a family of enzymes called ectonucleoside triphosphate diphosphohydrolases (E-NTPases). ATP directly can activate P2X and P2Y receptors while when is degraded to ADP and AMP it can activate $\text{P2Y}_T/\text{P2Y}_{12}$ receptors and P1 receptors, respectively [Burnstock and Williams, 2000].

2.1.2 Sarco/Endoplasmic Reticulum

The Sarco/Endoplasmic reticulum (SR/ER) is a multifunctional signaling organelle that is involved in the synthesis, folding, and transport of proteins and also plays an important role in Ca^{2+} signaling by functioning as a Ca^{2+} store. Opening of either inositol 1,4,5-trisphosphate receptors (IP_3 Rs) or ryanodine receptors (RYRs) located on the ER/SR membrane leads to leaking of Ca^{2+} from the ER into the cytoplasm. In low Ca^{2+} concentration, the opening of one channel stimulates opening of neighboring channels, called Ca^{2+} -induced Ca^{2+} release process, that generates a global Ca^{2+} wave in the cytosol. This repetitive mechanism of Ca^{2+} releasing is particularly important in the control of muscle cells and neurons [Berridge, 2002].

The two major functions of ER, protein synthesis and Ca^{2+} regulation can affect each other. Accumulation of misfolded proteins alter Ca^{2+} homostasis in the ER while changing the Ca^{2+} concentration within ER influences the process of protein synthesis. The ER is divided into three different regions based on their localization in the cell: rough ER, smooth ER and nuclear membrane. The rough ER is studded on its outer surface with ribosomes that is responsible for protein synthesis, called translation. In the lumen of the rough ER proteins are folded and also quality control of proteins is performed. Proteins that are folded incorrectly are rejected or are tagged and sent for recycling for the break down to amino acids. The smooth ER has a long network of a folded, tube-like structure and is involved in Ca^{2+} signaling as well as making lipids and steroid production. In muscle cells, this structure helps to release Ca^{2+} synchronously within the cell and create a rapid global signal in the

whole cell to contract the muscle.

The sarcoplasmic reticulum (SR) is an intracellular membranous network found in muscle cells. It serves to initiate muscle contraction by releasing calcium through the ryanodine receptors (RyR) into the cytosol and facilitates muscle relaxation by active reuptake of calcium by the sarcoendoplasmic reticulum Ca^{2+} - ATPase (SERCA) pumps. The SR/ER is highly sensitive to even minor perturbations in its environment, and is particularly sensitive to alterations in calcium homeostasis.

The function of ER and mitochondria is highly coupled. The released Ca^{2+} from ER is rapidly taken up by mitochondria and subsequently is released slowly to the cytosol that helps ER to refill instead of pumping to the extracellular space. Disturbance of Ca^{2+} concentration balance in the ER alters the function of chaperones that are responsible for folding the proteins. If mitochondria uptake more Ca^{2+} or don't release Ca^{2+} properly, it can lead to "ER stress". If a physiological and pathological stimuli can disrupt ER homeostasis resulting to an accumulation of misfolded and unfolded proteins, a condition known as ER stress. ER stress activates a complex signaling network referred as the Unfolded Protein response (UPR) to reduce ER stress and restore homeostasis [Oslowski and Urano, 2011]. A variety of physiologic conditions such as glucose deprivation, oxidative stress, ischemia, and infection can disrupt ER function that can result in ER stress.

Also if the amount of released Ca^{2+} is not controlled by ER, it can damage mitochondria by creating mitochondrial permeability transition pores (MPTP) within the mitochondrial membrane. Under conditions of mitochondrial calcium overload, especially when accompanied by oxidative stress, elevated phosphate concentrations and adenine nucleotide depletion, MPTP opens in the inner mitochondrial membrane. MPTP opening enables free passage into the mitochondria of molecules of < 1.5 kDa including protons. The resulting uncoupling of oxidative phosphorylation leads to ATP depletion and necrotic cell death [Halestrap, 2009].

IP₃ receptor (IP₃R) channels: IP₃ receptors (IP₃R) are a family of Ca^{2+} channels responsible for Ca^{2+} mobilization from Ca^{2+} stores and are generally located on the ER membrane, but in some tissues they have been seen on the plasma membrane and nuclei. IP₃Rs are tetrameric intracellular Ca^{2+} channels with four 313 kD subunits [Taylor and Laude, 2002]. IP₃Rs are expressed in three isoforms: IP₃R1, IP₃R2 and IP₃R3, but the structural organization of each subunit appears to be similar [Watras et al., 1991].

These channels are opened by binding one IP₃ molecule and one Ca^{2+} ion at low cytosolic Ca^{2+} concentration and are closed also by rising Ca^{2+} concentration. Thus, their open probability of IP₃Rs follow the biphasic regulation and bell-shaped curve in dependence on the local calcium level. The effect of Ca^{2+} on the IP₃Rs may be mediated by cytosolic

Ca^{2+} -binding proteins such as calmodulin (CaM) and the neuronal Ca^{2+} -binding protein 1 (CaBP1), which both have documented interaction sites with the IP_3R . The amount of Ca^{2+} in the ER also regulates IP_3R activity. Overloading luminal Ca^{2+} increases sensitivity of IP_3Rs to IP_3 which eventually leads to spontaneous Ca^{2+} release from permeabilized hepatocytes [Missiaen et al., 1991]. On the other hand, some studies have shown decreasing IP_3Rs activity to IP_3 by depletion of ER [Nunn and Taylor, 1992]. In common with cytosolic Ca^{2+} , ATP also has biphasic effects on IP_3 receptors. IP_3Rs activity increases by micromolar concentrations of ATP and decreases by presence of millimolar concentrations of ATP.

The most common pathway for producing IP_3 molecules is binding an agonist to G-protein coupled receptor on the cell membrane and activating phospholipase C (PLC). Then IP_3 diffuses into the cytosol and binds to IP_3 channels that leads to opening them and induce Ca^{2+} release from ER into cytosol due to the large concentration differences between the two compartments. In the low cytosolic Ca^{2+} concentration, binding Ca^{2+} and IP_3 to IP_3Rs increase their open probability and leads to releasing Ca^{2+} from these channels. Fluorescence imaging and modeling studies have shown that IP_3 -evoked Ca^{2+} signals are generated in a hierarchical process where Ca^{2+} releasing from one single IP_3R channel (blip) stimulates opening of neighbor channels at the same cluster, creating puffs and these puffs may activate adjacent clusters by diffusion of Ca^{2+} that may result in a global Ca^{2+} wave in the whole cell [Lipp et al., 1997, Skupin and Falcke, 2010]. IP_3 -evoked Ca^{2+} signals do not behave as regular oscillators since they are made from random sequences of Ca^{2+} spikes with not deterministic inter spike intervals (ISIs). Each ISI has a large stochastic period which leads to forming ISIs with different lengths and distributions [Skupin et al., 2008, Thurley et al., 2011]. Stochastic binding of IP_3 and Ca^{2+} to IP_3 receptors leads to stochastic opening and closing of each channel. These openings lead to the release of a small amount of Ca^{2+} , and are called 'blips'. When IP_3Rs are situated in clusters, the opening of one IP_3R can initiate the opening of neighboring IP_3R , leading to the simultaneous opening of a group of IP_3R . This is called a Ca^{2+} 'puff'. One Ca^{2+} puff can excite neighboring clusters of IP_3R , leading to large coordinated release of Ca^{2+} across an entire cell, called a Ca^{2+} spike. Each of these levels relies on the combination of stochastic events, and thus the time between Ca^{2+} waves follows a distribution, rather than being a fixed interval [Moenke et al., 2012, Dupont et al., 2016]. In contrast to random spikes, the relation between average of ISIs (T_{av}) and standard deviation of ISIs (σ) does not depend on channel and cluster properties and is determined by the global feedback processes in the Ca^{2+} signaling pathway, like global Ca^{2+} concentration, IP_3 metabolism or ER depletion [Thurley and Falcke, 2011].

Ca^{2+} oscillations start from IP_3R cluster area and then propagate through the cell as a Ca^{2+} wave. Ca^{2+} signals can spread into neighboring cells, generating intercellular Ca^{2+} waves. The complex Ca^{2+} oscillations contribute to diverse physiological processes such

as development, synaptic plasticity, fertilization, gene expression and apoptosis. Abnormal IP₃R-mediated Ca²⁺ signaling can disturb the communication between ER and mitochondria and lead to cell death. Type 1 IP₃R (IP₃R1) is the predominantly expressed in the central nervous system. Experiments on new born mice with genetically manipulated IP₃R1-knockdown led to the death of mice after 3 weeks. Lack of IP₃R1 cause long term depression which affect motor learning and coordination and also shown impairment in hippocampal synaptic plasticity. IP₃-evoked Ca²⁺ oscillations play important roles in astrocytes as increased Ca²⁺ concentration triggers release of neuroactive molecules from astrocytes, including glutamate, d-serine, ATP, adenosine, γ -aminobutyric acid and tumor necrosis factor α (TNF- α) [Hisatsune and Mikoshiba, 2012].

Sarco/Endoplasmic reticulum Ca²⁺-ATPase pump: Sarco/Endoplasmic reticulum Ca²⁺-ATPase pump (SERCA) pumps belong to P-type ATPase family that involves also plasma membrane Ca²⁺-ATPase (PMCA), Na⁺/K⁺ ATPase and H⁺/K⁺ ATPase channels. P-type ATPases move ions against the concentration gradient across a biological membrane by hydrolysis of ATP. The SERCA pump is a single polypeptide with molecular mass of 110 kDa and is localized on both the ER and the SR membrane. The family of SERCA pumps are encoded by three genes: SERCA1, SERCA2 and SERCA3 [Periasamy and Huke, 2001].

SERCA pumps push Ca²⁺ into the endoplasmic reticulum against the steep concentration gradient between ER and cytosol. They consume one molecule of ATP for pumping two calcium ions. SERCA activity impairment leads to an imbalance of the cellular Ca²⁺ level. This is implicated in many pathological processes, such as heart disease, Alzheimer's and Parkinson's diseases. In the muscles, SERCA pumps play two roles: first they cause muscle relaxation by lowering the cytosolic calcium, and second they restore calcium of SR necessary for muscle contraction. Contraction and relaxation cycle of the heart is tightly regulated by release and uptake of Ca²⁺ between the SR and the cytoplasm. Ca²⁺ enters the cell via L-type Ca²⁺ channels and as a consequence triggers Ca²⁺ release from SR through ryanodine receptor by CICR mechanism which leads to muscle contraction.

The SERCA pump is identified as an ER protein whose normal function is required by all cells and represents a potential therapeutic target for cancer therapy. It has been shown that inhibition of SERCA by thapsigargin directly leads to depletion of Ca²⁺ inside the ER and activation of ER-stress response and simultaneous activation of apoptotic pathways within the ER and the mitochondria. Anti-apoptotic members such as Bcl-2 prevent cell death in response to a wide variety of stimuli including thapsigargin. Overexpression of Bcl-2 in breast epithelial cells modulates ER Ca²⁺ store by upregulation of SERCA2 expression with little effect on IP₃R-3 expression [Kuo et al., 1998].

2.1.3 Mitochondria

Mitochondria are responsible for synthesis of most of the ATP in eukaryotic cells by oxidative phosphorylation. Besides this function, mitochondria also play a vital role in cell signaling by sensing and shaping Ca^{2+} signals. Fast uptaking and slow releasing mechanism of mitochondrial Ca^{2+} channels plus organelle movement profoundly influence Ca^{2+} dynamics and cellular function. Mitochondria uptake a large amount ($\sim 80\%$) of cytosolic Ca^{2+} through mitochondrial Ca^{2+} uniporter (MCU) and release it via $\text{Na}^+/\text{Ca}^{2+}$ (NCX) and $\text{H}^+/\text{Ca}^{2+}$ exchangers [Marhl et al., 2000]. Mitochondrial membrane potential ($\Delta\Psi$) which is mainly made by translocation of H^+ across the inner membrane of mitochondria make very large driving force for Ca^{2+} accumulation [Jacobson and Duchen, 2004]. MCUs are located close to IP_3 Rs and RYRs on the ER/SR as well as close VGCCs and SOCEs on the plasma membrane, thus they sense micro-domain of high cytosolic Ca^{2+} concentration which meets the low affinity of the MCUs and that dissipates rapidly, thus preventing mitochondrial Ca^{2+} overload and/or Ca^{2+} cycling across the mitochondrial membrane [Rizzuto et al., 2012].

Sensing the micro-domains of cytosolic calcium that dissipate rapidly by mitochondria has major functional consequences. Mitochondria sense highly localized cellular Ca^{2+} and act as a Ca^{2+} buffer while they can influence cell survival and various functions, such as metabolism, secretion and signaling [Rizzuto et al., 2012]. It has been shown that inhibition of mitochondrial Ca^{2+} uptake by compounds that dissipate mitochondrial membrane potential disturbs Ca^{2+} dependent inactivation of Ca^{2+} release-activated Ca^{2+} (CRAC) channels which can be due to the buffering capability of mitochondria that reduces the Ca^{2+} concentration near the sites that govern inactivation [Hoth et al., 2000].

The Ca^{2+} buffering by mitochondria also regulates Ca^{2+} release from IP_3 Rs on the ER. Opening IP_3 Rs and releasing Ca^{2+} from the ER creates a high cytosolic Ca^{2+} concentration locally which may inhibit IP_3 Rs and close these channels. But due to the presence of mitochondria in close contact with the ER, the Ca^{2+} is uptaken by mitochondria. Therefore mitochondrial Ca^{2+} uptake reduces the negative feedback inhibition of cytosolic Ca^{2+} and leads to further Ca^{2+} release from ER [Rizzuto et al., 2012]. Both GFP labelling of organelles in living cells and electron micrographs revealed the existence of close contacts (<200 nm) between mitochondria and the ER [Rizzuto et al., 1998]. The ER-mitochondrial junction and movement of Ca^{2+} between ER and mitochondria result in fundamental processes happens by Ca^{2+} like its role in energy production, cell fate and cell growth. A number of chaperones and regulatory proteins control the formation of the ER-mitochondria junction. Mitofusin 2 (MFN2) is involved in both mitochondrial fusion and in ER-mitochondria tethering.

The Ca^{2+} buffering capabilities of mitochondria also affect activity of Ca^{2+} dependent proteins. It can deactivate plasma membrane channels that are regulated by changes in Ca^{2+}

concentrations, like store-operated Ca^{2+} channels and voltage-gated Ca^{2+} channels. It has been shown that mitochondria can modulate the activity of SOCE by buffering the incoming Ca^{2+} or by generating ATP. In some cell types like T-lymphocytes, by opening the SOCs, mitochondria move close to plasma membrane and uptake the large amount of entering Ca^{2+} which leads to a more sustained Ca^{2+} influx. Mitochondria, by supplying ATP and slow release of Ca^{2+} through mitochondrial NCX, provide substrate and energy that PMCA needs to remove Ca^{2+} from cytoplasm. This process in the local domain close to the plasma membrane leads to relieving of Ca^{2+} -dependent inhibition mechanism in SOCEs and VGCCs which drastically change their temporal pattern and keep them active for longer time in the presence of nearby mitochondria. In contrast, mitochondria by providing ATP to SERCA pumps enhance the lumen Ca^{2+} concentration and reduce SOCE activity. The spatial organization of mitochondria and their contribution in Ca^{2+} buffering and supplying ATP for Ca^{2+} -ATPase pumps define their role in activating or inhibition of plasma membrane Ca^{2+} channels [Demaurex et al., 2009].

2.1.4 Calcium-Regulated Enzymes

Enzyme acts as a catalyst in living organisms, regulating the rate at which chemical reactions proceed without itself being altered in the process. The term kinase refers to a large category of enzymes that catalyze the transfer of phosphate from the gamma position of ATP to the hydroxyl group of Ser, Thr, or Tyr within protein substrates. So the importance of protein kinases in the regulation of protein function has become an integral part of our understanding of biology [Swulius and Waxham, 2008]. This process is known as phosphorylation. Three well-known kinases which are activated by Ca^{2+} ions are: Ca^{2+} /calmodulin-dependent protein kinase, Inositol 1,4,5-trisphosphate 3-kinase and protein kinase C.

Ca^{2+} /calmodulin-dependent protein kinase (CaM-kinase): Ca^{2+} binding proteins (CBP) are a heterogeneous and wide group of proteins that participate in numerous cellular functions. Although they have different structures and properties, most CBP selectively and reversibly bind Ca^{2+} in specific domains and the kinetics of this interaction being very fast. One group of intracellular CBPs exhibits EF-hand domains. This domain is found in a large family of proteins that includes some of the most important and ubiquitous CBP, such as calmodulin, troponin C or calcineurin. Calmodulin (CaM) is an ubiquitous Ca^{2+} binding protein that has been conserved throughout biological evolution. CaM has the capacity of binding four Ca^{2+} . Saturation of CaM with Ca^{2+} induces a conformational change in protein which makes it active to interact with diverse set of target enzymes. CaM itself has no enzymatic activity, and its function is to integrate with Ca^{2+} and transduce it to other downstream enzymes. The Ca^{2+} /CaM complex interacts with and modulates the functionality of a large number of proteins including several Ser/Thr protein kinases. Among many tar-

get enzymes, calmodulin-dependent protein kinases (CaM-kinases) are critically important for proper cellular functions like gene transcription, apoptosis, cytoskeletal reorganization, and learning and memory. In neurons Ca^{2+} /CaM-dependent protein kinase II (CaM-KII) is highly expressed and localized with certain subcellular structures. Upon activation, it can translocate to excitatory synapses where it regulates a number of proteins involved in synaptic transmission and its downstream signaling pathways [Soderling et al., 2001].

Inositol 1,4,5-trisphosphate 3-kinase (IP₃ 3-kinase): Inositol 1,4,5-trisphosphate 3-kinase (IP₃3-kinase/IP3K or ITP3K) is another calcium-regulated kinase which is activated directly by Ca^{2+} /CaM and also through protein kinase A (PKA or cAMP-dependent protein kinase) and Ca^{2+} /calmodulin-dependent protein kinase II (CAMKII). IP3K phosphorylates (consume ATP) second messenger Inositol 1,4,5-trisphosphate (IP₃) that mediates Ca^{2+} release from ER to the cytosol to another messenger Inositol 1,3,4,5-tetrakisphosphate (IP₄) responsible for mediating Ca^{2+} entry through plasma membrane. Thus, IP3K plays a key role in maintaining Ca^{2+} homeostasis by regulating the concentrations of IP₃ and IP₄. Another pathway of IP₃ metabolism is removal of the 5-phosphate from the inositol ring by inositol polyphosphate 5-phosphatases (IP5-ases) results in the production of Ins(1,4)P₂, an inactive inositol phosphate [Pattni and Banting, 2004].

Protein kinase C: Protein kinase C (PKC) is belong to a family of serine/threonine kinases that play important roles in several signal transduction cascades and is involved in receptor desensitization, in mediating immune responses, in regulating cell growth, and in learning and memory [Cole et al., 1988, Fenster et al., 1999, Dempsey et al., 2000]. PKC are activated by signals such as increases in the concentration of diacylglycerol (DAG) or calcium ions. DAG is known as second messenger signaling lipid. DAG and IP₃ are produced by hydrolysis of the phospholipid phosphatidylinositol 4,5-bisphosphate (PIP2) by the enzyme phospholipase C (PLC). IP₃ diffuses into the cytosol and stimulates Ca^{2+} release from ER, whereas DAG remains within the plasma membrane and activates PKC. The production of DAG in the membrane facilitates translocation of PKC from the cytosol to the plasma membrane. Disruption of PKC regulation is implicated in tumorigenesis and drug resistance.

2.1.5 Calcium Signaling in Electrically Non-Excitable Cells

Ca^{2+} signaling in electrically non-excitable cells have different dynamics from excitable cells. In excitable cells, changing the voltage of cellular plasma membrane leads to opening of voltage-gated Ca^{2+} channels and entering Ca^{2+} from extracellular space into the cytosol. Thus, excitable cells often have a cytosolic Ca^{2+} oscillator linked to a membrane potential oscillator, potentially giving rise to highly complex behaviours. However, in electrically non-excitable cells like astrocytes, the cytosolic Ca^{2+} dynamics occur independent of the cell

membrane potential and is governed by the periodic Ca^{2+} release from ER through IP_3R and RyR [Dupont et al., 2016].

Calcium signaling in Astrocytes: Calcium signaling is an important feature in the physiology of astrocytes. Indeed, astrocytes have developed various efficient ways to generate complex changes in intracellular calcium concentration. This machinery allows these cells to sense, integrate, and respond to external stimuli released mainly by neurons. Astrocytes are electrically non-excitatory cells for their lack of voltage-gated sodium channels. They make contact with most synapses in the central nervous system (CNS) and respond to synaptic activity with increases in cytosolic Ca^{2+} .

The widely accepted mechanism for astrocytic Ca^{2+} increases is the IP_3 pathway. Upon activation of G_q GPCR, phospholipase C (PLC) hydrolyzes the DAG and IP_3 , which leads to activation IP_3Rs and releasing Ca^{2+} from ER. It has been shown that $\text{IP}_3\text{R}2$ subtype is the primary functional IP_3R within hippocampus astrocytes [Petravicz et al., 2008]. In cultured and acutely prepared astrocytes, cytosolic Ca^{2+} concentration changes spontaneously or in response to mechanical stimulation, membrane potential depolarization, activation of metabotropic glutamate receptors and stimulation of purinergic receptors.

Astrocytes express receptors for most neurotransmitters, including glutamate. Glutamate evokes a calcium concentration rise in astrocytes (in culture, in brain slices, in whole retina and *in vivo*), which can propagate along astrocyte processes and even between glial cells [Dani et al., 1992, Porter and McCarthy, 1996, Newman and Zahs, 1997, Hirase et al., 2004, Wang et al., 2006, Parpura et al., 1994]. Ca^{2+} signaling in astrocytes may be limited to individual cells or may occur as a 'wave' of Ca^{2+} that is propagated from one cell to surrounding cells. Ca^{2+} wave propagation may happen through the gap junctions and has been correlated with the expression of connexins in multiple cell types [Giaume and Venancie, 1998]. Astrocytic Ca^{2+} waves may be mediated by purinergic receptors in the way that Ca^{2+} elevation in single astrocyte is propagated to neighboring cells, thereby recruiting a larger group of astrocytes. Astrocytes use ATP as a major extracellular messenger for propagating intracellular Ca^{2+} signaling to the neighboring cells [Guthrie et al., 1999].

Increases of astrocyte Ca^{2+} evoked by receptor agonists such as glutamate, GABA, ATP (ADP), or by uncaging of Ca^{2+} or IP_3 , were reported to release gliotransmitters from astrocytes, including glutamate, ATP, D-serine and GABA [Bazargani and Attwell, 2016]. The release of these gliotransmitters has been reported to generate a wide range of effects on neurons. The roles that astrocytic calcium elevations play in neurophysiology and especially in modulation of neuronal activity have been intensely researched in recent years.

In following of this chapter, we will describe the components of cellular energy metabolism

and show the link between Ca^{2+} signaling and energy metabolism in more detail. We also describe the medical relevance of Ca^{2+} and energy metabolism dysregulation in the pathogenesis of Alzheimer's and Parkinson's diseases.

2.2 Energy Metabolism

Energy metabolism is the process of generating energy (ATP) from nutrients. The major pathways that eukaryotic organism produce energy are glycolysis and mitochondrial oxidative phosphorylation [Erecińska and Wilson, 1982].

Carbohydrates, fats, and proteins are oxidized in the cells and produce large amount of energy. Energy metabolism is highly regulated through special cellular enzymes and substrates transfer systems that control chemical reactions and flow of metabolites along metabolic pathways. Eighty percent of digested carbohydrate is glucose and the rests are fructose and galactose which are rapidly converted to glucose via the liver. So the final product of almost all carbohydrates is glucose. Glucose is either metabolized in the cytosol through glycolysis or in the low energy demand is stored as glycogen or fat. Fatty acids that are another source of energy for the cells are degraded and oxidized in mitochondria where they go to beta-oxidation process and form acetyl coenzyme A. Proteins are made by amino acids that have peptide linkage with each other. Protein metabolism denotes the various biochemical processes responsible for the synthesis of proteins and amino acids, and the breakdown of proteins to α -keto acids which can be recycled in the body for generation of energy, and production of glucose or fat or other amino acids.

In order to produce ATP, cellular substrates go to Krebs cycle (also called citric acid cycle or tricarboxylic acid (TCA) cycle) in the matrix of mitochondria where they go through a series of chemical transformations and produce electron carrier molecules, NADH and FADH_2 . These molecules further go to electron transport chain (ETC) and generate electron gradient force for driving ATP synthesis.

Most metabolic reactions are catalyzed by enzymes, only some occur spontaneously. There are two types of regulations in cellular metabolism: (1) long-term (hours to days) or coarse regulation where regulation of cellular metabolism may start at the gene that encodes different enzyme isoform, followed by the transcriptional level that selects which genes are activated. Subsequently, alternative splicing, mRNA stability, translation, and protein degradation control enzyme abundances; (2) Short-term (seconds to minutes) or fine regulation that occurs by changing the activity of enzymes that already exist in the cell. Usually, they are triggered by changes in local concentrations of metabolites leading to an allosteric or post-translational regulation of enzyme activity [Wegner et al., 2015].

2.2.1 Glycolysis

The process of converting glucose with six carbons into two molecules of pyruvate with three carbons is called glycolysis that involves nine successive chemical reactions which produce two molecules of ATP per molecule of glucose. Glycolysis can produce ATP in the absence of oxygen.

This pathway can be divided into three stages. In the first stage glucose is transported to the cells by specific transport proteins and then is phosphorylated by consuming ATP that forms glucose 6-phosphate (G-6P). This reaction is catalyzed by hexokinase. Then G-6P is converted to Fructose 6-phosphate (F-6P) by phosphoglucose isomerase. The second phosphorylation happens after forming F-6P where it is phosphorylated by ATP to fructose 1,6-bisphosphate. This reaction is catalyzed by phosphofructokinase (PFK), an allosteric enzyme that sets the pace of glycolysis. Second stage of glycolysis is splitting fructose 1,6-bisphosphate into two 3-carbon molecules, glyceraldehyde 3-phosphate (GAP) and dihydroxyacetone phosphate (DHAP) by aldolase enzyme. GAP can directly move forward for the rest reactions in glycolysis whereas DHAP cannot and should first converted to GAP by the triose phosphate isomerase (TIM). This reaction is rapid and reversible. Stage three of glycolysis is where that ATP is produced from GAP. The initial reaction in this sequence is the conversion of GAP into 1,3-bisphosphoglycerate (1,3-BPG), a reaction catalyzed by glyceraldehyde 3-phosphate dehydrogenase. This reaction produce also one molecule of NADH. Then acyl phosphate of 1,3-BPG donates its phosphate group to ADP and forms one molecule ATP and 3-phosphoglycerate. In the remaining steps of glycolysis, 3-phosphoglycerate is converted into 2-phosphoglycerate and then into phosphoenolpyruvate (PEP). Finally, PEP is converted into pyruvate with the concomitant conversion of ADP into ATP [Berg et al., 2002] (see Figure 2.2). Therefore four molecules of ATP are created from two 3-carbons molecules in the stage three while two ATP molecules are consumed in the first stage of glycolysis. The produced pyruvate can go to mitochondria and TCA cycle and produce more ATP molecules or they can converted to lactate by lactate dehydrogenase.

In most mammalian cells, glycolysis is inhibited by the presence of oxygen, which allows mitochondria to oxidize pyruvate to CO_2 and H_2O . Conversion of glucose to lactic acid in the presence of oxygen is known as aerobic glycolysis or the 'Warburg effect'. Increased aerobic glycolysis is observed in cancers [Gatenby and Gillies, 2004]. In the astrocytes, taking up glutamate together with Na^+ leads to activating Na^+/K^+ -ATPase pumps for removing extra Na^+ from the cell. This process stimulates glycolysis, glucose utilization and lactate production. So glutamate uptake into astrocytes stimulates aerobic glycolysis which then produced lactate is transported to neurons as a important energy source for brain [Bélanger et al., 2011, Pellerin and Magistretti, 1994]

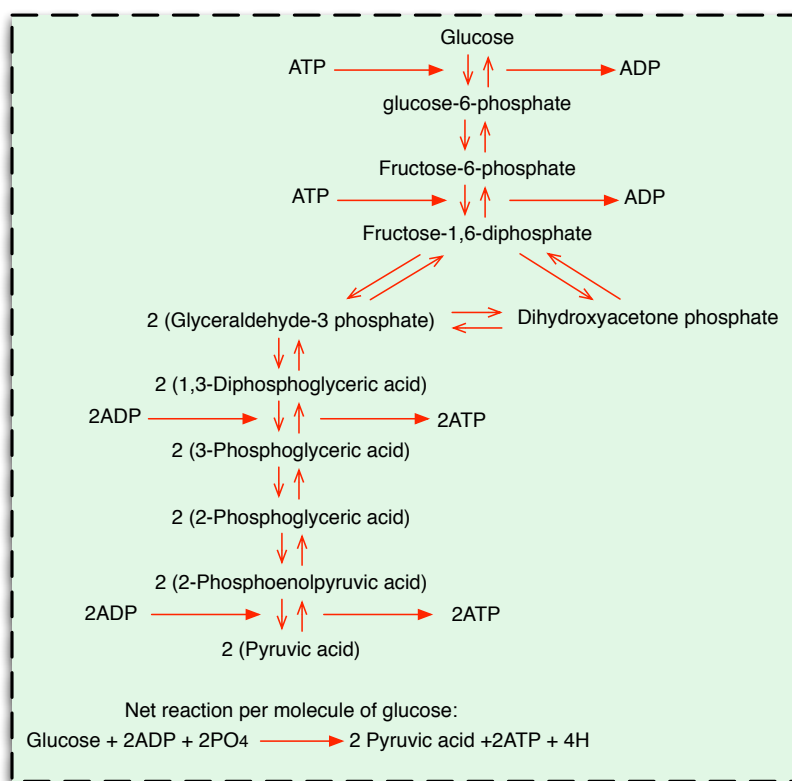


Figure 2.2. Sequence of reactions in the glycolysis process (inspired by [Hall and Guyton, 2006])

2.2.2 Tricarboxylic Acid (TCA) Cycle and Electron Transport Chain (ETC)

The energy production process continues with the mitochondrial reactions of the TCA cycle, which converts phosphoenolpyruvate (PEP) to malate and/or pyruvate in the cytosol. The pyruvate and/or malate are transported into mitochondria through mitochondrial carrier family (MCF). In mitochondria, these acids enter to the TCA cycle. TCA cycle is a series of chemical reactions used by all aerobic organisms to generate energy.

In mitochondria, pyruvate is either converted into acetyl-CoA or into oxaloacetate. Conversion of pyruvate into acetyl-CoA is catalyzed by pyruvate dehydrogenase (PDH). Acetyl-CoA which is a two carbon molecule enters TCA cycle. The TCA cycle includes eight enzymes: citrate synthase, aconitase, isocitrate dehydrogenase, α -ketoglutarate dehydrogenase, succinate thiokinase, succinate dehydrogenase, fumarase, and malate dehydrogenase [Bubber et al., 2005]. During one TCA cycle three molecules of nicotinamide adenine dinucleotide (NAD^+) are converted into NADH and one molecule of flavin adenine dinucleotide (FAD) is converted into FADH_2 and one equivalent each of guanosine diphosphate (GDP) and inorganic phosphate (Pi) into one equivalent of guanosine triphosphate (GTP).

In TCA cycle some carbon molecules enter mitochondria to replenish the TCA cycle intermediates to ensure its continued function. This process is termed anaplerosis. Pyruvate carboxylase, which synthesizes oxalacetate from pyruvate in the mitochondrial matrix, is a anaplerotic enzyme. Also some carbon compounds cannot fully oxidize and must be removed from the cycle by a process termed cataplerosis. Cataplerosis may be linked to biosynthetic processes such as fatty acid synthesis in the liver and gluconeogenesis in the liver and kidney cortex.

The enzymes of TCA cycle are primarily located in the mitochondrial matrix, with the exception of succinate dehydrogenase, which is bound to the inner membrane, forming part of complex II of the electron transport chain. The major regulators of TCA cycle enzymes are ADP and NAD⁺ and calcium. The reduced amount of ADP leads to increasing the production of NADH. Also the high amount of NADH and ATP inhibit dehydrogenases like pyruvate dehydrogenase, isocitrate dehydrogenase, α -ketoglutarate dehydrogenase in TCA cycle. Calcium is another regulator in TCA cycle. It activates pyruvate dehydrogenase, isocitrate dehydrogenase and α -ketoglutarate dehydrogenase. This increases the reaction rate of many of the steps in the cycle, and therefore increases flux throughout the pathway. In the TCA cycle itself, only 2 molecules of ATP are produced: only in one chemical reaction during changing α -ketoglutaric acid to succinic acid. Thus, for each molecule of glucose metabolized, two acetyl-CoA molecules pass through the TCA cycle, each forming a molecule of ATP, or in total two molecules of ATP are formed. Figure 2.3 shows mitochondrial compartments, TCA cycle and electron transport chain.

The mitochondrial ATP production relies on the electron transport chain (ETC), composed of respiratory chain complexes I-IV, which transfer electrons in a stepwise fashion until they finally reduce oxygen to form water. The NADH and FADH₂ formed in glycolysis, fatty-acid oxidation and the citric acid cycle donate their electrons to the ETC. Electrons move toward electron transporting complexes and the energy of electron transport leads to pumping protons to intermembrane space, resulting in a mitochondrial membrane potential of around 150-180 mV. ATP synthase occurs by F₁F₀-ATPase molecule that utilizes the proton motive force to convert ADP and phosphate ATP, thereby coupling electron transport and proton pumping to ATP synthase [Fontanesi, 2001, Bratic and Trifunovic, 2010]. The rate of mitochondrial respiration depends on the phosphorylation potential expressed as a [ATP]/[ADP] [Pi] ratio across the inner mitochondrial membrane that is regulated by the adenine nucleotide translocase (ANT). In the case of increased cellular energy demand when the phosphorylation potential is decreased and more ADP is available, a respiration rate is increased and leads to an increased ATP synthesis [Slater et al., 1973].

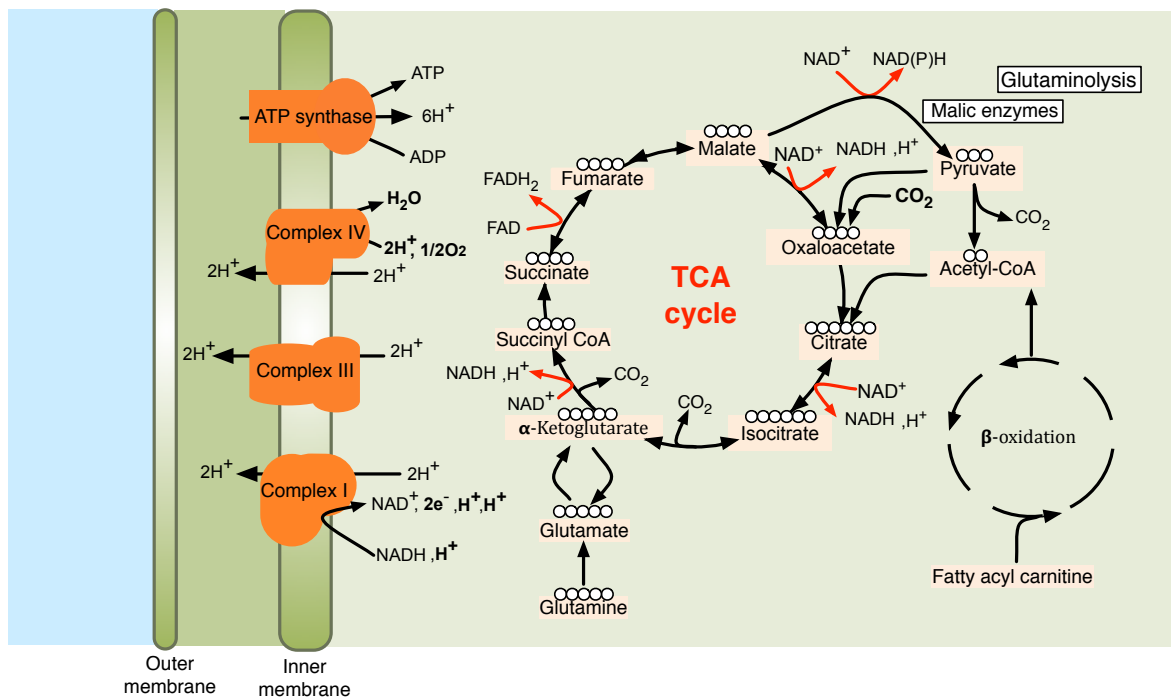


Figure 2.3. Overview of the tricarboxylic acid (TCA) cycle and electron transport chain (ETC) in mitochondria. Mitochondria is responsible for synthesis of most of the ATP in eukaryotic cells by oxidative phosphorylation. In order to produce ATP, cellular substrates go to TCA cycle in the matrix of mitochondria where they goes through a series of chemical transformations and produce electron carrier molecules, three NADH and one FADH₂. These molecules donate their electrons to the ETC. Electrons move toward electron transporting complexes and the energy of electron transport leads to pumping protons to intermembrane space, resulting in a mitochondrial membrane potential. ATP synthase happens by F₁F₀-ATPase molecule that utilizes the proton motive force to convert ADP and phosphate to ATP.

2.2.3 Glycogenesis and Glycogenolysis

Forming glycogen from glucose is called glycogenesis that happens when glucose demand is low. Glycogenolysis is the breakdown of glycogen to glucose-6-phosphate and glycogen. When glucose intake is reduced as during a period of starvation, glycogen is metabolized to release energy substrate in the form of glucose (or glucose-related substrates). In the liver glycogen is break down to glucose when the glucose level in blood decrease and is released into the systemic circulation. In skeletal muscle glycogen has a different function. It is metabolized when energy demand is high to provide ATP to muscles via glycolysis and the produced lactate is released into blood which then can be absorbed by brain or heart as energy source. Thus the dogmatic view is that liver glycogen is used for the benefit of the entire body, whereas skeletal muscle glycogen is used solely by that tissue or by brain.

The brain contains glycogen but at low concentration compared with liver and muscle cells. In the adult brain, glycogen is found predominately in astrocytes. Neurons have two

main sources of neural energy substrates, the first one is direct entry of glucose into neurons from blood vessel and the second source is lactate which is provided by astrocytes. The stored glycogen by astrocytes can be rapidly metabolized, converted to lactate and transported to neurons as efficient energy substrate. Thus, astrocytic storage of glycogen provides a supplemental energy reserve available to neurons when demand is high [Gibbs, 2015].

2.2.4 Glutaminolysis

Glutaminolysis, which catabolizes glutamine to generate ATP and lactate, is a mitochondrial pathway that involves the initial deamination of glutamine (Gln) by glutaminase, yielding glutamate (Glu) and ammonia. Glutamate is then converted via a second deamination step to a TCA cycle intermediate, α -ketoglutarate (α -KG). The conversion of glutamate to α -KG is catalyzed by either glutamate dehydrogenase (GDH) or transaminases, such as glutamate pyruvate transaminases (GPTs, that is, alanine aminotransferases) and glutamate oxaloacetate transaminases (GOTs, that is, aspartate aminotransferase), which convert α -KG acids into their corresponding amino acids. Glutamine not only provides a major substrate for respiration but also for the synthesis of other macromolecules, such as nucleotides, proteins and hexosamines.

Glutamine is transported into the cells through transporters such as SLC1A5 and SLC7A5. Glutaminolysis produces α -KG and replenishes the TCA cycle, which not only provides intermediates for other biosynthetic pathways but also supports energy production. Glutamine becomes conditionally essential when the demand for glutamine surpasses the supply, especially for rapidly proliferating cells such as cancer cells. Cancer cells display enhanced and unusual metabolic activities compared with normal differentiated cells, as they reprogram their metabolic machinery in order to satisfy their bioenergetic and biosynthetic requirements. One of these metabolic abnormalities is that cancer cells take up glucose at higher rates than normal tissue, yet use less glucose for oxidative phosphorylation (OXPHOS) and favor the incomplete oxidation of glucose through the glycolytic pathway even in the presence of oxygen. Pyruvate generated from the glycolytic pathway is converted to lactate, rather than being used in the TCA cycle. Although the requirement for mitochondrial ATP production is decreased in tumor cells, the demand for biosynthetic precursors and NADPH is increased. To compensate for these changes and to maintain a functional TCA cycle, cancer cells often rely on elevated glutaminolysis [Jin et al., 2015].

2.2.5 Regulation of Cellular Metabolism

Organisms and cells have evolved systems to modulate metabolic flux over short and long time scales. Extracellular signals like hormones and growth factors communicate signals

between tissues to regulate metabolic function [Metallo and Vander Heiden, 2013]. Most metabolic reactions are catalyzed by enzymes.

Regulation of cellular metabolism can start from genes that encode several enzymes and followed by transcriptional level that selects which genes are activated and the abundance of enzyme is controlled by mRNA transcription, splicing, mRNA stability and translation. This kind of enzyme regulation takes time from hours to days and are called long-term or coarse regulations. The more rapid adjustment (seconds to minutes) of enzymes also can happen by changing the activity of enzyme which is already present in the cell. This kind of regulation is called short-term or fine regulation. Regulation of enzymes by substrate and product concentration, allosteric regulation and reversible covalent modifications of enzymes are different means for fine regulation of enzymes.

All metabolic reactions are dependent on both the concentration of substrate and product. Since the concentration of many intracellular substrates are in the range of K_M , an increase in substrate concentration causes an increase in enzyme activity which tends to returns the concentration of substrate toward normal. The K_M value is the substrate concentration at which the reaction rate is half of the maximum rate achieved by the system for a given enzyme concentration. Allosteric regulation of enzyme activity is a more precise means for finely controlling cellular metabolism on a short time scale. In allosteric regulation, enzymes are regulated by binding specific ligand at a site other than enzyme's active site which induces conformational change modulating the enzyme's activity. Allosteric enzymes show reaction kinetics that deviate from classical Michaelis-Menten kinetics, changing from hyperbolic to sigmoidal saturation [Wegner et al., 2015].

Understanding the role of Ca^{2+} homeostasis and mitochondrial metabolism in the diseases, requires a mechanistic understanding of the crosstalk between these two systems. In the next section, we will give the background information about the crosstalk between Ca^{2+} signaling and mitochondrial metabolism.

2.3 Crosstalk Between Intracellular Ca^{2+} Signaling and Mitochondrial Metabolism

An early hypothesis about controlling the rate of oxidative phosphorylation was that the feedback of ADP and inorganic phosphate (P_i) from the cytosol to mitochondria determine the rate of ATP production. This hypothesis is based on the economic law of supply and demand where ATP is the currency of energy in biological systems [Gunter et al., 2004]. Today, although we accept the supply and demand process, we know that it is not the usual

2.3. Crosstalk Between Intracellular Ca^{2+} Signaling and Mitochondrial Metabolism

process by which ATP production is controlled. It is found that the metabolic rate and the work performed by the perfused heart and other samples can vary up to a factor of around four without observed changes in ADP, ATP or P_i concentrations [Balaban, 2002]. Therefore something else must act as the metabolic mediator in these circumstances.

The link between Ca^{2+} ions and its regulatory role in cellular metabolic activity has been discovered more than 50 years ago, when Krebs found that phosphorylase kinase becomes highly active in rabbit muscle extracts when incubated for a short period of time with Ca^{2+} ions [Krebs et al., 1959]. Many studies have suggested that increases in cytosolic Ca^{2+} concentration lead to increasing mitochondrial calcium that is important for stimulation oxidative metabolism. The work by Denton and McCormack in the 1980s showed that the activity of pyruvate dehydrogenase (PDH) can increase 3-fold in rat hearts stimulated with adrenaline for 5 minutes. They concluded that the increased activity of PDH is induced by the increase in cytoplasmic Ca^{2+} concentration followed by increasing mitochondrial Ca^{2+} concentration that leads to activation of PDH. This view further is supported by studies that found the effects of adrenaline on pyruvate oxidation and the amount of PDH were greatly diminished in the presence of two agents: verapamil and ionophore A23187 which alter the normal distribution of Ca^{2+} in the perfused heart [Hiraoka et al., 1980, McCormack and England, 1983, McCormack and Denton, 1984, McCormack and Denton, 1981]. It has been proposed that stimulation of hepatocytes with vasopressin evokes increases in cytosolic and mitochondrial Ca^{2+} that increase NAD(P)H production and PDH activity [Robb-Gaspers et al., 1998]. A wide range of studies on isolated enzymes, separated mitochondria and intact cell preparations have shown that the activation of pyruvate dehydrogenase upon increasing cytoplasmic Ca^{2+} is due to the stimulation of pyruvate dehydrogenase phosphatase. In eukaryotes, pyruvate dehydrogenase complex is tightly regulated by its own specific pyruvate dehydrogenase kinase (PDK) and pyruvate dehydrogenase phosphatase (PDP), deactivating and activating it respectively. In mammalian mitochondria, there appears to be two isoforms of pyruvate dehydrogenase phosphatase, PDP1 and PDP2, but calcium ions activate just PDP1 isoform [Denton, 2009].

PDH is not the only intramitochondrial dehydrogenase which is activated by calcium ions. Oxoglutarate dehydrogenase and NAD^+ -isocitrate dehydrogenase are also activated, but in these cases Ca^{2+} acts directly on the enzymes to greatly diminish the K_M values for their respective substrates [Denton et al., 1978, McCormack and Denton, 1979]. Mitochondrial calcium also activates FAD-glycerol phosphate dehydrogenase, which is located on the cytoplasmic surface of the inner membrane of mitochondria [Denton, 2009, Griffiths and Rutter, 2009]. Thus Ca^{2+} stimulates both glycogen breakdown and glucose oxidation leading to increased ATP supply. The effect of calcium ions is to lower the K_M for glycerol phosphate very substantially. In addition, mitochondrial calcium has been suggested to ac-

tivate electron transport chain, adenine nucleotide translocase (ANT) [Gunter et al., 2000] and F1F0 ATP synthase [Territo et al., 2001].

Mitochondria are also a critical component of the cell signaling machinery, via their ability to sense and shape Ca^{2+} signals that control fundamental cellular functions. Measurement of mitochondrial Ca^{2+} concentration in the matrix demonstrated rapid fluctuation of mitochondrial Ca^{2+} upon cell stimulation that is in parallel with cytosolic Ca^{2+} [Rizzuto et al., 1992]. Ca^{2+} can traverse the outer mitochondrial membrane through voltage dependent anion-selective channels (VDAC). The protein mediating the Ca^{2+} transport across the inner mitochondrial membrane is referred as the uniporter channel and has been identified as a Ca^{2+} selective ion channel. Mitochondrial Ca^{2+} uniporter (MCU) channel passes Ca^{2+} along the electrochemical gradient due to the highly negative mitochondrial membrane potential [Hajnóczky et al., 2006]. Thus transport by the MCU is membrane potential dependent and sensitive to ruthenium red or its derivative Ru360 [Gunter and Pfeiffer, 1990]. Ca^{2+} leaves mitochondria in exchange for sodium ions, a process catalyzed by the $\text{Na}^+/\text{Ca}^{2+}$ exchanger (mNCX). The mitochondrial Ca^{2+} uptake and release has numerous effect on Ca^{2+} homeostasis. The shuffling of Ca^{2+} by mitochondria alters the amplitude of Ca^{2+} signals as well as their spatial and temporal dimensions. Modifying any of MCU or mNCX pathways affects the frequency of the oscillations. Increasing the activity of the MCU can both increase and decrease the frequency of oscillations [Wacquier et al., 2016]. In addition to its effect on the frequency of the oscillations, the MCU controls the width of the spikes and the sustainability of the oscillations, as knocking down the MCU broadens Ca^{2+} oscillations and accelerates the rundown of the oscillations in rat basophilic leukemia (RBL)-1 cells [Dupont and Combettes, 2016].

Mitochondria act like a Ca^{2+} buffer and can activate or deactivate plasma membrane channels that are regulated by changes in Ca^{2+} concentrations or restrict Ca^{2+} signals to specific cellular domains. Mitochondria are dynamic organelles that actively move, fuse, and divide within cells. Mitochondria also act like a Ca^{2+} relay that can propagate Ca^{2+} signals and funnel Ca^{2+} inside the cells to reload intracellular Ca^{2+} stores [Demaurex et al., 2009]. Because of their slow dynamics, mitochondria continue releasing Ca^{2+} between subsequent releases of Ca^{2+} from the ER, thus playing a key role in determining the baseline cytosolic Ca^{2+} level [Dupont and Combettes, 2016]. Mitochondria are located in close proximity to the Ca^{2+} channels that elicit the rise in Ca_c , including IP₃R and RYRs on the ER and sarcoplasmic reticulum as well as different classes of channels on the plasma membrane (for example, voltage-operated channels and store-operated channels). Therefore, mitochondria sense a microdomain of high Ca_c that meets the low affinity of the MCU and that dissipates rapidly, thus preventing mitochondrial Ca^{2+} overload. Thereby, mitochondrial Ca^{2+} uptake can profoundly influence cell survival and various functions, such as metabolism, secretion

and signalling [Rizzuto et al., 2012].

After activating different cellular processes, the released Ca^{2+} from internal and external sources should be removed from the cytosol to prevent toxic effects. The $\text{Na}^+/\text{Ca}^{2+}$ exchanger (NCX) and the plasma-membrane Ca^{2+} -ATPase (PMCA) extrude Ca^{2+} to the outside, whereas the SERCA pumps Ca^{2+} back into the ER. In addition to the role of mitochondria as a sensor and regulator of Ca^{2+} signals, mitochondria play significant role in Ca^{2+} homeostasis by producing ATP as a substrate for Ca^{2+} -ATPase pumps and also providing enough energy to keep ion gradients that are maintained with ATP-dependent pumps [Berridge et al., 2003]. Several studies proposed that the metabolic demand created by these ATP-dependent steps in Ca^{2+} homeostasis should increase oxidative phosphorylation in mitochondria and the production of damaging ROS. Although this design helps prevent bioenergetic failure when activity needs to be sustained, it leads to basal mitochondrial oxidative stress. ROS damage mitochondrial proteins such as complex I and mtDNA, reducing the efficiency of oxidative phosphorylation. Over decades, this basal oxidative stress could compromise mitochondrial function and increase mitophagy [Chan et al., 2009, Surmeier et al., 2016].

2.4 Medical Relevance in the Neurodegenerative Diseases

Neurodegenerative diseases are defined by the progressive loss of specific neuronal cell populations and are associated with protein aggregates. In this section, we will describe the role of Ca^{2+} dyshomeostasis and mitochondrial deficiency in the Parkinson's and Alzheimer's diseases.

2.4.1 Parkinson's Disease

Parkinson's disease (PD) is a common neurodegenerative disorder which loss of dopamine (DA) neurons in substantia nigra pars compacta (SNc) cause motor symptoms as indicated by the effective treatment with levodopa (a dopamine precursor). SNc dopaminergic neurons have three features that might link them to their selective vulnerability: 1) they rely on dopamine as a neurotransmitter; 2) they have long axons; 3) they rely on Ca^{2+} and L-type Ca^{2+} channels for making pacemaker that leads to increasing mitochondrial oxidative stress. The reliance on DA and Ca^{2+} and also their long axons is hypothesized to increase DA, cytosolic Ca^{2+} and α -synuclein where these combinations are toxic especially in axon terminals [Surmeier et al., 2016].

The pacemaking property of SNc dopaminergic neurons lead to the generation of action potential in a clockwise manner with 2-10 Hz even in the absence of synaptic input. SNc

dopamine neurons express $\text{Ca}_v1.3$ L-type Ca^{2+} channels, which are open at relatively hyperpolarized potentials, leading to elevated intracellular Ca^{2+} concentration [Ritz et al., 2010]. Because of the existing steep concentration gradient between intra and extra cellular space, the entered Ca^{2+} during pacemaking has to be pumped out by slow membrane transporters. This process requires energy either in the form of ATP or ion gradients that are maintained with ATP-dependent pumps. The ER and mitochondria are partners in Ca^{2+} homeostasis and are two organelles most closely linked to PD. The ER uses SERCA pumps to sequester Ca^{2+} and when it is filled up, the cytosolic Ca^{2+} may trigger RyR and IP_3 receptors which leads to releasing Ca^{2+} from ER. Since ER and mitochondria are in close contact, mitochondria uptake a large amount of Ca^{2+} through MCU into its matrix. Accumulation of Ca^{2+} in the mitochondrial matrix stimulate oxidative phosphorylation and enhance free radical generation.

Stimulating oxidative phosphorylation in the absence of strong ATP demand (that is, most of the time) leads to mitochondrial hyperpolarization and then dissipation of electrochemical gradient by moving back electron flux through the electron transport chain and increased production of reactive oxygen species (ROS) and reactive nitrogen species (RNS) [Surmeier et al., 2016]. ROS damage mitochondrial proteins such as complex I and mtDNA, reducing the efficiency of oxidative phosphorylation. In extreme cases, the stress on mitochondria induces mPTP opening, swelling and the release of cytochrome c and other pro-apoptotic proteins such as apoptosis-inducing factor. ROS also can damage ER proteins and increase the concentration of misfolded proteins. Genetic mutations or environmental toxins are other factors compromising mitochondrial or ER function, rendering them more vulnerable to Ca^{2+} -induced stress [Chan et al., 2009]. This model has been particularly popular to explain the increased vulnerability of SNC DA neurons, since this neuronal population is characterized by a high oxidative burden and a low antioxidant capacity [Exner et al., 2012].

Mitochondrial respiratory complex deficits, disturbed mitochondrial calcium buffering, altered mitochondrial morphology and mitophagy have been seen in PD models. The first evidence for the involvement of mitochondria in PD resulted from the observation that human exposure to 1-methyl-4-phenyl-1, 2, 3, 6 tetrahydropyridine (MPTP) and rotenone, two inhibitors of complex I of the mitochondrial electron transport chain, leads to a PD-like syndrome in humans [Hala et al., 1983]. Changes in the subunits of proteins or function of complex II, III, IV, and V have also been reported in PD [Zhu and Chu, 2010]. In the muscle of PD patients, a reduction in mitochondrial number and disruptions of the mitochondrial membrane are noted [Ahlqvist et al., 1975]. In addition, impairment of mitochondrial calcium buffering in cells enhances the vulnerability of SNC DA neurons to genetic and environmental challenges.

PINK1 mutation also alters the Ca^{2+} buffer capacity of mitochondria and leads to accumulation of Ca^{2+} in mitochondria and respiration reduction [Gandhi et al., 2009, Soman et al., 2016]. Mutations in PINK1 cause autosomal recessive Parkinson's disease. In human PD increased autophagy has been seen [Anglade et al., 1997]. Mitochondrial autophagy (mitophagy) refers to selective sequestration of mitochondria by autophagosomes, which subsequently deliver them to lysosomes for destruction. Elimination of damaged mitochondria protects against cell death, as well as stimulates mitochondrial biogenesis [Thomas and Gustafsson, 2013]. As concerning autophagy, PINK1 and Parkin have been extensively linked to the selective removal of damaged mitochondria through the mitophagy pathway. PINK1 overexpression has been reported to enhance autophagy through interaction with the pro-autophagic protein Beclin1, whereas the opposite was observed upon PINK1 knock-down. Parkin overexpression, in contrast, has been reported to impair autophagy through the stabilization of the autophagy inhibitory protein Bcl-2 [Cieri et al., 2016].

2.4.2 Alzheimer's Disease

Alzheimer's disease (AD), is a chronic and progressive neurodegenerative disorder caused by an increase in amyloid metabolism [LaFerla, 2002]. The progressive impairment of memory and cognition is strongly correlated with death of neurons in the hippocampus and neocortex [Qi and Shuai, 2016]. The series of events underlying the pathogenesis of AD is unknown. The most widely accepted hypothesis is called the amyloid cascade, based on the observation that the brains of AD patients contain high levels of extracellular plaques, composed mainly of amyloid-beta ($\text{A}\beta$), and intracellular tangles, composed of hyperphosphorylated forms of the microtubule-associated protein tau (τ) [Area-Gomez and Schon, 2016]. AD is now known as multiple stage disease where $\text{A}\beta$ and τ dysfunctions are aggravated by oxidative stress, intracellular Ca^{2+} imbalance and metabolic disturbance.

Constant dysregulation in the Ca^{2+} signaling affect health and functionality of neurons over time. Recent studies have linked the accumulation of $\text{A}\beta$ to the Ca^{2+} dysregulation [LaFerla, 2002, Supnet and Bezprozvanny, 2010]. The basis of the Ca^{2+} hypothesis is that abnormal amyloid metabolism results in an upregulation of neuronal Ca^{2+} signaling to induce an initial decline in memory and then progresses to a later phase of apoptosis. One of the major and widely accepted mechanisms of Ca^{2+} dyshomeostasis is $\text{A}\beta$ forms Ca^{2+} -permeable channels on the cell membrane which leads to increase of Ca^{2+} influx to the cell. The β -amyloid peptides, which aggregate to form complexes may enhance entry either directly by forming channels in the membrane or by stimulating pre-existing channels such as the N-Methyl-D-aspartate receptors (NMDARs) and voltage-operated Ca^{2+} channels (VOCCs) as well as store-operated channels (SOCCs). Any Ca^{2+} that enters through these amyloid-dependent mechanisms will contribute to the remodeling of the Ca^{2+} signaling sys-

tem that occurs during AD. [Berridge, 2013].

In addition to Ca^{2+} entry from extracellular space, many studies have shown increasing Ca^{2+} release from ER through IP_3Rs and RyRs with presenilin mutation in the early stage of AD progression, while there are evidences that show $\text{A}\beta$ also affects Ca^{2+} signaling at later disease stages. Disruption of Ca^{2+} regulation in the ER mediates the most significant signal transduction cascades that are associated with Alzheimer's disease. Perturbations in Ca^{2+} signaling pathway are causal factors in excitotoxicity, synaptic degeneration, and cell death, whereas reduced Ca^{2+} release is neuroprotective. Both neuroprotective and pathogenic Ca^{2+} cascades can be triggered sequentially. For example, increasing cellular Ca^{2+} level initially protect cells by activating genes and proteins that promote cell survival like $\text{NF}\kappa\text{B}$ and cAMP while it also can lead to mitochondrial Ca^{2+} overload and produce proapoptotic mitochondrial proteins such as caspases and cytochrome c, which are linked to cell death and neurodegeneration in several AD models [Demuro et al., 2010]. Hence, calcium signaling dyshomeostasis seems to be central to the pathogenesis of Alzheimer's disease and targeting this process might be therapeutically beneficial [LaFerla, 2002].

Mitochondrial dysfunction and oxidative stress also play important role in the early pathology of Alzheimer's disease (AD). There are strong indications that oxidative stress occurs prior to the onset of symptoms in AD and oxidative damage is found not only in the vulnerable regions of the brain affected in disease but also peripherally.

AD is associated with impaired glucose utilization, deficits in mitochondrial activity and metabolic dysfunction. Although the brain represents only 2% of the body weight, it accounts for 20% of total body oxygen consumption. This highly energy demand is continuous and even brief periods of oxygen or glucose deprivation result in neuronal death. Glucose is the primary source of fuel for any energy demanding activity in brain that together with oxygen is delivered by the circulation for the metabolic chores that keep brain cells healthy. When glucose delivery to the brain stops, catastrophic neurological consequences or even death can develop. There is increasing amount of evidence suggesting that insulin present in CNS is a regulator of central glucose metabolism.

Recently, Kim et al. [Kim et al., 2005] reported that low glucose metabolic rate of early onset AD patients is much greater in magnitude and extent than that of late onset patients, though both groups are similar in dementia severity. These abnormalities in cerebral glucose utilization include a diminished activity of key enzymes involved in intermediary metabolism notably the activity of glutamine synthetase, pyruvate dehydrogenase and α -ketoglutarate dehydrogenase [Moreira et al., 2007]. A decreased concentration of acetyl-CoA may decrease the formation of intracellular cholesterol [Michikawa and Yanagisawa, 1999]. Choles-

terol is important for normal cell function. Cholesterol levels are markedly decreased in brain membranes and in the cerebrospinal fluid of AD patients [Moreira et al., 2007].

Swerdlow and Khan proposed that mitochondrial dysfunction is the primary event that cause amyloid-beta (A β) deposition, synaptic degeneration, and NFTs (intracellular neurofibrillary tangles) formation. Patients exhibiting cognitive impairment have shown reduced changes in neuronal TCA cycle rate, glucose oxidation and metabolization into cerebral glutamate and glutamine [Lin et al., 2003]. Furthermore, treatments directed toward overcoming these deficits appear to be beneficial to AD patients. For example, glucose and insulin improves memory in AD patients at least transiently. In the patients with AD, significant decreases were observed in the activities of pyruvate dehydrogenase complex, isocitrate dehydrogenase, and the alpha-ketoglutarate dehydrogenase complex, whereas the activities of succinate dehydrogenase (complex II) and malate dehydrogenase were increased [Bubber et al., 2005].

Another major change associated with AD is the impairment in oxidative phosphorylation (OXPHOS) due to the inhibition of the electron transport chain at complex IV. In agreement with brain studies, complex IV deficiency has been reported in fibroblasts and platelets from AD patients [Bosetti et al., 2002, Cardoso et al., 2004]. Studies in both human cortical neuronal cells and in a transgenic mouse model for AD showed that Amyloid beta precursor protein (plasma membrane protein, which is known to be the source of the toxic amyloid β) accumulates in mitochondria and impairs mitochondrial function inducing a decline in complex IV activity and ATP levels and disruption of mitochondrial membrane potential [Anandatheerthavarada et al., 2003, L Ferreira et al., 2010].

Deficiency of the interplay between Ca $^{2+}$ signaling and mitochondrial metabolism also have been seen in the other neurological diseases such as Leigh syndrome. In the recent study on the patients carrying the mutation in the MT-ATP6 gene for ATP synthase the decrease in the ATP production, high mitochondrial membrane potential and altered mitochondrial and cytosolic Ca $^{2+}$ homeostasis have been observed [Lorenz et al., 2017].

The interaction between intracellular Ca $^{2+}$ signaling and cellular energy metabolism is a complex system since already each subsystem is itself complex. Thus, for dissecting the crosstalk between Ca $^{2+}$ signaling and mitochondrial metabolism, we need a mechanistic representation of the whole system to help us understanding the dynamics of this complex system as depicted by Figure 1.1. For this purpose, we use mathematical modeling which we will describe a background information in the next section.

2.5 Describing Biological Systems by Mathematical Models

Experiments lead to biological hypotheses about individual cellular processes, but it often remains unclear if these hypotheses can be combined into a larger coherent picture because it is often difficult to foresee the global behavior of a complex system from knowledge of its parts. Mathematical modeling and computer simulations can help us to understand the internal nature and dynamics of these processes and to arrive at predictions about their future development as well as the effect of interactions with the environment. A model is an abstract representation of objects or processes that explains their features. A biochemical reaction network can be represented by a graphical sketch showing dots for metabolites and arrows for reactions, the same network could also be described by a system of ordinary differential equations (ODEs), which allows simulating and predicting the dynamic behavior of that network. If a model is used for simulations, it needs to be ensured that it faithfully predicts the system behavior at least those aspects that are supposed to be covered by the model [Klipp et al., 2016].

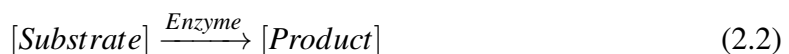
2.5.1 General Biochemical Models

Biochemical signaling ODEs are generally made by combination of mass action equations and Michaelis-Menten approximations for enzyme-catalyzed reactions and other non-linear equations reflecting the molecular dynamics of the system. In the law of mass action, the rate of an elementary reaction (a reaction that proceeds through only one transition state, that is one mechanistic step) is proportional to the product of the concentrations of the participating molecules:



Then rate of C production is (concentration/time): $k^+[A][B]$.

In the Michaelis-Menten equations, the model describes the rate of enzymatic reactions by relating reaction rate to the concentration of a substrate. Its formula is given by:

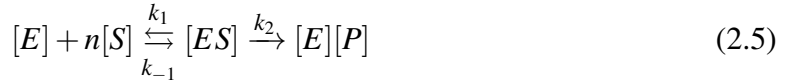


where $[S]$ is concentration of free substrate, $[E]$ is concentration of free enzyme and $[P]$ is the concentration of product. The rate of P production is computed as:

$$\frac{dP}{dt} = \frac{V_{max}[S]}{K_M + [S]} \quad (2.4)$$

where $V_{max} = k_2[E]_{tot}$ is the maximum rate achieved by the system at saturating substrate concentration, k_2 is catalytic constant of enzyme and $K_M = \frac{k_{-1}+k_2}{k_1}$ is the substrate concentration at which the reaction rate is half of the V_{max} .

Sometimes several substrates need to bind the enzyme for the enzymatic reaction to take place. When this is the case, the enzymatic reaction is said to be cooperative.



where ES represents the enzyme-n-substrates complex and n is called the cooperativity coefficient. Then the first order nonlinear ODE model is obtained by the following Hill equation:

$$\frac{dP}{dt} = \frac{V_{max}[S]^n}{K_M + [S]^n} \quad (2.6)$$

where $V_{max} = nk_2[E]_{tot}$ and $K_M = \frac{k_{-1}+k_2}{k_1}$.

Periodic behaviors are very important in biology, appearing in diverse areas such as neural signaling, circadian rhythms, calcium signaling, etc. It is possible to simulate periodic behaviors by linear ODE models of order 2, but they are fragile or non-robust to small perturbations in the model and also their oscillation characteristics depend on the initial condition. Thus, biological systems which exhibit periodic behavior are modeled by nonlinear ODEs which create limit cycles. A limit cycle is an isolated closed trajectory. Isolated means that neighboring trajectories are not closed; they spiral toward or away from the limit cycle. Stable limit cycles are robust meaning that: first, if a small perturbation moves the state to a different initial state away from the cycle, the system will return to the cycle by itself and second, If the dynamics change a little (e.g., small perturbation), the limit cycle will still exist, close to the original one. Limit cycles are inherently nonlinear phenomena and they cannot occur in linear systems, therefore we model calcium oscillation by nonlinear ODEs that reflect known molecular mechanisms.

2.5.2 Modeling Calcium Oscillations with ODEs

Several models have been proposed for simulating the calcium signal oscillation with ordinary differential equations. In 1990, Goldbeter suggested a minimal model for Ca^{2+} oscillation based on Ca^{2+} -induced Ca^{2+} release from intracellular stores that demonstrates how IP_3 molecules activated by external stimulation can develop sustain Ca^{2+} oscillations. In the Goldbeter model, with opening IP_3 -sensitive Ca^{2+} channels on the intracellular stores a certain amount of Ca^{2+} release that in turn triggers Ca^{2+} release from a second Ca^{2+} store

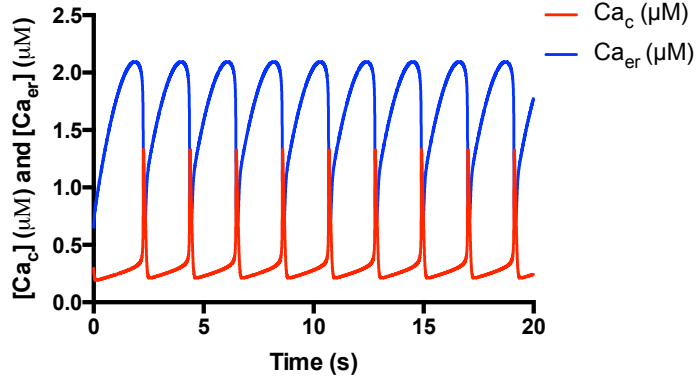


Figure 2.4. Calcium oscillation in cytosol and ER, simulated by the Goldbeter model.

that is not sensitive to IP_3 . In this model, two variables are considered, the concentration of free Ca^{2+} in the cytosol and the Ca^{2+} concentration in the ER/SR, denoted by Z and Y , respectively:

$$\frac{dZ}{dt} = v_0 + v_1\beta - v_2 + v_3 + k_fY - kZ \quad (2.7)$$

$$\frac{dY}{dt} = v_2 - v_3 - k_fY \quad (2.8)$$

where v_0 reflects Ca^{2+} leakage from extracellular space into the cytosol, kZ is Ca^{2+} efflux out of the cell. $v_1\beta$ is Ca^{2+} influx from IP_3 -sensitive pool that is proportional to the IP_3 concentration. When the cell receives an external signal, this triggers an increase in $[\text{IP}_3]$, which leads to a rise in the saturation function β and, subsequently, to an increase in the cytosolic Ca^{2+} concentration. v_2 denotes the rate of pumping Ca^{2+} into the ER/SR by SERCA pump and v_3 refers to the rate of Ca^{2+} transport from ER/SR into the cytosol.

$$v_2 = V_{m_2} \frac{Z^n}{K_2^n + Z^n} \quad (2.9)$$

$$v_3 = V_{m_3} \frac{Y^m}{K_R^m + Y^m} \cdot \frac{Z^p}{K_A^p + Z^p} \quad (2.10)$$

where V_{m_2} and V_{m_3} are maximum rates of Ca^{2+} pumping into and Ca^{2+} releasing from the intracellular store. K_2 , K_R , and K_A are threshold constants for pumping, release, and activation. These equations exhibit nonlinearity and therefore can describe the intracellular Ca^{2+} oscillation. But they don't consider the stochasticity of IP_3 Rs channels and the random behavior of IP_3 Rs. The defined parameter values for Ca^{2+} oscillation in physiological range are: $v_0 = 1 \mu\text{s}^{-1}$, $k = 10 \text{s}^{-1}$, $k_f = 1 \text{s}^{-1}$, $v_1 = 7.3 \mu\text{s}^{-1}$, $V_{m_2} = 65 \mu\text{s}^{-1}$, $V_{m_3} = 500 \mu\text{s}^{-1}$, $K_2 = 1 \mu\text{M}$, $K_R = 2 \mu\text{M}$, $K_A = 0.9 \mu\text{M}$, $m = n = 2$ and $p = 4$ [Goldbeter et al., 1990].

2.6 Summary

Ca^{2+} is a universal intracellular messenger that regulates many cellular processes. Because of its involvement in nearly every aspect of cellular life, Ca^{2+} is under very tight homeostatic control. Expression of different signaling components and the self-assessment system in the Ca^{2+} signaling toolkit make this signaling system robust to small perturbations. In this chapter, we provided a background information about the Ca^{2+} signaling toolkit. We described the role of different Ca^{2+} channels, proteins, ER and mitochondria in Ca^{2+} homesostasis. Ca^{2+} dysregulation affects health and functionality of neurons and may cause neurodegenerative diseases like Parkinson's and Alzheimer's diseases. Ca^{2+} signaling is not independent of energy metabolism. Mitochondria, the main source of ATP production in the cell works also as component for buffering and shaping Ca^{2+} signals. Mitochondria not only act as local calcium buffers, but also respond to calcium uptake by upregulating the TCA cycle, thus reacting metabolically to local signaling. Mitochondrial dysfunction also can lead to neurodegenerative diseases since neurons are highly energy demanding.

Chapter 3

Material and Methods

This chapter explains our developed model for the interplay between Ca^{2+} signaling and mitochondrial metabolism. Then we validate our model by performing parameter scan and comparing the results with the published experimental and modeling results. Section 3.2 provides a background information about HEK293 and C8-D1A cell lines that are used in our experiments. Section 3.3 explains the setup of experiments, medium composition and protocols for each experiment. Then the methods of calcium imaging experiments and measurement of extracellular metabolites are explained. We also describe how intracellular ADP/ATP ratio is measured. Finally, we explain the used statistics methods for analyzing experimental results.

3.1 Developed Model for the Crosstalk of Ca^{2+} Signaling and Mitochondrial Metabolism

The ER is a major store of calcium inside the cell and in most of the cells oscillatory changes in free cytosolic calcium concentration result from the periodic release of calcium from ER. Upon stimulation of GPCRs on the cell membrane, the PLC enzyme is activated. PLC induces formation of IP_3 second messenger. Binding IP_3 and Ca^{2+} to an IP_3Rs channels on the ER/SR membrane make them open and Ca^{2+} enters the cytosol due to the large concentration gradients between the two compartments. Released cytosolic Ca^{2+} makes a positive feedback on IP_3Rs at low Ca^{2+} concentration leading to propagation of the Ca^{2+} signal in form of a global Ca^{2+} wave. This mechanism is called Ca^{2+} - induced Ca^{2+} release (CICR). After performing its signaling functions, the released Ca^{2+} is removed from the cytoplasm by various pumps and exchangers. Since this process is against the ion concentration gradient, it needs the energy which is stored in ATP. Ca^{2+} is extruded to the outside of the cell through the PMCA pumps and is pumped back into the ER through the SERCA pumps.

Hence, ATP which is mainly produced by mitochondria plays a vital role in Ca^{2+} homeostasis. In most eukaryotic cells, mitochondria play an important role in ATP production and act as Ca^{2+} stores, both functions of these organelles are tightly connected. Mitochondria sequester and release Ca^{2+} , thereby affecting the shape, the frequency and the amplitude of the Ca^{2+} spikes in the cytosol. In turn, increased mitochondrial Ca^{2+} stimulates mitochondrial metabolism and allows the coupling of ATP supply with energy demand. The ER and mitochondria are partners in calcium homeostasis. They not only buffer calcium, but also increase cell metabolism activity. Any perturbation in ER function or mitochondrial function leads to calcium dyshomeostasis and will have profound implications for cell function.

Several models have been proposed for modeling Ca^{2+} dynamics, but most of them neglect mitochondria although it is an effective organelle which can shape spatio-temporal properties of Ca^{2+} signals [Goldbeter et al., 1990, De Young and Keizer, 1992, Li et al., 1994]. Many do also not consider Ca^{2+} signaling as an energy demanding process and they don't take into account the ATP consumption of SERCA and PMCA pumps [Bertram and Arceo II, 2008, Fall and Keizer, 2001]. Thus, most of the existing Ca^{2+} and mitochondrial models do not focus on the crosstalk between Ca^{2+} signaling and mitochondrial metabolism.

3.1.1 Model Implementation

Here we extend the previous studies to propose a mathematical model which can simulate the crosstalk between calcium signaling and mitochondrial metabolism in the electrically non-excitable cell. Thus we integrate a well-established model of IP_3 -mediated Ca^{2+} signaling with a simplified model of mitochondrial Ca^{2+} handling and metabolic function. The model consists of three compartments: Cytosol (c), ER (er) and mitochondria (m). With this model, we are able to address the open questions such as: how mitochondrial carbon inputs and cytosolic ATP affect Ca^{2+} dynamics and how the activity of mitochondrial Ca^{2+} channels, IP_3Rs channels and SERCA pumps change the frequency of Ca^{2+} signals. Our model is a simple and is mainly built by combination of previously published kinetic expressions. We built a new Ca^{2+} signaling model and combined it to the Bertram mitochondrial model which is a simplified version of Magnus and Keizer model, developed for modeling of oxidative phosphorylation [Bertram et al., 2006]. Figure 3.1 shows the components and variables which are defined in the mitochondrial-calcium model.

All fluxes that are considered in the model are shown in Figure 3.2. Concentrations are described by ordinary differential equations. Since we neglect the spatial scale, thus all fluxes are averages on the volume of a given intracellular compartment. The model is defined by 7 ordinary differential equations, 16 fluxes, 3 conservation relations and 40 parameters.

Ordinary differential equations:

3.1. Developed Model for the Crosstalk of Ca^{2+} Signaling and Mitochondrial Metabolism

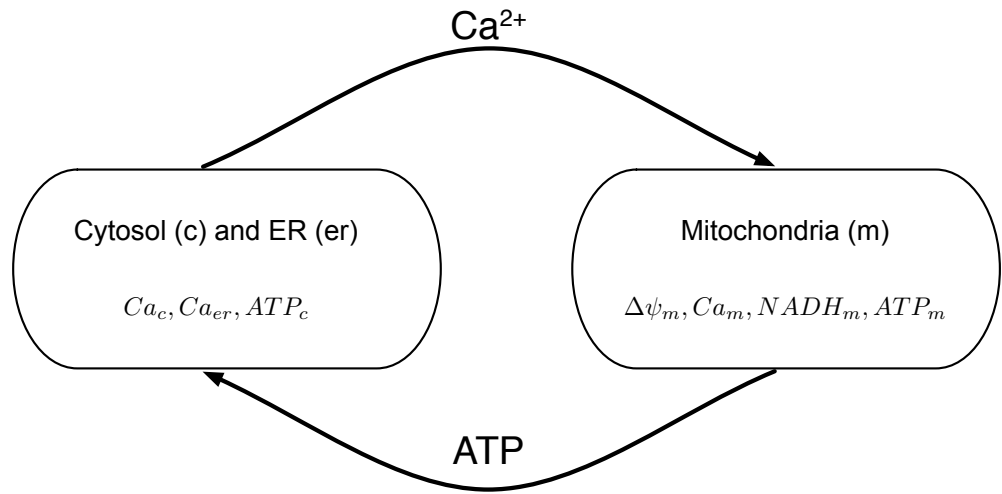


Figure 3.1. Illustration of the two model components. Calcium which is the output of the cytosol and ER component is the input of mitochondrial model component and the by mitochondria produced ATP is the input of cytosol/ER component.

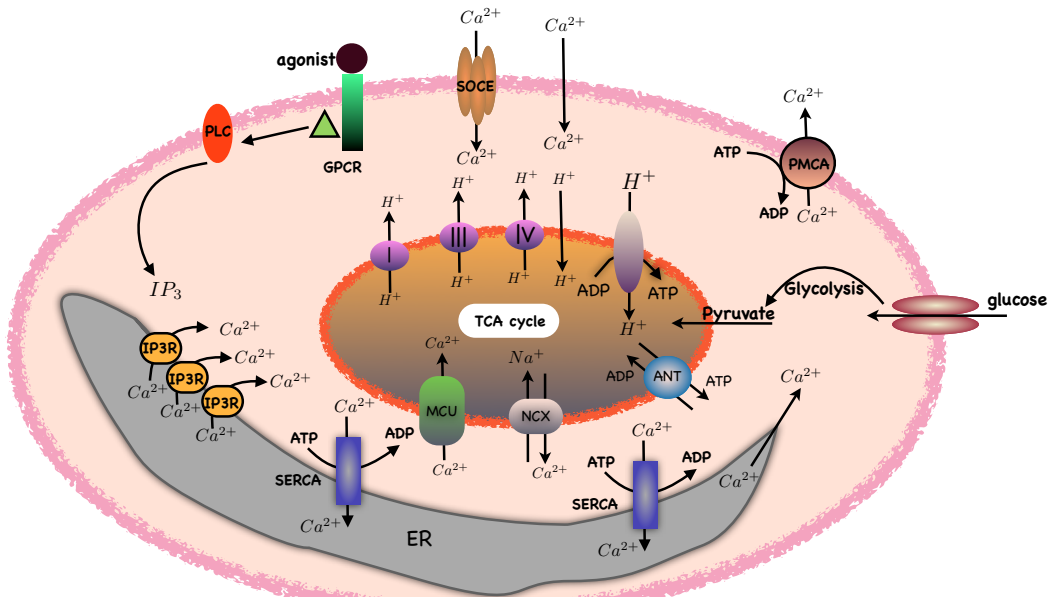


Figure 3.2. Schematic representation of the calcium-mitochondrial metabolism model. Binding an agonist to GPCRs forms IP₃ molecules. Binding IP₃ and Ca^{2+} to IP₃Rs channels increases their open probability and leads to leaking Ca^{2+} from ER into the cytosol. We considered other Ca^{2+} influxes from extracellular space through SOCE channel and also Ca^{2+} leakage from extracellular space. Ca^{2+} also can leak into the cytosol from the ER because of the large Ca^{2+} concentration gradient. By increasing cytosolic Ca^{2+} concentration, mitochondria uptake a large amount of Ca^{2+} which subsequently leads to activating enzymes in TCA cycle and producing NADH. NADH molecules loose their electrons during ETC and produce enough force for converting ADP to ATP. Produced ATP by mitochondria is translocated into the cytosol through ADP/ATP translocator (ANT) and is partly used by SERCA and PMCA pumps for regulating Ca^{2+} signals inside the cell.

- Dynamics of cytosolic Ca^{2+} concentration:

$$\frac{dC_{a_c}}{dt} = f_{cyt} \left(J_{ext} + v_{m/c} (J_{NCX} - J_{MCU}) - J_{SERCA} + J_{release} + J_{leak,er} - J_{PMCA} \right) \quad (3.1)$$

where f_{cyt} is the fraction of free cytosolic Ca^{2+} and $v_{m/c}$ is mitochondria to cytosol volume ratio. J_{ext} and $J_{leak,er}$ are Ca^{2+} influx from extracellular space and Ca^{2+} leakage from ER into the cytosol, respectively. $J_{release}$ denotes to Ca^{2+} releasing from the ER and J_{SERCA} is the Ca^{2+} flux into the ER by SERCA pumps. J_{PMCA} is the efflux of Ca^{2+} across the cell membrane through plasma membrane Ca^{2+} -ATPase pumps. Since mitochondria act as Ca^{2+} buffer and can shape cytosolic Ca^{2+} signals, Ca^{2+} release from mitochondria into the cytosol through $\text{Na}^+/\text{Ca}^{2+}$ channel (J_{NCX}) and Ca^{2+} uptake into the mitochondria through mitochondrial Ca^{2+} uniporter channels (J_{MCU}) are considered in the equation of cytosolic Ca^{2+} .

- ER Ca^{2+} concentration:

$$\frac{dC_{a_{er}}}{dt} = f_{er} v_{c/er} \left(J_{SERCA} - J_{release} - J_{leak,er} \right) \quad (3.2)$$

where f_{er} is the fraction of free Ca^{2+} in ER compartment. $v_{c/er}$ is cytosolic to ER volume ratio. ER Ca^{2+} concentration increases by pumping Ca^{2+} through SERCA pumps and decreases by releasing Ca^{2+} from IP_3 Rs and also Ca^{2+} leakage from ER.

- Mitochondrial Ca^{2+} concentration:

$$\frac{dC_{a_m}}{dt} = f_m (J_{MCU} - J_{NCX}) \quad (3.3)$$

where f_m is the fraction of free Ca^{2+} in mitochondrion compartment. Mitochondrial Ca^{2+} concentration increases by uptaking Ca^{2+} through MCU channels and decreases by Ca^{2+} efflux through NCX channels.

- Cytosolic ADP concentration:

$$\frac{dADP_c}{dt} = -v_{m/c} J_{ANT} + J_{hyd,bas} + 2J_{PMCA} + J_{SERCA} \quad (3.4)$$

where J_{ANT} indicates the nucleotide transport flux through adenine nucleotide translocases (ANT) which transport produced mitochondrial ATP into the cytosol and also move ADP from cytosol into the matrix of mitochondria. $J_{hyd,bas}$ is the basal rate of ATP consumption by sources of hydrolysis other than SERCA and PMCA pumps in the cell. SERCA pumps two Ca^{2+} and PMCA pumps one Ca^{2+} per ATP hydrolyzed [Clapham, 1995]. In contrast to the most existing models, we considered the ATP consumption of SERCA and PMCA pumps as one source of ATP hydrolysis and these expressions link Ca^{2+} signaling to energy metabolism.

- Mitochondrial NADH concentration:

$$\frac{dNADH_m}{dt} = \gamma (J_{PDH} - J_o). \quad (3.5)$$

3.1. Developed Model for the Crosstalk of Ca^{2+} Signaling and Mitochondrial Metabolism

This equation is adapted from [Bertram and Arceo II, 2008]. J_{PDH} represents the reaction rate for the sum of the dehydrogenases in TCA cycle that is proportional to the reaction rate of pyruvate dehydrogenase complex (PDH). Pyruvate, the main product of glycolysis process is rapidly oxidized and decarboxylated by the PDH in mitochondria. This reaction produces acetyl coenzyme A (acetyl CoA) that enters the citric acid cycle, where more NADH is produced by additional dehydrogenases. J_o is the rate of oxygen consumption in the electron transport chain (ETC) where NADH is converted to NAD^+ and oxygen is consumed. The scaling parameter $\gamma = 0.001$ converts NADH_m to units of mM.

- Mitochondrial ADP concentration:

$$\frac{dADP_m}{dt} = \gamma(J_{ANT} - J_{F_1F_0}) \quad (3.6)$$

ADP (with mM unit) inside mitochondrial increases by the rate of nucleotide transporter (J_{ANT}) and decreases by the rate of ATP synthase ($J_{F_1F_0}$), both in unit $\mu\text{M} \cdot \text{ms}^{-1}$. The scaling parameter $\gamma = 0.001$ converts ADP_m to units of mM. This equation is adapted from [Bertram and Arceo II, 2008].

- Mitochondrial membrane potential:

$$\frac{d\Delta\Psi}{dt} = (J_{H,res} - J_{H,atp} - J_{ANT} - J_{H,leak} - J_{NaCa} - 2J_{uni}) / C_m \quad (3.7)$$

where $J_{H,res}$ is the proton ejection from the matrix into the outer chamber between inner and outer mitochondrial membranes which creates positive charge in this chamber and negative electrical charge in the matrix. $J_{H,atp}$ is the proton influx thorough the ATP synthesis and $J_{H,leak}$ is the proton leak into the matrix. Mitochondrial $\text{Na}^+/\text{Ca}^{2+}$ exchanger (NCX) that extrude two Ca^{2+} from mitochondrial matrix and import 3 Na^+ in exchange, creates one negative electrical charge in matrix. This equation is taken from [Bertram and Arceo II, 2008]. C_m represents mitochondrial inner membrane capacitance divided by Faraday constant. $\Delta\psi$ has units of mV.

In addition to the differential equations related to the calcium and ADP dynamics, we also considered three conservation equations, taken from [Bertram et al., 2007]:

- Conservation of total mitochondrial nicotinamide adenine dinucleotide:

$$\text{NAD}_m + \text{NADH}_m = \text{NAD}_{m,tot} \quad (3.8)$$

- Conservation of total mitochondrial adenine nucleotides:

$$ADP_m + ATP_m = A_{m,tot} \quad (3.9)$$

- Conservation of total cytosolic adenine nucleotides:

$$ADP_m + ATP_m = A_{c,tot} \quad (3.10)$$

Expressions for fluxes: We explained the ODEs and conservation equations and now we will explain the expression of the fluxes in the ODEs. Equations 3.11 to 3.19 are taken from Bertram mitochondrial model [Bertram and Arceo II, 2008] which are the modified and simplified form of expressions of the Magnus and Keizer mitochondrial model in the pancreatic β -cell [Magnus and Keizer, 1997, Magnus and Keizer, 1998, Magnus and Keizer, 1998]. Equations 3.20 to 3.26 are built in this work based on the molecular dynamics of channels which are known from experimental observations in previously published literatures.

- Bertram et al. considered the activity of glyceraldehyde 3-phosphate dehydrogenase (GPDH) as the input of PDH rather than pyruvate concentration since its reaction rate reflects the flux through the glycolytic pathway. In the equilibrium state the GPDH reaction rate can be described by an algebraic function of the substrate fructose 1,6-bisphosphate (FBP) [Bertram et al., 2007]. In our model FBP is considered as the mitochondrial carbon input instead of pyruvate and is a constant parameter:

$$J_{GPDH} = K_{GPDH} \sqrt{FBP/(1\mu M)} \quad (3.11)$$

- The pyruvate dehydrogenase flux J_{PDH} is linearly dependent to the flux of GPDH, which reflect the rate of glycolysis and pyruvate production. J_{PDH} increases by increasing mitochondrial Ca^{2+} concentration and decreasing $NAD_m/NADH_m$ ratio:

$$J_{PDH} = \left(\frac{p_1}{p_2 + NADH_m/NAD_m} \right) \left(\frac{Ca_m}{p_3 + Ca_m} \right) J_{GPDH} \quad (3.12)$$

- The oxygen consumption flux (J_o) increases with $NADH_m$ concentration since they are electron carrier molecules and donate their electrons. Increasing mitochondrial membrane potential ($\Delta\psi$) decreases the J_o , since it is more difficult to pump protons against a large potential:

$$J_o = \left(\frac{p_4 NADH_m}{p_5 + NADH_m} \right) \left(\frac{1}{1 + \exp((\Delta\psi - p_6)/p_7)} \right) \quad (3.13)$$

- $J_{H,res}$ is the flux of proton ejection to the inner mitochondrial space which increases with $NADH_m$ concentration since NADH oxidation provides driving force for proton ejection. $J_{H,res}$ decreases with increasing $\Delta\psi$, since it is more difficult to pump protons against a large potential:

$$J_{H,res} = \left(\frac{p_8 NADH_m}{p_9 + NADH_m} \right) \left(\frac{1}{1 + \exp((\Delta\psi - p_{10})/p_{11})} \right) \quad (3.14)$$

- $J_{H,atp}$ is the flux of proton flow into the matrix though the F_1F_0 ATP synthase which has an increasing sigmoidal dependence on $\Delta\psi$ and a weak decreasing dependence on ATPm, since increasing mitochondrial ATP concentration decreases rate of respiration:

$$J_{H,atp} = \left(\frac{p_{13}}{p_{13} + ATP_m} \right) \left(\frac{p_{12}}{1 + \exp((p_{14} - \Delta\psi)/p_{15})} \right) \quad (3.15)$$

3.1. Developed Model for the Crosstalk of Ca^{2+} Signaling and Mitochondrial Metabolism

- $J_{H,F1F0}$ is the flux of ADP phosphorylation. Because $J_{H,F1F0}$ is determined by the proton flux through the F_1F_0 ATP synthase, its expression is similar to that of $J_{H,atp}$. In fact, $J_{H,F1F0}$ is a constant multiple of $J_{H,atp}$:

$$J_{H,F1F0} = \left(\frac{p_{13}}{p_{13} + ATP_m} \right) \left(\frac{p_{16}}{1 + \exp((p_{14} - \Delta\psi)/p_{15})} \right) \quad (3.16)$$

- $J_{H,leak}$ is the flux of proton leakage from inner mitochondrial space into the matrix which is larger for larger values of the electrical potential:

$$J_{H,leak} = p_{17}\Delta\psi + p_{18} \quad (3.17)$$

- J_{ANT} is the flux of exchanging mitochondrial ATP with cytosolic ADP through adenine nucleotide translocator (ANT). This is a carrier that exchanges one molecule of mitochondrial ATP^{4-} and for one molecule of cytosolic ADP^{3-} . It tends to keep the ATP/ADP ratio in the cytosol equal to that in the mitochondria. $FRT = F/RT$, where R is the gas constant, T is the temperature in Kelvin, and F is Faraday's constant:

$$J_{ANT} = p_{19} \left(\frac{RAT_m}{RAT_m + p_{20}} \right) e^{0.5FRT\Delta\psi} \quad (3.18)$$

- RAT_m indicates mitochondrial ATP to ADP ratio:

$$RAT_m = \frac{ATP_m}{ADP_m} \quad (3.19)$$

The following equations express Ca^{2+} fluxes in the cytosol, ER and mitochondria and are made from combination of expressions in published papers:

- J_{MCU} expresses Ca^{2+} uptake by mitochondrial Ca^{2+} uniporter (MCU) which increases with increasing cytosolic Ca^{2+} concentration and also with mitochondrial membrane potential [Gunter et al., 1994]:

$$J_{MCU} = P_{MCU} (p_{21} \frac{Ca_c^2}{p_{22}^2 + Ca_c^2} e^{0.0016\Delta\Psi}) \quad (3.20)$$

- J_{NCX} is the Ca^{2+} efflux from and Na^+ influx into the mitochondria. The $\text{Na}^+/\text{Ca}^{2+}$ exchanger exchanges 3 Na^+ with one Ca^{2+} and therefore leads to one inward flow of positive charge into the mitochondria. In this equation, we did not consider any dependency on Na^+ concentration as we assumed it to be constant. J_{NCX} increases with increasing $\Delta\psi$ and Ca_m and decreases when Ca_c is increasing:

$$J_{NCX} = P_{NCX} \left(p_{23} \left(\frac{Ca_m}{Ca_m + p_{24}} \right) \left(\frac{p_{25}^2}{p_{26}^2 + Ca_c^2} \right) e^{p_{27}\Delta\Psi} \right) \quad (3.21)$$

- J_{serca} is the SERCA pump flux which consumes one mole ATP for pumping two moles Ca^{2+} , since movement against Ca^{2+} concentration gradient. J_{serca} increases with increasing cytosolic Ca^{2+} and cytosolic ATP:

$$J_{serca} = p_{28} \left(\frac{Ca_c^2}{p_{29}^2 + Ca_c^2} \right) \left(\frac{ATP_c}{p_{30} + ATP_c} \right) \quad (3.22)$$

- $J_{release}$ is Ca^{2+} releasing flux from ER through IP_3R channels. $J_{release}$ has bell-shape dependency on cytosolic Ca^{2+} . At low cytosolic Ca^{2+} concentration, $J_{release}$ increases with increasing Ca_c because of CICR mechanism which is due to the positive feedback of Ca^{2+} on the IP_3R channels. By further increasing Ca_c , calcium has negative feedback on the IP_3Rs and leads to closing them. Increasing IP_3 increases open probability of IP_3Rs :

$$J_{release} = p_{31} \left(\frac{ip_3^2}{p_{32}^2 + ip_3^2} \right) \left(\frac{Ca_c^2}{p_{33}^2 + Ca_c^2} \right) \left(\frac{p_{34}^4}{p_{35}^4 + Ca_c^4} \right) (Ca_{er} - Ca_c) \quad (3.23)$$

- J_{pmca} is the flux of Ca^{2+} pump to the extracellular space through plasma membrane Ca^{2+} -ATPase channels which consume one mole ATP for pumping one mole Ca^{2+} since they move calcium ions against the concentration gradient:

$$J_{pmca} = p_{36} \left(\frac{Ca_c^2}{p_{37}^2 + Ca_c^2} \right) \left(\frac{ATP_c^2}{p_{38}^2 + ATP_c^2} \right) \quad (3.24)$$

- J_{ext} is combination of Ca^{2+} leakage from extracellular space into the cytosol and also Ca^{2+} entry through store-operated calcium (SOC) channels. Increasing cytosolic Ca^{2+} concentration decreases the Ca^{2+} leakage flux from extracellular space. Ca^{2+} entry from SOC channels decreases when Ca^{2+} concentration inside the ER rises:

$$J_{ext} = J_{ext,base} - p_{39}Ca_{er} - p_{40}Ca_c \quad (3.25)$$

- $J_{leak,er}$ indicates Ca^{2+} leakage from ER into the cytosol which happens because of large Ca^{2+} concentration gradient between cytosol and ER:

$$J_{leak,er} = p_{41} (Ca_{er} - Ca_c) \quad (3.26)$$

- $J_{hyd,base}$ is the basal rate of ATP consumption by sources of hydrolysis other than SERCA and PMCA pumps in the cell [Bertram et al., 2007]:

$$J_{hyd,base} = K_{hyd,base} ATP_c \quad (3.27)$$

The parameter values are presented in Table 3.1. For the equations taken from the Bertram model, also the parameters and conservation assumptions are kept [Bertram et al., 2007]. For the developed equations for the Ca^{2+} model (3.20 to 3.26), the parameter values

3.1. Developed Model for the Crosstalk of Ca^{2+} Signaling and Mitochondrial Metabolism

$p_1 = 400$	$p_2 = 1$	$p_3 = 0.06 \mu\text{M}$
$p_4 = 0.6 \mu\text{Mms}^{-1}$	$p_5 = 0.1 \text{ mM}$	$p_6 = 177 \text{ mV}$
$p_7 = 5 \text{ mV}$	$p_8 = 7 \mu\text{Mms}^{-1}$	$p_9 = 0.1 \text{ mM}$
$p_{10} = 177 \text{ mV}$	$p_{11} = 5 \text{ mV}$	$p_{12} = 120 \mu\text{Mms}^{-1}$
$p_{13} = 10 \text{ mM}$	$p_{14} = 190 \text{ mV}$	$p_{15} = 8.5 \text{ mV}$
$p_{16} = 35 \mu\text{Mms}^{-1}$	$p_{17} = 0.002 \mu\text{Mms}^{-1}\text{mV}^{-1}$	$p_{18} = -0.03 \mu\text{Mms}^{-1}$
$p_{19} = 35 \mu\text{Mms}^{-1}$	$p_{20} = 2$	$\text{FRT} = 0.037 \text{ mV}^{-1}$
$p_{21} = 0.1 \mu\text{Mms}^{-1}$	$p_{22} = 1 \mu\text{M}$	$p_{23} = 0.3 \mu\text{Mms}^{-1}$
$p_{24} = 0.6 \mu\text{M}$	$p_{25} = 1 \mu\text{M}$	$p_{26} = 10 \mu\text{M}$
$p_{27} = 0.016 \text{ mV}^{-1}$	$p_{28} = 0.455 \mu\text{Mms}^{-1}$	$p_{29} = 1 \mu\text{M}$
$p_{30} = 60 \mu\text{M}$	$p_{31} = 0.02 \mu\text{Mms}^{-1}$	$p_{32} = 0.5 \mu\text{M}$
$p_{33} = 0.9 \mu\text{M}$	$p_{34} = 1.3 \mu\text{M}$	$p_{35} = 1.3 \mu\text{M}$
$p_{36} = 0.01 \mu\text{Mms}^{-1}$	$p_{37} = 0.7 \mu\text{M}$	$p_{38} = 5 \mu\text{M}$
$p_{39} = 3 \times 10^{-6} \text{ ms}^{-1}$	$p_{40} = 15 \times 10^{-6} \text{ ms}^{-1}$	$p_{41} = 0.001 \text{ ms}^{-1}$
$J_{\text{ext,base}} = 0.0035 \mu\text{Mms}^{-1}$	$f_{\text{cyt}} = 0.015$	$f_{\text{er}} = 0.03$
$v_{\text{er}} = 1$	$v_c = 3$	$\text{FBP} = 5 \mu\text{M}$
$C_m = 1.8 \mu\text{MmV}^{-1}$	$f_m = 0.01$	$K_{\text{GPDH}} = 5 \times 10^{-4} \mu\text{Mms}^{-1}$
$\text{NAD}_{\text{m,tot}} = 10 \text{ mM}$	$A_{\text{m,tot}} = 15 \text{ mM}$	$A_{\text{m,tot}} = 3000 \mu\text{M}$
$\text{IP}_3 = 0.3 \mu\text{M}$	$K_{\text{hyd,base}} = 0.003 \text{ ms}^{-1}$	$P_{\text{MCU}} = 1$
$P_{\text{NCX}} = 1$	$V_{\text{m/c}} = 0.07$	

Table 3.1. Parameter values of model

are obtained by performing parameter scan with the goal that variables sweeps in the physiological range with the objective of oscillating Ca^{2+} concentrations and in accordance to the experimental observation. The full system of equations are solved with the Euler's method and are simulated using C++ language.

Figure 3.3 exhibits the Ca^{2+} dynamics in the cytosol, the ER and mitochondria as well as the dynamics of mitochondrial variables. Mitochondrial Ca^{2+} increases with increasing cytosolic Ca^{2+} concentration due to J_{MCU} flux. Mitochondria sequester cytosolic Ca^{2+} rapidly when $[\text{Ca}_c]$ increases and release it with slower rate indicating the mitochondrial Ca^{2+} buffering system. Releasing Ca^{2+} from mitochondria continues while cytosolic and ER Ca^{2+} are still increasing. Therefore, release of mitochondrial Ca^{2+} is responsible for the increase in the cytosolic Ca^{2+} concentration, which itself allows the replenishment of the ER. The Ca_m does not reach to its basal level during the time that Ca_c is decreasing. This

result highlights the effect of mitochondria in stimulating IP₃Rs by releasing Ca²⁺ during the silent phase of cytosolic Ca²⁺ oscillations which is in agreement with publications [Rizzuto et al., 2012, Wacquier et al., 2016, Ishii et al., 2006]. By increasing the Ca_c, more IP₃Rs open leading to decreasing Ca_{er}. When Ca_c reaches to its maximum value, the ER Ca²⁺ concentration becomes minimal showing that ER is the main Ca²⁺ store (see Figure 3.3 A, B). Mitochondrial Ca²⁺ accumulation depends on mitochondrial membrane potential ($\Delta\psi_m$) and mitochondrial metabolic function is, in turn, dependent on mitochondrial Ca²⁺. The flux of positive Ca²⁺ into the mitochondria first depolarizes the mitochondrial membrane but then due to the activating PDH and increasing NADH_m, the inner membrane is hyperpolarized (see Figure 3.3 C, D). By increasing the mitochondrial Ca²⁺ concentration, respiration and ATP production increases. By releasing mitochondrial Ca²⁺ into the cytosol, mitochondrial ATP also releases into the cytosol as the cytosolic ATP starts to increase (see Figure 3.3 E). Cytosolic ATP decreases by increasing ER Ca²⁺ concentration indicating the ATP consumption of SERCA pumps.

3.1.2 Model Parameter Scan

Figure 3.4 shows how expression level of different Ca²⁺ channels affect frequency of Ca²⁺ signals. For these simulations, we limited the parameter range to values that model show Ca²⁺ oscillations.

3.2 Cell Lines

In order to investigate the crosstalk between intracellular calcium oscillation and mitochondrial metabolism, we select two cell lines, HEK 293, human embryonic kidney cell line and C8-D1A, mouse cerebella astrocytic cell line. Both cell types are electrically non-excitable cells. Thus the main mechanism for intracellular Ca²⁺ oscillation is Ca²⁺ release from intracellular stores and Ca²⁺ uptake by SERCA pumps. We exposed these cell lines to ligands that activate phospholipase C (PLC) through G protein (heterotrimeric guanine nucleotide-binding protein)-coupled receptors (GPCRs), thereby stimulating production of IP₃ and Ca²⁺ release from the ER.

3.2.1 Human embryonic kidney (HEK) 293 cells

HEK 293 cells were generated in 1973 by transformation of cultures of normal human embryonic kidney cells in Alex van der Eb's laboratory in Leiden (the Netherlands). The human embryonic kidney cells were obtained from a single apparently healthy fetus legally aborted under Dutch law. They are called HEK since they originated in human embryonic kidney cultures, while the number 293 came from Graham's habit of numbering his experiments.

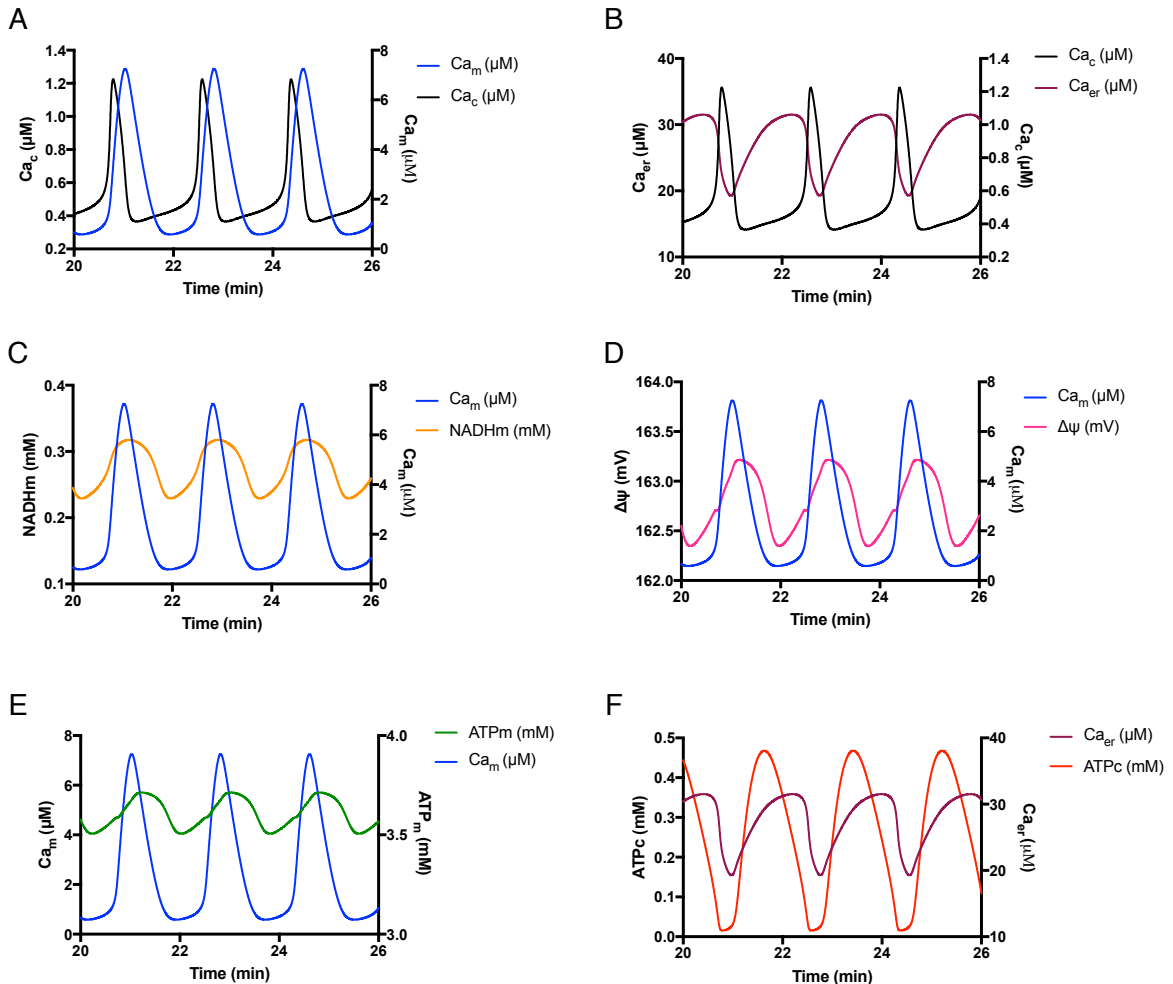


Figure 3.3. Calcium dynamics in relation to other variables. (A) mitochondrial Ca^{2+} increases with increasing cytosolic Ca^{2+} concentration. (B) ER is an intracellular Ca^{2+} store. Releasing Ca^{2+} from ER leads to increasing cytosolic Ca^{2+} concentration. (C) mitochondrial Ca^{2+} stimulate NADH production in mitochondria. (D) Increasing Ca^{2+} concentration in mitochondria first depolarizes the inner membrane and then increasing mitochondrial NADH leads to hyperpolarization of the membrane. (E) Increasing mitochondrial Ca^{2+} enhances respiration and ATP production. (F) The ATP is consumed by SERCA pump and leads to increasing Ca^{2+} concentration in the ER.

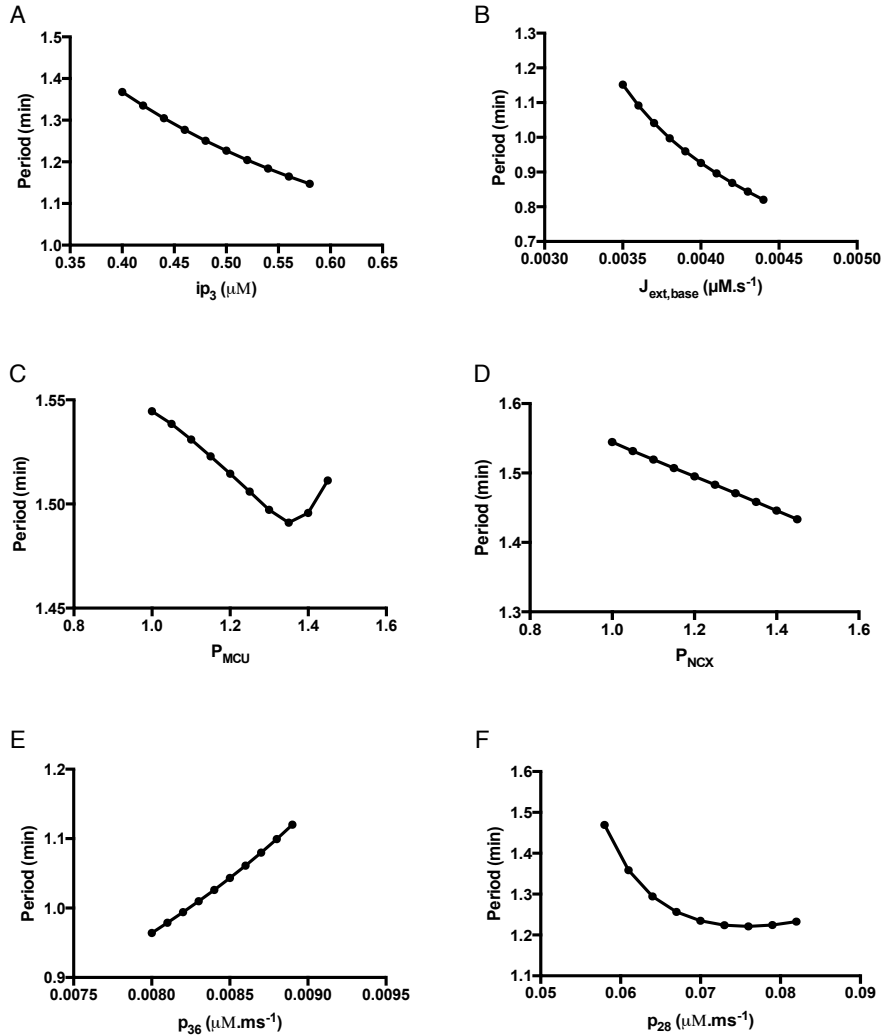


Figure 3.4. Model parameter scan. Effect of Ca^{2+} fluxes strength on the frequency of Ca^{2+} signals. (A) Increasing the IP_3 concentration increases frequency of Ca^{2+} signals since it rises the open probability of IP_3R channels, which is in agreement with experiment in [Thurley et al., 2014]. (B) Increasing Ca^{2+} influx from extracellular space decreases the periods of Ca^{2+} signals which is in agreement with experiments in [Perez and Sanderson, 2005]. (C) P_{MCU} controls the activity of MCU channel. Increasing P_{MCU} first decreases and then increases the period of Ca^{2+} signals. Low values of P_{MCU} leads to less Ca^{2+} uptake by mitochondria and subsequently less Ca^{2+} release from mitochondria which inhibits the positive effects of Ca^{2+} on IP_3Rs and thus increase periods of Ca^{2+} signals, in agreement with experiments in [Wacquier et al., 2016]. Period of Ca^{2+} signals also increases in high values of P_{MCU} . Our interpretation is that increasing P_{MCU} increases the buffer capacity of mitochondria which slows down the ER-cytosol Ca^{2+} exchanges. (D) P_{NCX} controls the Ca^{2+} release from mitochondrial NCX channel. Increasing P_{NCX} decrease periods of Ca^{2+} signals which is due to releasing more Ca^{2+} from mitochondria and increasing the positive effect of Ca^{2+} on IP_3Rs , in agreement with experiments in [Wacquier et al., 2016]. (E) p_{36} indicates the level of PMCA expression. Increasing Ca^{2+} efflux through PMCA channel leads to increasing period of Ca^{2+} signals in agreement with the prediction of deterministic and stochastic models implemented in [Cao et al., 2014]. (F) Increasing the level of SERCA pump expression by increasing p_{28} first decreases and then increases periods of Ca^{2+} signals which is in agreement with the prediction of stochastic model implemented in [Komin et al., 2015] and also in agreement with experiments done in [Falcke et al., 2003].

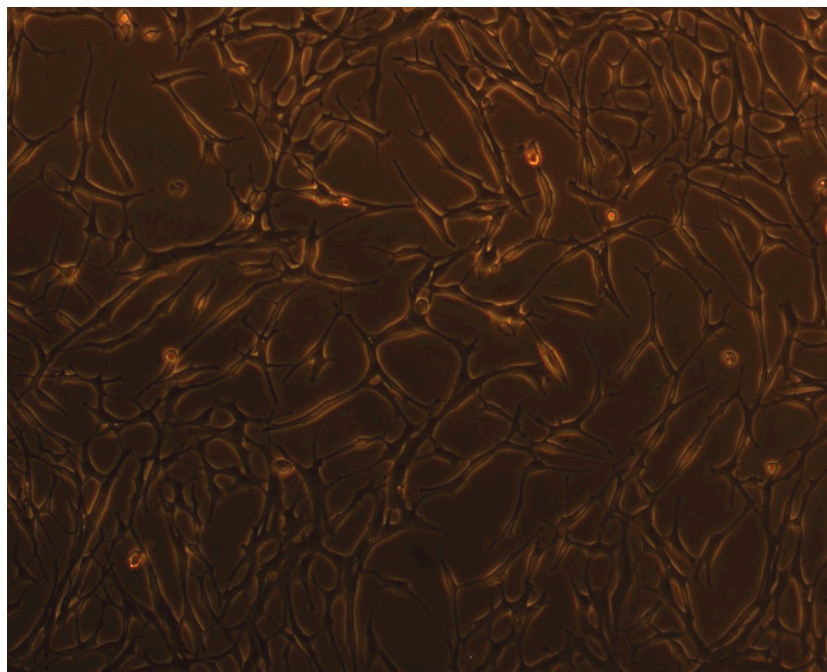


Figure 3.5. C8-D1A astrocytic cell line.

HEK 293 cells are straightforward to grow in culture and to transfect, and so have been widely used to study gene expression and Ca^{2+} signaling.

3.2.2 C8-D1A: Astrocyte type I clone

The C8-D1A type I is a clonal permanent cell line with astrocytic properties that have been established from explant cultures of 8-day postnatal mouse cerebella after in vitro spontaneous transformation, i.e. without the addition of carcinogens or oncogenic viruses. The C8-D1A type I has small somata and several short processes [Alliot and Pessac, 1984]. The cell line is bought from ATCC. Figure 3.5 shows the snapshot of cultured cells.

3.3 Experimental Protocols

We cultured both cell lines, C8-D1A and HEK293 in the Dulbecco's modified Eagle's medium supplemented with D-Glucose (25 mM), L-Glutamine (4 mM), 10% fetal bovine serum and 1% penicillin streptomycin in a humidified atmosphere (95% air, 5% CO_2 , 37°C).

3.3.1 Media Used for Experiments

We prepared a medium for growing and starving cells. This medium was composed of Dulbecco's Modified Eagle Medium (DMEM), no glucose, no glutamine, no phenol red plus

2 mM glucose, 4 mM L-glutamine, 10% fetal bovine serum and 1% penicillin streptomycin. We call this medium "starvation medium" in the rest of this thesis.

We also prepared a medium for a growing cells in a non-starvation condition. This medium is like starvation medium but it contains 25 mM glucose instead of 2 mM glucose. We call this medium "non-starvation medium" in the rest of this thesis. Cells were plated in 22 mm round glass coverslips coated with 0.01% poly-L-lysine and were grown with 1ml of prepared medium during three days in the humidified incubator gassed with 95% air, 5% CO₂, 37°C.

For all experiments, we prepared a "basic medium" containing DMEM, no glucose, no glutamine, no phenol red supplemented with 10% fetal bovine serum and 1% penicillin streptomycin. Then based on the experiment protocol, different amount of the glucose or glutamine were added to the basic medium.

3.3.2 Single-Cell Imaging of Calcium in C8-D1A cells

Experiment I: In this experiment, cells (around 1×10^5 cells/well) were starved in poly-L-lysine-coated cover-slips for three days with starvation medium. Then they were washed with phosphate buffered saline (PBS) and new medium was added to the cells at different time points.

Cells were loaded with 1 ml of two different media: 1) high glucose medium that was composed of basic medium and glucose (25 mM) and glutamine (4 mM); 2) no glucose medium that was composed of basic medium and glutamine (4 mM). Then cells loaded with 250 μ l of Fluo-4 Direct from ThermoFisher for 30 min in incubator and then immediately transferred to an imaging chamber at 37°C. Cells were imaged with inverted Nikon fluorescence microscope using excitation at 490 to 510 nm (ET500/20x filter from Chroma) were collected at 3-s intervals and with LED light source. The exposure time is set to 80 ms. During imaging cells are exposed to 80 μ M of ATP from Sigma-Aldrich (A1852-1VL), an agonist for stimulating purinergic receptors.

Experiment II: This experiment is performed like experiment I, but cells are loaded with 1 ml of medium composed of basic medium plus 1 mM glucose. During imaging cells are stimulated with different concentrations of ATP.

Experiment III: This experiment is performed like experiment I, but cells are loaded with 1 ml of medium composed of basic medium plus 1 mM L-glutamine. During imaging cells are stimulated with different concentrations of ATP.

Experiment IV: This experiment is performed like experiment I, but cells are loaded with 1 ml of medium composed of basic medium plus 5 mM glucose and 4 mM L-glutamine.

3.3.3 Single-Cell Imaging of Calcium in HEK293 cells

HEK293 cells (around 1×10^5 cells/well) were plated in poly-L-lysine-coated cover-slips for three days with non-starvation medium. Then they are washed with phosphate buffered saline (PBS) and 1 ml of new medium composed of basic medium plus 5 mM glucose and 4 mM is added to cells. Then cells are imaged like Experiment I. During imaging cells are exposed to different concentrations of carbachol (CCh), an agonist of muscarinic acetylcholine receptors.

3.3.4 Measuring Extracellular Metabolites

For all experiments described in Sections 3.3.2 and 3.3.3, we also measured the extracellular metabolic flux. Cells are loaded with new medium as described and then C8-D1A are exposed to different concentrations of ATP and HEK293 are exposed with different concentration of carbochol. Then cells are incubated for 1 hour and also different time points as indicated. The medium of each well was filtered and $150 \mu\text{l}$ of it were loaded in 96-well plate and used for measuring the remaining metabolites, glucose, glutamine, lactate and glutamate.

Measurement of the metabolites inside the medium is done by the YSI 2900 Series machine. In the YSI 2900, for measuring the amount of glucose, the enzyme glucose oxidase is immobilized in the enzyme membrane. This is a direct reading of glucose in solution at the enzyme sensor: $\text{Glucose} + \text{O}_2 \rightarrow \text{H}_2\text{O}_2 + \text{D-Glucono-}\gamma\text{-Lactone}$.

For measuring the amount of glutamate, the enzyme L-Glutamate Oxidase is immobilized in the YSI Glutamate Membrane. This is a direct reading of L-glutamate in solution at the enzyme sensor: $\text{Glutamate} + \text{O}_2 \rightarrow \text{H}_2\text{O}_2 + \alpha\text{-Ketoglutarate} + \text{NH}_3$.

For measurement the amount of glutamine, two enzymes are co-immobilized in the YSI in Glutamine Membrane: Glutaminase and Glutamate Oxidase. Through the following chain of reactions the amount of hydrogen peroxide liberated is directly proportional to the amount of glutamine: $\text{L-Glutamine} \rightarrow \text{L-Glutamate} + \text{NH}_3$; $\text{L-Glutamate} + \text{O}_2 \rightarrow \text{H}_2\text{O}_2 + \alpha\text{-Ketoglutarate} + \text{NH}_3$.

For measurement the amount of lactate in solution, the enzyme L-Lactate Oxidase is immobilized in the enzyme membrane: $\text{L-Lactate} + \text{O}_2 \rightarrow \text{H}_2\text{O}_2 + \text{Pyruvate}$.

In the all reactions the amount of produced H_2O_2 is proportional to the concentration of

substrates. In the next step, YSI performs another electrochemical reaction which is common to all YSI enzyme sensors: $\text{H}_2\text{O}_2 \rightarrow 2\text{H}^+ + \text{O}_2 + 2\text{e}^-$. The electron flow is measured by a platinum electrode which is proportional to the concentration of the substrate. Then the absolute amount of glucose, glutamine, lactate and glutamate in the solution is calculated through plotting standard curve for each metabolite. The amount of glucose/glutamine consumption was determined by subtracting glucose in control medium (medium without cells) from glucose/glutamine in the plating medium. The amount of lactate/glutamate secretion is calculated by subtracting lactate/glutamate in the plating medium from lactate/glutamate concentration in control medium. The concentration of metabolites were normalized to the cell number.

3.3.5 ADP/ATP Ratio Measurement

Around 1×10^4 of C8-D1A cells were plated in 96-well plate for 3 days in $100 \mu\text{l}$ of starvation medium. We starved our cells to be sure that they uptake glucose from the new medium. Subsequently, cells were washed with PBS. The high glucose medium and low glucose medium were added to the cells and then the amount of ADP/ATP ratio is measured in different time points by the ADP/ATP ratio assay kit from abcam. This assay is based on the bioluminescent detection of the ADP and ATP levels in the sample. In this assay, luciferase catalyzes the conversion of ATP and luciferin to light, which in turn can be measured using a luminometer. ADP level is measured by its conversion to ATP (by adding ADP converting enzyme) that is subsequently detected using the same reaction. The assay can be fully automatic for high throughput and is highly sensitive.

In another experiment, cells were seeded in the same condition but the medium is changed with DMEM, no glucose, no glutamine, no phenol red plus 5 mM glucose, 4 mM glutamine, 10% fetal bovine serum and 1% penicillin streptomycin. Then cells are exposed to different concentration of carbochol (CCh) for one hour and ADP/ATP ratio was measured.

3.3.6 Statistics

For comparing the average period of Ca^{2+} signals (T_{av}), data is representative for more than 100 cells and T_{av} is the average of ISIs in the Ca^{2+} signals that have more than 12 Ca^{2+} spikes. For analyzing extracellular metabolic flux 3 or more independent experiments are presented. For measuring ADP/ATP ratio, the data represent measurements of 5 replicates for each condition. The bar plots are represented as mean \pm SEM. We used unpaired t test for comparing two different groups and for comparing more than 2 groups of data we used one-way ANOVA. Statistical analyses were done using GraphPad Prism software. The P values are shown by the following symbols: 'ns' $P > 0.05$, * $P \leq 0.05$, ** $P \leq 0.01$, *** $P \leq 0.001$.

3.4 Summary

In this chapter, we developed a new model for IP_3 -induced Ca^{2+} oscillations and coupled it to simplified mitochondrial model developed by Bertram in order to simulate the interplay between Ca^{2+} signaling and mitochondrial metabolism. Equations 3.11 to 3.19 are taken from Bertram mitochondrial model [Bertram and Arceo II, 2008] while equations 3.20 to 3.26 are our contributions for developing a new model for IP_3 -induced Ca^{2+} oscillations. By coupling Ca^{2+} model to the mitochondrial model, we could investigate the dependency of Ca^{2+} dynamics to the mitochondrial metabolism and vice versa. Then we validate our model by investigating the effect of different parameters on the frequency of Ca^{2+} signals and showed that our deterministic model can reproduce the main experimental features. Then we described the cell lines and the protocols which were used in our experiments. We explained how Ca^{2+} imaging and the flux of metabolites were measured.

Chapter 4

Results

The crosstalk between Ca^{2+} signaling and mitochondrial metabolism is known since 1959 when Krebs discovered that Ca^{2+} regulates metabolism by activating phosphorylase kinase [Krebs et al., 1959]. In 1961, Vasington and Murphy [Vasington and Murphy, 1961] and Deluca and Engstrom [DeLuca and Engstrom, 1961] discovered that isolated kidney mitochondria could accumulate large amounts of Ca^{2+} in an energy driven process. Upon increasing cytosolic Ca^{2+} concentration mitochondria sequester large amount of Ca^{2+} resulting in lower cytoplasmic Ca^{2+} levels. Mitochondria are active participants in cellular Ca^{2+} signaling, whose unique role is determined by their ability to rapidly accumulate and then release large quantities of Ca^{2+} [Babcock et al., 1997]. Subsequently in the 1960s and 70s, Ca^{2+} at physiological concentrations was found to regulate dehydrogenase enzymes: FAD-glycerol phosphate dehydrogenase, which is located on the cytoplasmic surface of the inner membrane of mitochondria, pyruvate dehydrogenase, NAD-isocitrate dehydrogenase and oxoglutarate dehydrogenase, all found in the matrix of mitochondria [Denton, 2009, Griffiths and Rutter, 2009]. Hence, the known interaction between calcium signaling and mitochondrial metabolism is that calcium regulates TCA cycle enzymes for ATP production and the ATP which is mainly produced by mitochondria is used by calcium pumps for calcium homeostasis (see Figure 4.1).

Understanding the role of ATP in Ca^{2+} homeostasis and also the role of Ca^{2+} in mitochondrial metabolism is important since impaired Ca^{2+} homeostasis and mitochondrial ATP production is now thought to contribute to several neurodegenerative diseases. As detailed in Section 2.4, it has been shown that the impaired interaction between Ca^{2+} signaling and mitochondrial metabolism is the potential reason for selective vulnerability of dopamine neurons in the substantia nigra pars compacta (SNc) [Chan et al., 2009, Surmeier et al., 2010]. These neurons express $\text{Ca}_{v1.3}$ Ca^{2+} channels that enable Ca^{2+} to enter the cytoplasm during pacemaking, leading to elevated intracellular Ca^{2+} concentrations. Ca^{2+} entry

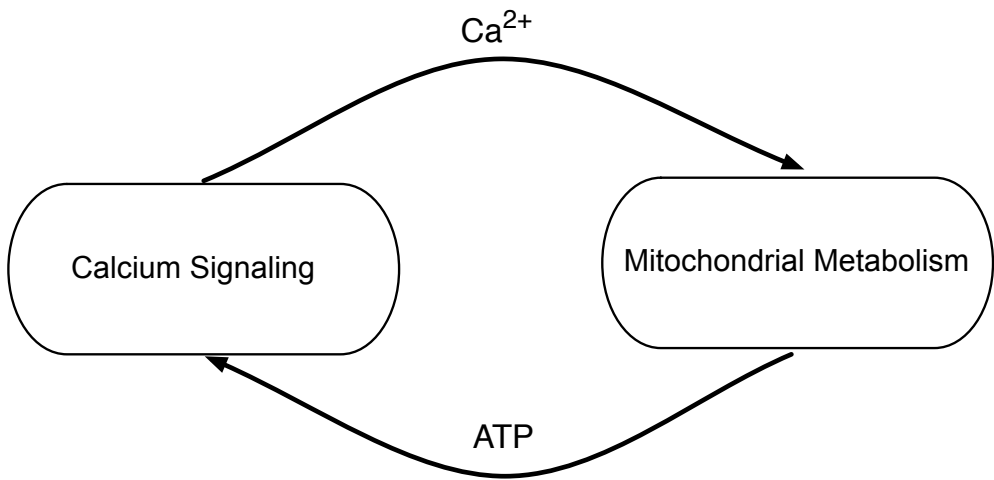


Figure 4.1. Components and interactions in the calcium-mitochondrial system.

through plasma membrane $\text{Ca}_v1.3$ Ca^{2+} channels during pacemaking is either pumped back across the plasma membrane or rapidly sequestered in the ER or mitochondria. Both processes require energy stored in the form of ATP. The metabolic demand created by these ATP-dependent steps in Ca^{2+} homeostasis should increase oxidative phosphorylation in mitochondria and the production of damaging ROS. ROS are capable of damaging ER proteins, elevating the concentration of misfolded proteins. Mitochondrial Ca^{2+} overload could further compromise their ability to generate ATP, leading to a functionally important drop in cytosolic ATP levels. Such a drop would compromise ER proteins and promote the formation of protein aggregates such as Iwrey bodies [Chan et al., 2009].

There is a lot known about the Ca^{2+} signaling and mitochondrial metabolism, but the goal of this work is having a systematic understanding of the interaction between Ca^{2+} signaling and mitochondrial metabolism without focusing too much on the functionality of each subsystem. We want to quantitatively answer the questions like how intracellular ATP affect calcium homeostasis and how different profiles of calcium signals affect mitochondrial metabolism and ATP production.

This chapter we first describes the model implications. We show the robustness of our model with respect to ATP perturbation. Then we illustrate the effect of mitochondrial carbon inputs on the profile of Ca^{2+} signals and intracellular ATP. In the Section 4.2, we will show the experimental results. Section 4.2.1 provides an overview of the astrocytic Ca^{2+} signaling and energy metabolism. In section 4.2.3, we explore the impact of glucose availability on the intracellular ATP and Ca^{2+} signals and show how glutamine uptake rate is affected. Sections 4.2.5 and 4.2.6 describe the effect of extracellular stimuli on the period of Ca^{2+} signals and glucose and glutamine uptake rates. Finally, we investigate the metabolic decoding of intracellular Ca^{2+} signals in our cell lines and also explore the effect of IP_3 -mediated Ca^{2+}

signaling on the mitochondrial ATP production.

4.1 Model Implications

4.1.1 ATP-Dependent Model versus ATP-Independent Model

The proposed model in Section 3.1 considers SERCA and PMCA pumps as the sources of ATP consumption and therefore couples Ca^{2+} signaling and ATP dynamics. We name this model ATP-dependent model. Most of the existing models neglect the ATP consumption of SERCA and PMCA pumps. We developed a similar model that does not take into account the ATP hydrolysis of SERCA and PMCA pumps and called it ATP-independent model. In the ATP-independent model the expression of SERCA and PMCA pumps and the equation of ADP_c have the following form:

$$J_{serca} = p_{28} \frac{Ca_c^2}{p_{29}^2 + Ca_c^2}, \quad (4.1)$$

$$J_{pmca} = p_{36} \frac{Ca_c^2}{p_{37}^2 + Ca_c^2}, \quad (4.2)$$

$$\frac{dADP_c}{dt} = -v_{m/c} J_{ANT} + J_{hyd,bas}. \quad (4.3)$$

All other equations and expressions and also parameters of the ATP-independent model are similar to the ATP-dependent model. The only parameter which takes different value in the ATP-independent model is p_{29} that is set to 0.2 to ensure a similar oscillation behavior. Figure 4.2 shows the dynamics of cytosolic and mitochondrial Ca^{2+} and ATP in the ATP-dependent model and ATP-independent model. The dynamics of Ca_c , Ca_m and ATP_m are similar in both models but ATP_c shows different behavior (see Figure 4.2 A, C). In contrast to ATP-dependent model, ATP_c barely changes by varying Ca_c in the ATP-independent model. As Figure 4.2 B and D show, by decreasing ATP_c , Ca_c increases indicating lower rates of SERCA and PMCA pumps for removing Ca^{2+} from cytoplasm that results in rising Ca_c . Thus the ATP-dependent model shows more coupling between cytosolic ATP and calcium. By establishing the crosstalk between calcium and ATP, we can investigate the effect of ATP on the Ca^{2+} homeostasis.

ATP-dependent model is more robust to the intracellular ATP perturbation: In order to investigate the effect of ATP dependency of SERCA and PMCA pumps on the Ca^{2+} homeostasis, we increased the rate of ATP consumption by increasing $J_{hyd,base}$ as the step function. As shown in Figure 4.3, increasing the rate of ATP hydrolysis increases the frequency of Ca^{2+}

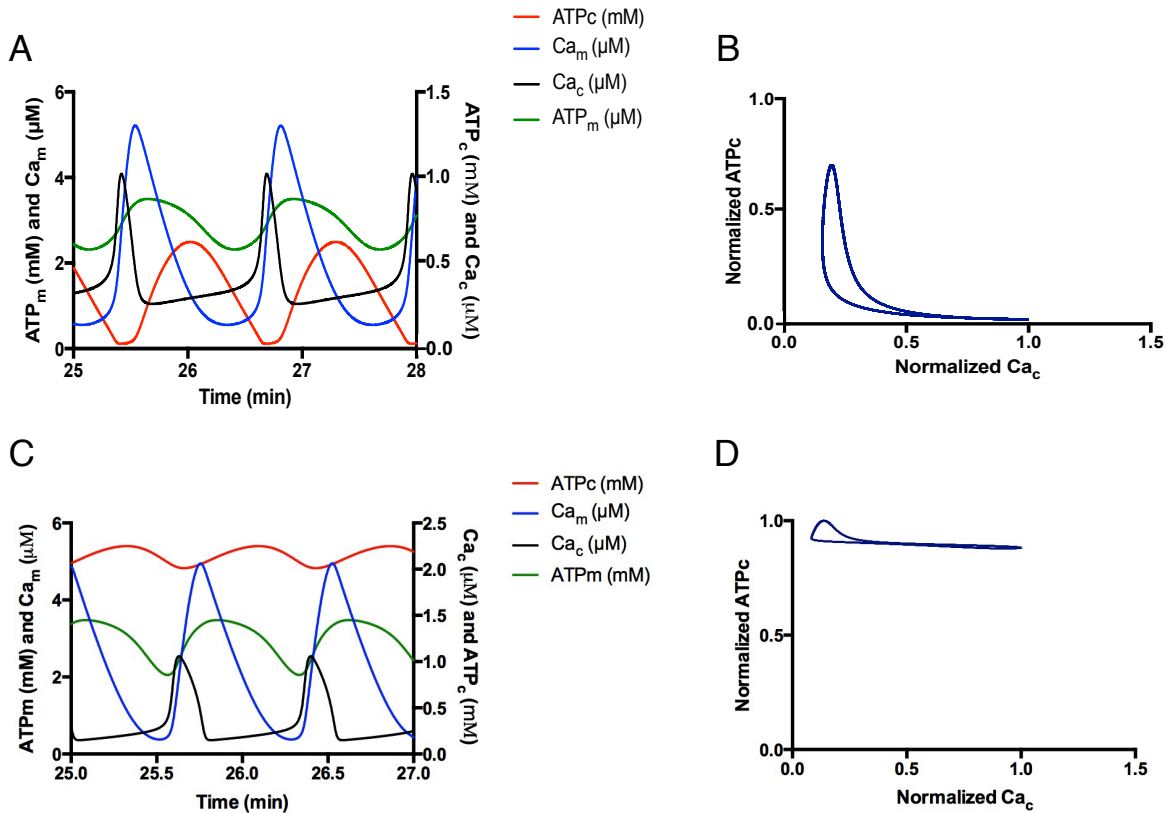


Figure 4.2. Calcium and ATP dynamics in ATP-dependent model (A, B) versus ATP-independent model (C, D). In B and D, the ATP_c and Ca_c concentrations are normalized between 0 and one in order to show their variability with respect to each other.

signals and decreases the amplitude of the spikes in the ATP-dependent model while it does not affect the Ca^{2+} signaling profile in the ATP-independent model. In the ATP-dependent model, increasing $J_{\text{hyd},\text{base}}$ leads to around 26% reduction of cytosolic ATP while it leads to 47% reduction in cytosolic ATP in ATP-independent model. These results indicate that ATP-dependent model is more robust to the cytosolic ATP perturbation. Meaning that increasing the rate of ATP consumption cause less dropping in the average of cytosolic ATP. It also shows the crosstalk between Ca^{2+} signaling and cytosolic ATP in the ATP-dependent model since changing the ATP level affects Ca^{2+} signaling profile and subsequently the cytosolic calcium affects the profile of cytosolic ATP.

4.1.2 Impact of Mitochondrial Substrates on Ca^{2+} Signaling

Ca^{2+} signaling is an energy demanding process. ATP which is mainly produced by mitochondria, is partly consumed by SERCA and PMCA pumps to extrude Ca^{2+} into ER or extracellular space in order to keep the cytosolic Ca^{2+} concentration at ~ 100 nM (see Figure 4.4). The question is: what happens for calcium regulation if cytosolic ATP drops? In

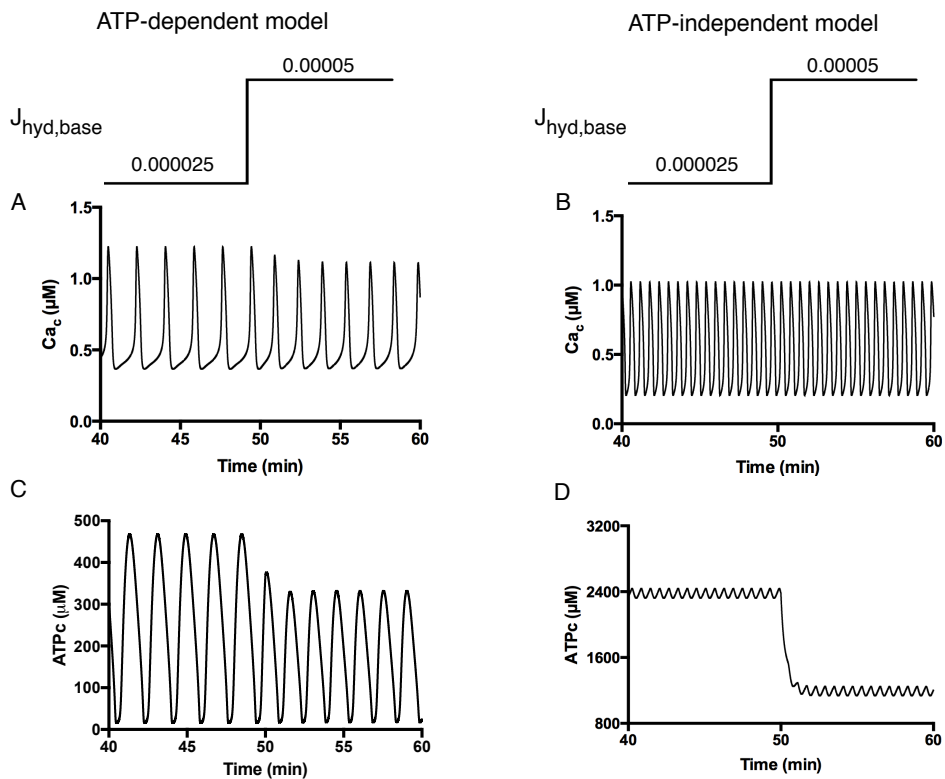


Figure 4.3. Changing the cytosolic Ca^{2+} and ATP with respect to varying the rate of ATP hydrolysis in the cell. Increasing cytosolic ATP consumption affect the profile of Ca^{2+} signals in ATP-dependent model.

order to see the impact of cytosolic ATP on the Ca^{2+} homeostasis, we simulate the calcium-mitochondrial system behavior while decreasing the mitochondrial carbon inputs. Figure 4.5 C and E shows the profile of cytosolic calcium and ATP while decreasing the level of FBP as the exponential function. As described before, FBP is considered as mitochondrial carbon input instead of pyruvate and is constant parameter. Decreasing mitochondrial carbon inputs leads to increasing frequency of calcium signals. Our interpretation of this result is that decreasing mitochondrial substrates cause decreasing mitochondrial NADH production and also decreasing mitochondrial membrane potential which subsequently decreases mitochondrial ATP production. This results in decreasing cytosolic ATP and decreasing Ca^{2+} pump into the ER through the SERCA pumps. Therefore mitochondria are exposed to large amount of Ca^{2+} which leads to mitochondrial Ca^{2+} overload. Increasing mitochondrial Ca^{2+} leads to increasing mitochondrial NCX activity and therefore rises the positive feedback effect of Ca^{2+} on the IP_3 Rs channels which ends up with increasing frequency of Ca^{2+} signals. Frequently opening IP_3 channels and slow calcium removal mechanism lead to an increase in the cytosolic and mitochondrial calcium concentration. Although decreased mitochondrial membrane potential should decrease Ca^{2+} entry into mitochondria through the MCU channels, but due to the high cytosolic Ca^{2+} concentration even the small values

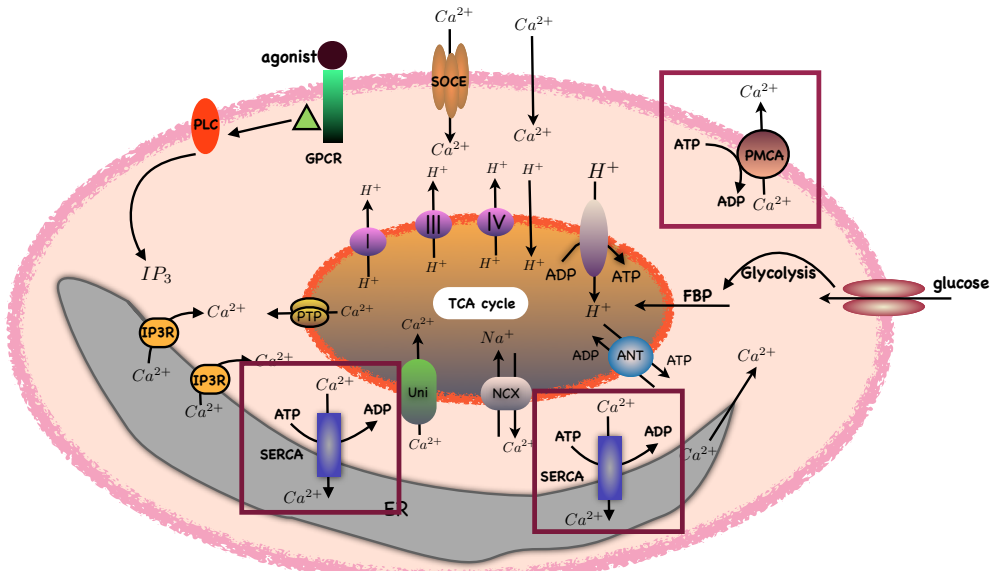


Figure 4.4. Ca^{2+} homeostasis is an energy demanding process. ATPase pumps push Ca^{2+} uphill into the ER (via SERCA pumps) or out of the cell (via PMCA) to maintain low cytoplasmic Ca^{2+} concentration.

of mitochondrial membrane potential leads to a large Ca^{2+} input into the mitochondria and leads to mitochondrial Ca^{2+} overload. Figure 4.5 shows the dynamics of mitochondrial Ca^{2+} fluxes, membrane potential, NADH, ATP and other Ca^{2+} fluxes with respect to decreasing mitochondrial FBP input. In Sections 4.2.6 and 4.2.8, we will show that increasing the frequency of Ca^{2+} signals upon decreasing mitochondrial carbon substrates is a mechanism for compensating the reduced amount of ATP production.

In another simulation, we performed parameter scan for the different values of FBP while increasing IP₃ concentration and Ca^{2+} influx through MCU channel into the mitochondria in order to test if decreasing FBP values leads to increasing frequency of Ca^{2+} signals in different profiles of Ca^{2+} signals. Increasing IP₃ concentration increases the frequency of Ca^{2+} oscillations and increasing MCU value increases mitochondrial Ca^{2+} concentration. Figure 4.6 shows that decreasing mitochondrial substrates leads to increasing frequency of Ca^{2+} signals independent of the rate of Ca^{2+} entry into the mitochondria. We also measured the average cytosolic ATP, mitochondrial Ca^{2+} and periods of Ca^{2+} signals for two different values of FBP concentration while changing the level of IP₃. As Figure 4.7 shows low concentration of FBP decreases cytosolic ATP. The reduced ATP level in the cell leads to lower SERCA pump activity, causing an increase in Ca^{2+} levels in the cytosol. Increasing cytosolic Ca^{2+} concentration cause increasing mitochondrial Ca^{2+} concentration. It also has positive feedback on the IP₃Rs which leads to decreasing the periods of Ca^{2+} signals. Figure 4.7 also indicates that different values of IP₃ lead to the same results.

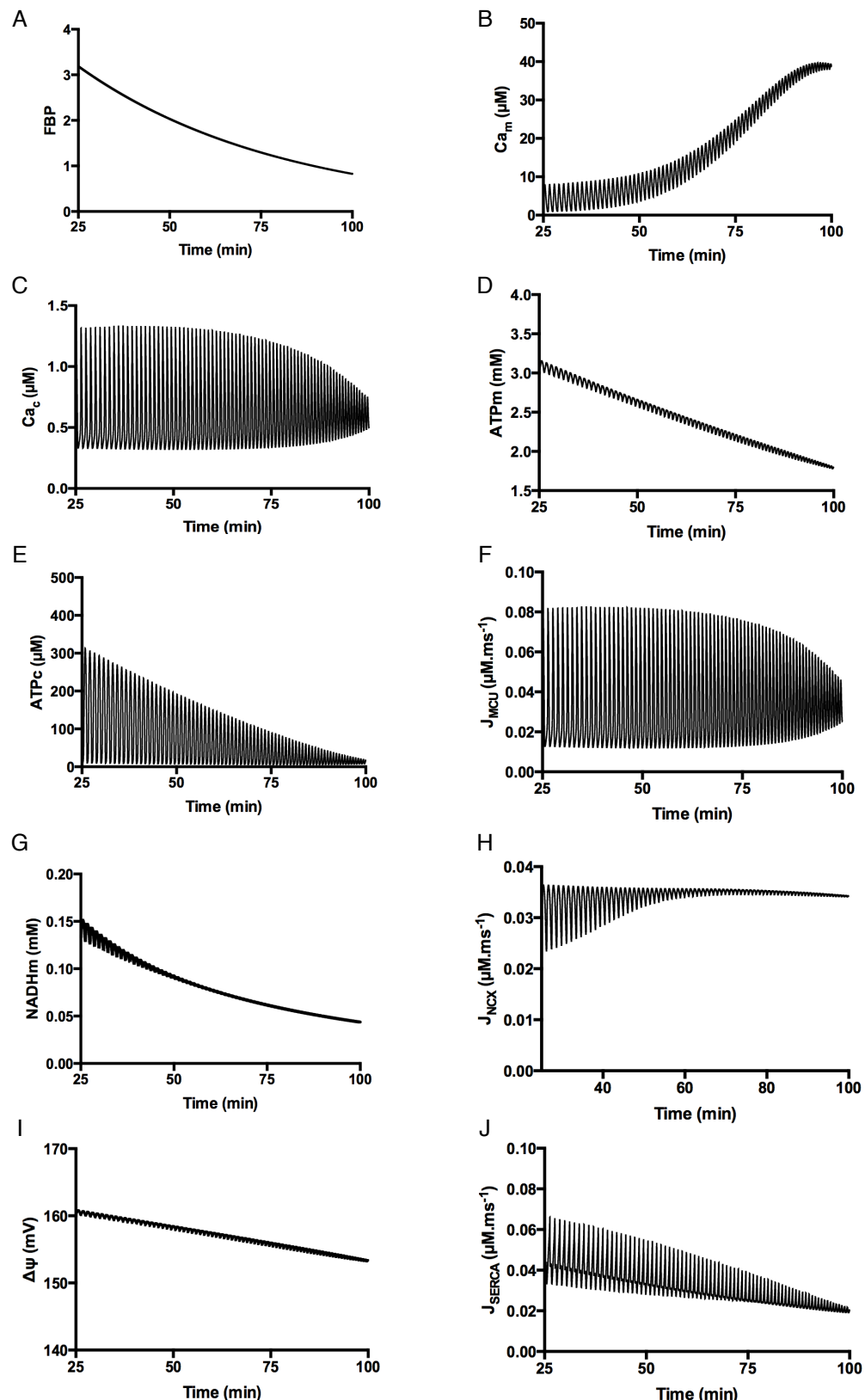


Figure 4.5. Dynamics of calcium and ATP fluxes in cytosol and mitochondria while decreasing FBP exponentially.

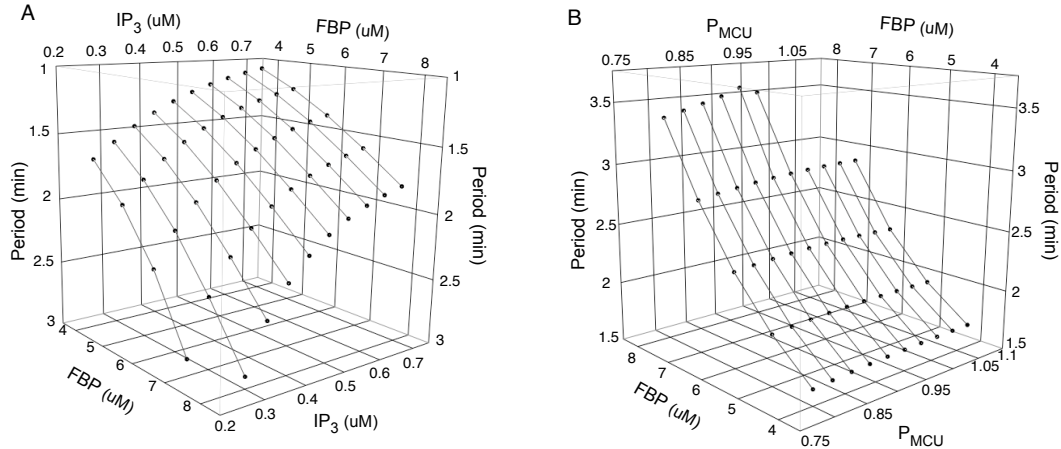


Figure 4.6. Decreasing FBP concentration cause to decreasing periods of Ca²⁺ signals. (A) Parameter scan on the IP₃ concentration shows that decreasing periods of Ca²⁺ signals by decreasing FBP concentration is not dependent on the concentration of IP₃. (B) Parameter scan on the P_{MCU} parameter which controls the amount of mitochondrial Ca²⁺ entry shows that decreasing periods of Ca²⁺ signals by decreasing FBP concentration is not dependent on the mitochondrial Ca²⁺ concentration.

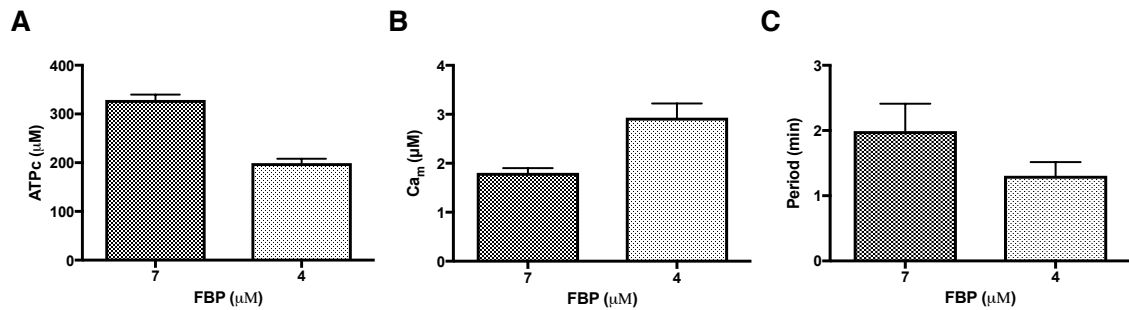


Figure 4.7. Decreasing FBP concentration leads to decreasing cytosolic ATP and increasing mitochondrial calcium, and frequency of calcium signals. The variations are due to the measurements of average values in different concentrations of IP₃ which indicates the results are independent of IP₃ variations.

Based on these simulations, we make the following hypothesis: decreasing mitochondrial substrates leads to decreasing cytosolic ATP and increasing frequency of Ca^{2+} signals. In order to test the proposed hypothesis, we used the astrocytic mouse cell line C8-D1A. Astrocytes are electrically non-exitable cells and their main mechanism for Ca^{2+} oscillation is IP_3 -mediated Ca^{2+} signaling which is compatible with our mathematical model. Before going through the experiments for examining the proposed hypothesis, we give first an overview of the astrocytic calcium-energy metabolism system that will support our understanding of the experimental results.

4.2 Experimental Results

4.2.1 Astrocytic Calcium-Energy Metabolism System

Astrocytes are a sub-type of glia and electrically non-exitable cells in the central nervous system that have been implicated in controlling the dynamics of neural networks. Astrocytes exhibit calcium excitability. Their excitation which is chemically induced can be revealed by imaging assays of Ca^{2+} transients [Volterra and Meldolesi, 2005]. Astrocyte Ca^{2+} excitation can occur spontaneously by Ca^{2+} releasing from internal stores when IP_3R receptors are activated or it can be induced by chemical signals like neurotransmitters (e.g. glutamate and purins) from neurons or neighboring astrocytes which is of crucial importance because it indicates the existence of neuron-to-astrocyte and astrocyte-to-astrocyte communication [Sofroniew and Vinters, 2010]. Astrocytes play direct roles in synaptic transmission through release of synaptically active molecules including glutamate, purines (ATP and adenosine), GABA and D-serine. Astrocytes express a wide variety of functional neurotransmitter receptors. They express metabotropic and purinergic receptors which are G proteins and stimulate phospholipase C and IP_3 formation, which increases the intracellular Ca^{2+} concentration through the release of Ca^{2+} from IP_3 receptors on the ER. Astrocytic Ca^{2+} waves are mediated primarily by release of ATP and activation of purine receptors. Studies have shown that ATP is released from single cell and then diffuses to neighboring cells which leads to increasing intracellular Ca^{2+} level in response to P2Y-receptor activation but the Ca^{2+} wave is not further amplified by release of additional ATP [Nedergaard et al., 2003].

Astrocytes have processes that on the one hand contact blood vessels and on the other hand contact neural axons and synapses. So they are well positioned to take up glucose from the blood vessel and provide energy substrates to neurons. Astrocytes exhibit a high glycolytic rate. A large portion of the glucose entering the glycolytic pathway in astrocytes is released as lactate in the extracellular space and neuron can efficiently use lactate as an energy substrate. Astrocytes are well-characterized in rapid removal of neurotransmitters released into the synaptic cleft. Astrocytes uptake glutamate by the astrocyte-specific

sodium-dependent high-affinity glutamate transporters GLT-1 and glutamate aspartate transporter (GLAST). A large portion of released glutamate from the neurons at the synapse is taken up by astrocytes together with 3 sodium ions and in turn astrocytes release glutamine to be taken up into neurons. This cycle is called glutamate-glutamine cycle. Removing sodium ions from astrocytes is performed by Na^+/K^+ ATPase which triggers glucose uptake from the blood vessel through the glucose transporter GLUT1 [Bélanger et al., 2011]. Glutamate uptake by astrocytes stimulates aerobic glycolysis and lactate production. Astrocytes store glycogen which then can be converted into glucose either for the cell's own use or for the export to neurons in the form of lactate. Figure 4.8 shows the schematic representation of the calcium-energy metabolism system in astrocytes.

4.2.2 Astrocytes Nutrients Utilization

As described in Section 4.1.2, we want to experimentally investigate how reduced mitochondrial carbon inputs impact Ca^{2+} signaling. In our experiments, we changed the glucose concentration since pyruvate derived from glucose is the main mitochondrial substrate. In order to have more precise experiments for characterizing the effect of mitochondrial substrates on the Ca^{2+} signaling, we decided to first starve our cells during 72 h before performing treatment to ensure that cells are lacking substantially glucose and will take up the newly provided sources.

To test at which glucose concentration astrocytes are starved, we prepared six media containing different concentrations of glucose and grew 0.1×10^6 cells in each well of a 12-well plate for 3 days. Then we measured the amount of glucose and glutamine uptake as well as the amount of lactate and glutamate secretion. As Figure 4.9 A and B show, cells which have access to lower level of glucose consume less glucose, but more glutamine. In all conditions, the amount of produced lactate is high and even in low glucose media astrocytes are able to keep up the lactate production. This indicates the cellular astrocyte role to providing lactate to neurons. This result further indicates the activation of the glutaminolysis pathway in cells which have access to low amount of glucose, where glutamine is oxidized in the mitochondria and converted to pyruvate via malic enzymes.

4.2.3 Frequency of Ca^{2+} Spikes is High in the Cells with no Glucose Accessibility

In Section 4.1.2, we hypothesized by model simulations that decreasing mitochondrial carbon input leads to decreasing cytosolic ATP and increasing frequency of Ca^{2+} signals. In this section we will show experimentally that this hypothesis is true in the C8-D1A astrocytic cell line. For this purpose, we measured the cytosolic ADP/ATP ratio of the cells

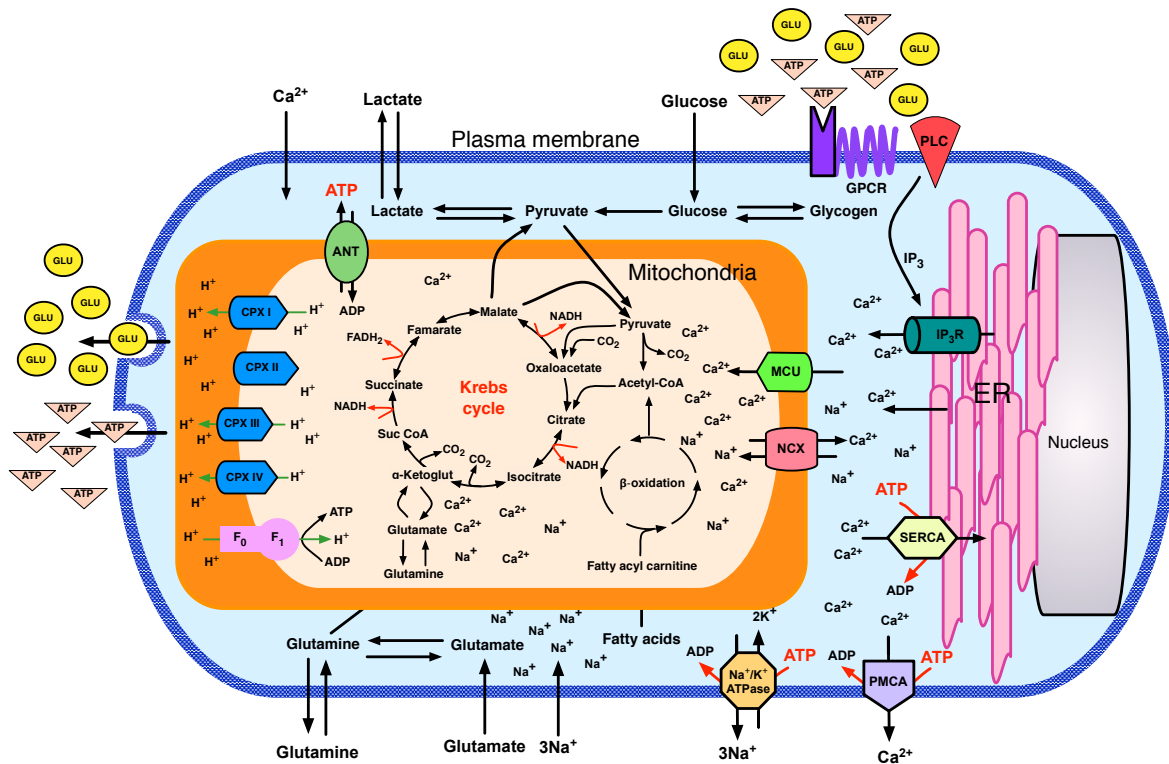


Figure 4.8. Schematic representation of astrocytic calcium-energy metabolism system. Glucose which is taken up from the blood vessel is either converted into glycogen or pyruvate. Pyruvate may enter into mitochondria and TCA cycle or converted into lactate. Glutamate is co-transported with Na^+ , resulting in an increase in the intra-astrocytic concentration of Na^+ , leading to an activation of the astrocyte Na^+/K^+ -ATPase. Activation of the Na^+/K^+ -ATPase stimulates glycolysis and lactate production. Lactate, once released by astrocytes, can be taken up by neurons and serves them as an adequate energy substrate. Following glutamate uptake by astrocytes, it is converted to glutamine by the action of glutamine synthetase and shuttled to neurons, where it is converted back to glutamate by glutaminases. Astrocytes release ATP to the extracellular space. Releasing ATP from astrocytes leads to propagating Ca^{2+} waves in neighboring cells since they express purine receptors. Astrocytes also can release glutamate upon increasing intracellular Ca^{2+} concentration which has variety of actions on neurons [Innocenti et al., 2000, Rossi et al., 2007]. Astrocytes express metabotropic receptors which stimulate phospholipase C and IP_3 formation. Binding IP_3 to IP_3 receptors on the ER membrane open them and leads to elevation of intracellular Ca^{2+} concentration. Ca^{2+} after performing its functions is removed back into the ER through SERCA pumps or extruded to extracellular space through PMCA pumps. GPCRs: G protein-coupled receptors, PLC: phospholipase C, MCU: mitochondrial Ca^{2+} uniporter, NCX: $\text{Na}^+/\text{Ca}^{2+}$ exchanger, ANT: adenine nucleotide translocase, GLU: glutamate.

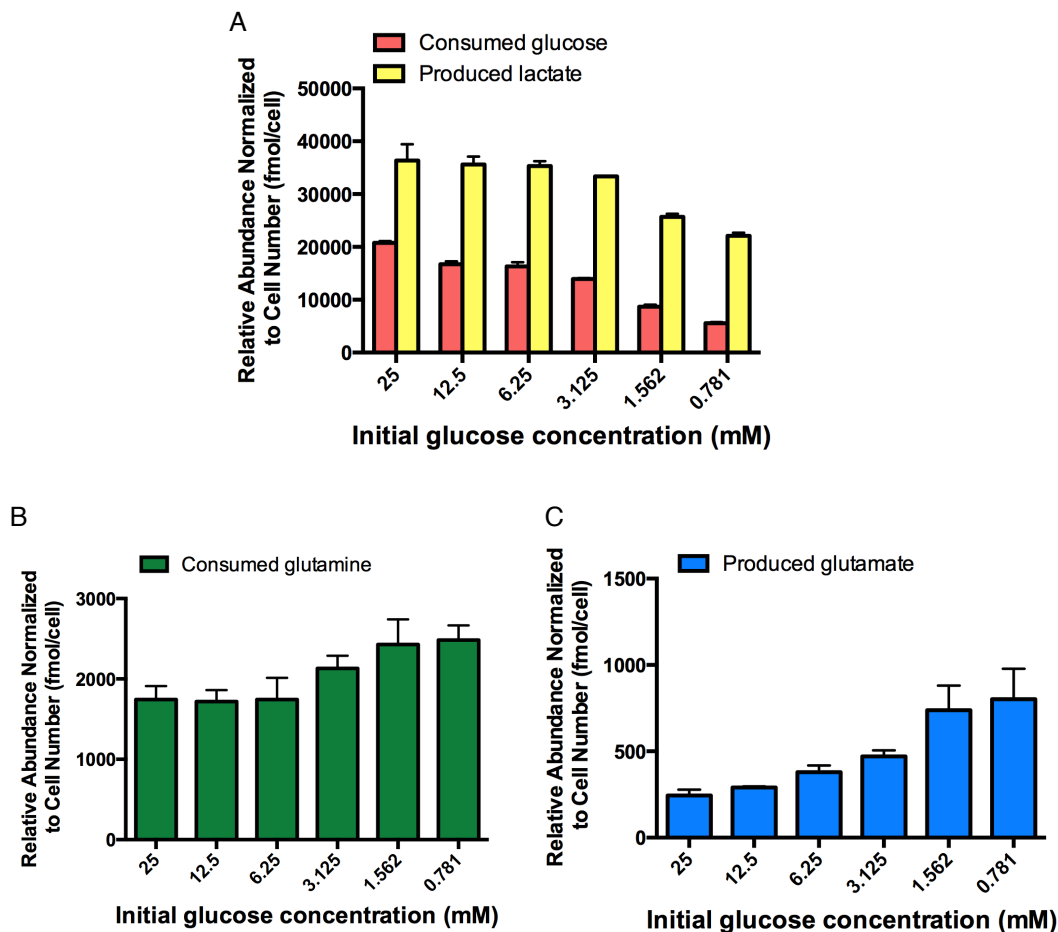


Figure 4.9. Glucose and glutamine uptake, and lactate and glutamate secretion in media containing different amount of glucose. Cells which are in low glucose medium take up more glutamine to compensate partially the lack of glucose.

that have been for 30 min and 90 min in medium with no glucose and medium containing 25 mM glucose. After 30 min there was no difference in the ADP/ATP ratio between cells in two different media. However, the level of ADP/ATP ratio increased significantly after 90 min in the cells with no glucose medium (see Figure 4.10 A). Thus, removing glucose from the medium and decreasing mitochondrial carbon input decreases intracellular ATP after 90 min. To explore the effect of intracellular ATP on the calcium signaling, we performed Ca^{2+} imaging as described in Section 3.3.2 Experiment I. Calcium imaging was done 1 h and 2 h after changing medium with no glucose and 25 mM glucose medium. Computing the period of Ca^{2+} signals by getting the average of interspike intervals revealed that periods of Ca^{2+} signals of the cells which were in no glucose medium are significantly smaller than cells in 25 mM glucose (See figure 4.10 B, C). These results indicate that decreasing mitochondrial carbon inputs, decrease intracellular ATP and increase frequency of Ca^{2+} signals which is in agreement with the model prediction.

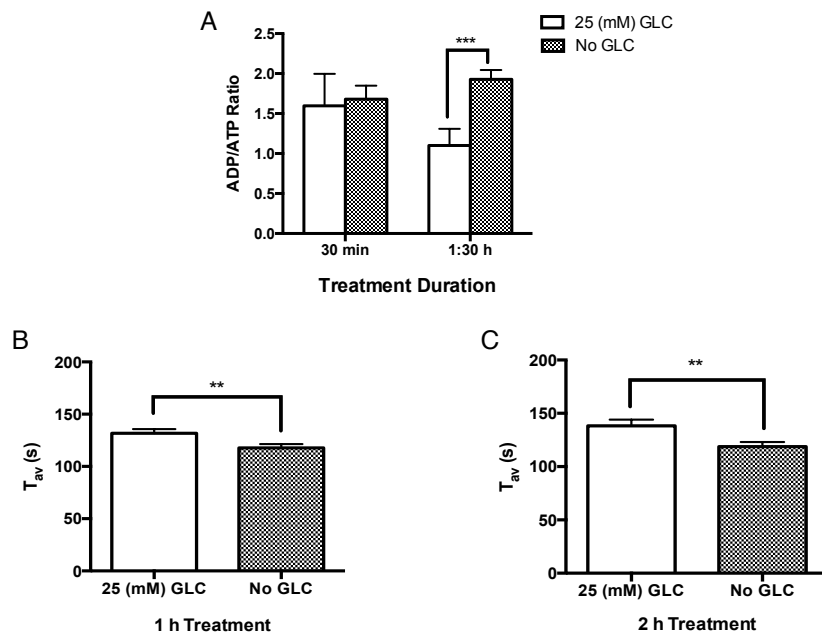


Figure 4.10. Effect of glucose availability on the intracellular ATP and period of Ca^{2+} signals. (A) The ADP/ATP ratio increases in cells inside no glucose medium after 1:30 hour. (B, C) Cells in no glucose medium show lower period of Ca^{2+} oscillations after 1 hour and 2 hours of changing the medium. These graphs indicate that glucose deprivation leads to increasing ADP/ATP ratio and rises the frequency of Ca^{2+} signals.

4.2.4 Glutamine Uptake Rate is High in the Cells with no Glucose Accessibility

It is known that pyruvate dehydrogenase complex (PDH), NAD-isocitrate dehydrogenase (ICDH) and α -ketoglutarate/oxaglutarate dehydrogenase (KGDH) are activated by calcium ions [Denton et al., 1980, Denton, 2009]. PDH is activated by a Ca^{2+} - stimulated pyruvate dehydrogenase phosphatase (PDP) and inactivated by a Ca^{2+} - independent kinase. The activity of the PDH can directly be inhibited by increasing the concentrations of acetylCoA/CoA, NADH/NAD⁺ and ATP/ADP ratios. ICDH and KGDH are two other enzymes that are allosterically regulated by Ca^{2+} and their sensitivity to Ca^{2+} is increased by increasing the ADP/ATP ratio. The activation of these enzymes is important in stimulation of the respiratory chain and increasing ATP supply under condition of increased ATP demands in mammalian cells [Denton, 2009]. In addition, the activity of glutamate dehydrogenase (GLDH) increases by rising the ADP/ATP ratio level (see Figure 4.11).

Measuring glutamine uptake rate of cells in no glucose medium and cells in 25 mM glucose (described in Section 3.3.4, Experiment I) shows that cells in no glucose medium have higher glutamine uptake rate after 4 h and 8 h of incubation (see Figure 4.12 A). We also showed that cells in no glucose medium have higher frequency of Ca^{2+} spikes (Figure 4.10

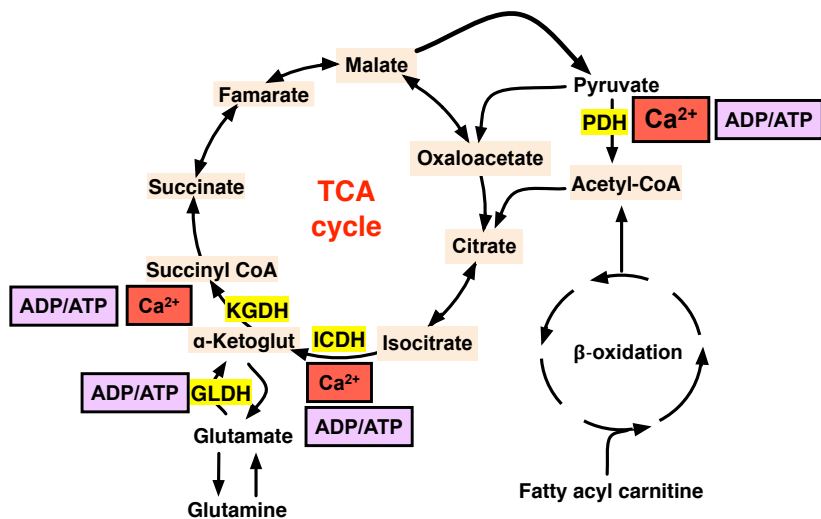


Figure 4.11. Schematic representation of the effect of Ca^{2+} and ADP/ATP ratio on the TCA cycle enzymes. (A) Calcium ions activates pyruvate dehydrogenase (PDH), NAD-isocitrate (ICDH) and oxoglutarate dehydrogenases (KGDH). The sensitivity of these enzymes to the Ca^{2+} increases by increasing the ADP/ATP concentration. Also the activity of glutamate dehydrogenase (GLDH) elevates by increasing the ADP/ATP ratio.

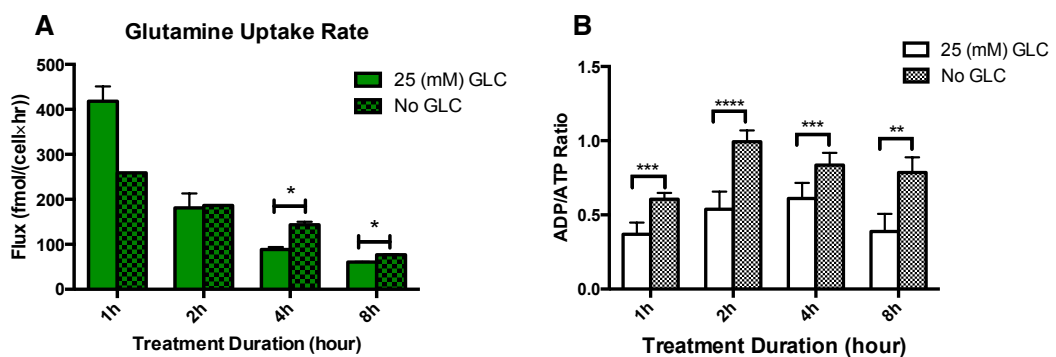


Figure 4.12. Effect of glucose deprivation on the ADP/ATP ratio and glutamine uptake rate. (A) Cells in no glucose medium have higher rate of glutamine uptake after 4 hours and 8 hours of incubation. (B) Cells in no glucose medium have higher ADP/ATP ratio compare to cells in 25 mM glucose. High ADP/ATP ratio leads to increasing glutamine uptake rate in cells in no glucose medium.

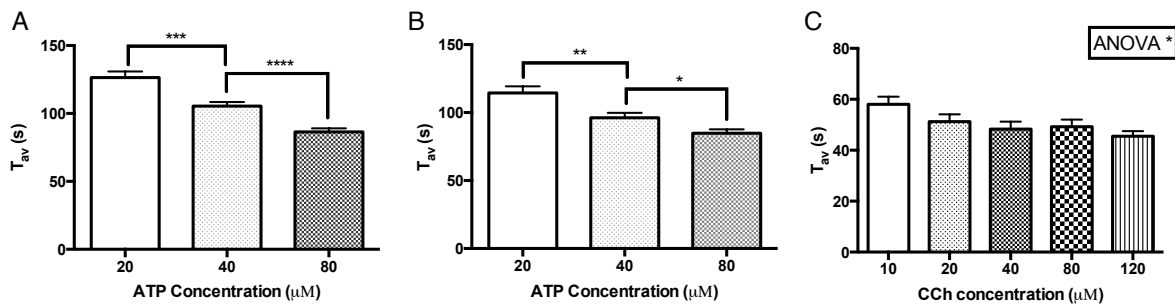


Figure 4.13. Period of Ca^{2+} spikes evoked by stimulation of GPCRs. (A) C8-D1A cells are in the medium containing 1 mM glucose. Increasing ATP concentration, increases frequency of Ca^{2+} spikes. (B) C8-D1A cells are in the medium containing 1 mM glutamine. Increasing ATP concentration, increases frequency of Ca^{2+} spikes. (C) HEK293 cells are in medium containing 5 mM glucose and 4 mM glutamine. Increasing CCh concentration increases frequency of Ca^{2+} signals.

B and C) and higher level of ADP/ATP ratio (Figure 4.12 B). Since glutamine is the substrate of KGDH enzyme and this enzyme is activated by Ca^{2+} and high ADP/ATP ratio (see Figure 4.11), we speculate that KGDH enzyme activity and subsequently glutamine uptake rate are regulated by the frequency of Ca^{2+} spikes. In other words, high ADP/ATP ratio leads to increasing frequency of Ca^{2+} signals (Figure 4.10) and subsequently high frequency of Ca^{2+} signals leading to increasing glutamine uptake rates in order to refill the TCA cycle and increase mitochondrial respiration. To test this hypothesis, we exposed cells with different concentrations of ATP, an agonist for stimulating GPCRs and releasing Ca^{2+} from IP_3R receptors, and then performed Ca^{2+} imaging which is described in the next section.

4.2.5 Stimulation of GPCRs Increases Frequency of Ca^{2+} Spikes

To explore the effect of Ca^{2+} frequency on the glutamine uptake rate, we first performed Ca^{2+} imaging of individual cells while exposing them to ligands that activate phospholipase C through GPCRs, thereby stimulating production of IP_3 and Ca^{2+} release from ER. We imaged C8-D1A astrocytic cell line and HEK293 while exposing them to ATP and carbochol (CCh), respectively. As Figure 4.13 shows increasing the concentration of ATP and CCh lead to increasing frequencies of Ca^{2+} spikes. Therefore we used these agonists in our other experiments to increase the frequency of Ca^{2+} spikes. Ca^{2+} imaging experiments are done according to the descriptions in Section 3.3.2 experiment II and III, and in the section 3.3.3.

4.2.6 Stimulation of GPCRs Increases Glucose and Glutamine Uptake Rate

As shown in the previous section, increasing the concentration of extracellular stimuli leads to increasing frequencies of Ca^{2+} signals. Therefore, to explore the effect of Ca^{2+} frequencies on the glutamine uptake rate, we exposed C8-D1A cells with different concentration of ATP. As Figure 4.14 A shows increasing ATP concentration leads to increasing glutamine uptake rates. We also measured the glucose uptake rate upon stimulation of GPCRs. The results show that increasing ATP and CCh concentration and as the result increasing frequencies of Ca^{2+} spikes lead to rising glucose uptake rate in C8-D1A (Figure 4.14 B, C) and HEK293 (Figure 4.14 D, E) in non-starved and starved cells, respectively.

4.2.7 Metabolic Decoding of Ca^{2+} Signals in Astrocytes and HEK293

We showed that increasing the concentration of extracellular stimuli increases frequency of Ca^{2+} spikes and also it leads to rising glucose and glutamine uptake rates. Putting together the results of Ca^{2+} imaging and metabolic flux analysis reveals that there is a well-defined relation between periods of Ca^{2+} signals and metabolic activity. To explore the relation between periods of Ca^{2+} signals and metabolite fluxes, we combined the plots of the periods of Ca^{2+} signals with the plots of the glucose and glutamine fluxes (Figure 4.15 C, F). The results indicate that glucose and glutamine fluxes decreases by increasing period of Ca^{2+} signals. In order to characterize the relation between metabolic flux and periods of Ca^{2+} signals, we measured periods and glucose fluxes of C8-D1A and HEK293 cells in 5 different concentrations of extracellular stimuli. The results reveals a sigmoidal like relation between glucose flux and period of Ca^{2+} signals (see Figure 4.16 C and F).

4.2.8 Effect of Ca^{2+} on Regulation of ATP Production

We showed that stimulating cells with extracellular stimuli increases the frequency of Ca^{2+} signals and also rises the glucose and glutamine uptake rate. To explore the consequences of these changes on the cellular ATP level, we measured the ADP/ATP ratio of C8-D1A cells while stimulating them with different concentrations of carbochol. In this experiment we stimulated cells with CCh instead of ATP because we wanted to prevent the possible mixture of ATP as the agonist with the intracellular ATP. The results show that increasing the concentration of CCh leads to decreasing ADP/ATP ratio. Thus, stimulating cells with extracellular agonist leads to increasing ATP supply (see Figure 4.17). The reason can be increasing frequency of Ca^{2+} signals and elevating the metabolite uptake rate as the result of increasing the concentration of extracellular stimuli which can lead to activating TCA enzymes through the stimulating Ca^{2+} -sensitive enzymes.

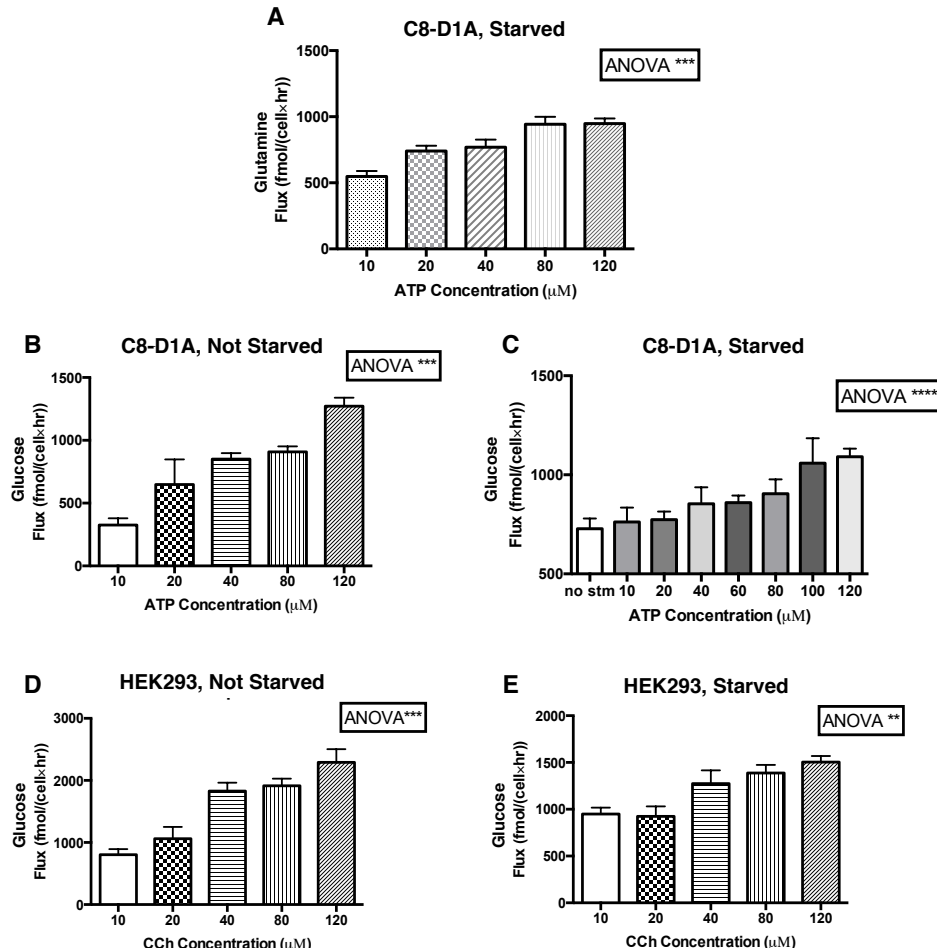


Figure 4.14. Glutamine and glucose uptake rate over stimulation of GPCRs in C8-D1A and HEK293 cells. Glucose and glutamine uptake rate increase by increasing the concentration of extracellular stimuli in the not starved and starved cells. (A) C8-D1A cells are starved and then medium is exchanged with medium containing 4 mM glutamine. Increasing the concentration of agonist increases glutamine uptake rate. (B) C8-D1A cells are not starved and the exchanged medium contains 5 mM glucose. Increasing ATP concentration elevates glucose uptake rate. (C) C8-D1A cells are starved and then medium is exchanged with medium containing 5 mM glucose and 4 mM glutamine. Increasing ATP concentration rises glucose uptake rate. (D) HEK293 cells are not starved and the medium is exchanged with the medium containing 5 mM glucose. Increasing CCh concentration increases glucose uptake rate. (E) HEK293 cells are starved and then medium is exchanged with medium containing 5 mM glucose. Increasing CCh concentration elevates glucose uptake rate.

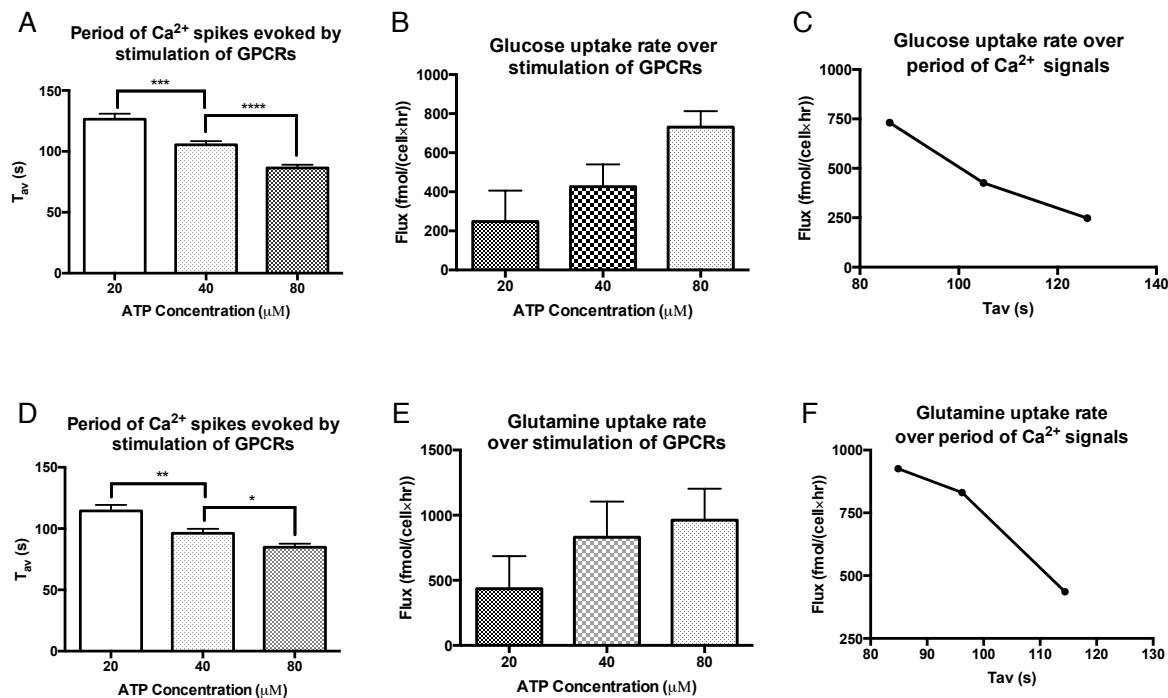


Figure 4.15. Glucose and glutamine uptake rates decrease with increasing periods of Ca^{2+} signals in C8-D1A cells. (A, B) Cells are starved and then medium is exchanged with medium containing 1 mM glucose. Calcium imaging experiment shows increasing ATP concentration leads to faster frequency of Ca^{2+} spikes. Measuring the glucose uptake rate shows that increasing ATP concentration leads to increasing glucose uptake rate. (C) Combining the A and B plots indicates that glucose uptake rate decreases with increasing periods of Ca^{2+} signals. (D, E) Cells are starved and then medium is exchanged with medium containing 1 mM glutamine. Stimulating cells with ATP indicates that increasing ATP concentration increases frequency of Ca^{2+} spikes and also elevates glutamine uptake rate. (F) Combining the plots D and E reveals that glutamine uptake rate decreases with increasing periods of Ca^{2+} signals.

4.3 Simulation of PINK1 Deficiency Using Ca^{2+} -mitochondrial Model

Mutations in PTEN-induced putative kinase 1 (PINK1) are a cause of early onset Parkinson's disease (PD). Loss of PINK1 function causes dysregulation of mitochondrial calcium homeostasis, resulting in mitochondrial dysfunction and neuronal cell death. In our recent paper, we reported that inactivation of the mitochondrial calcium uniporter (MCU), located in the inner mitochondrial membrane, prevents dopaminergic neuronal cell loss in pink1 mutant zebrafish via rescue of mitochondrial respiratory chain function [Soman et al., 2016].

PINK1 loss of function is associated with reduction in glucose uptake through the plasma membrane in human and mouse neurons. Reduced substrate delivery causes the impairment of respiration and reduced mitochondrial membrane potential in cells that lack PINK1.

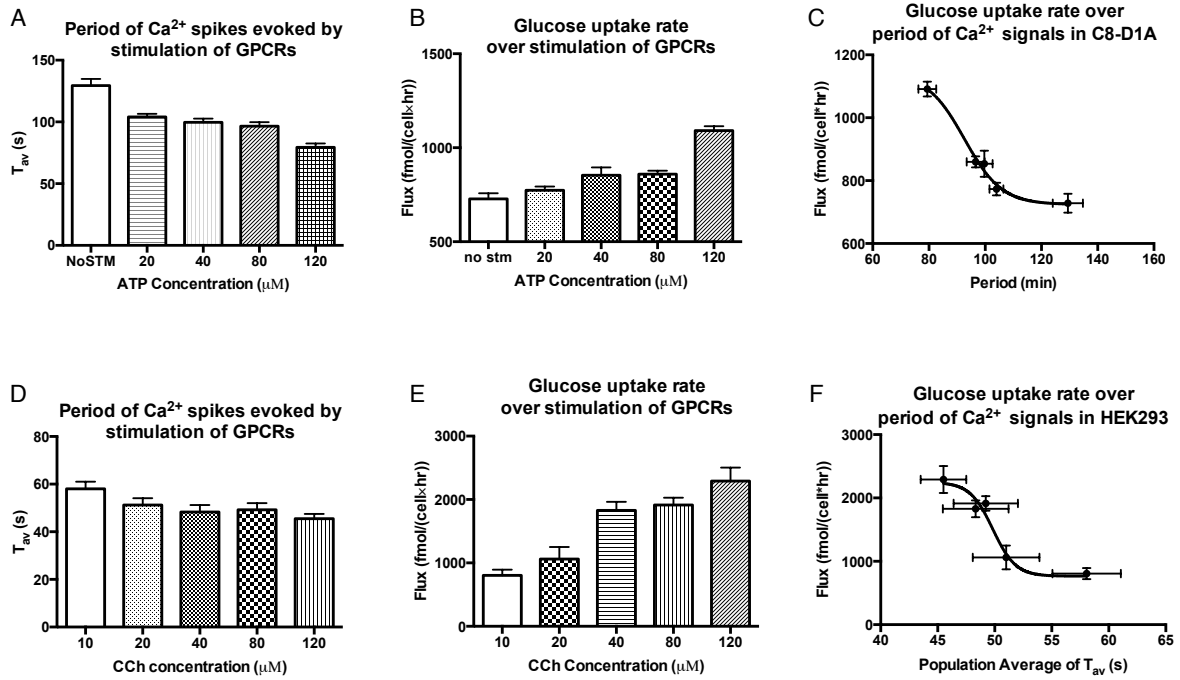


Figure 4.16. Metabolic decoding of Ca^{2+} signals in astrocytes and HEK293 cells. Increasing the concentration of extracellular agonist increase frequency of Ca^{2+} spikes and elevates glucose uptake rate in astrocytes (A, B) and in HEK293 (D, E) cells. The C and F plots reveal a sigmoidal relation between glucose flux and periods of Ca^{2+} signals.

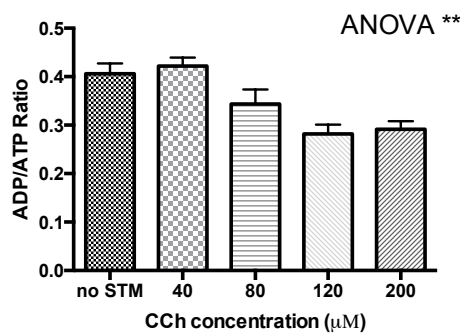


Figure 4.17. Increasing ATP supply upon stimulation of GPCRs.

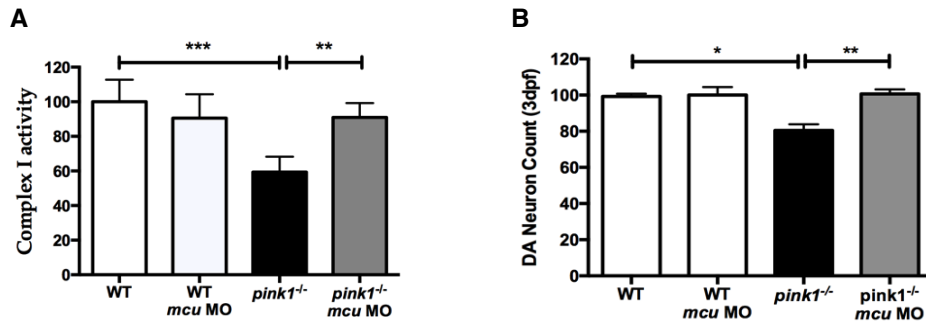


Figure 4.18. Effect of PINK1 deficiency on the zebrafish larvae DA neural cells and the rescue mechanism. A) Mitochondrial complex I activity is restored in 5 dpf (days post fertilized) *pink1^{-/-}* following *mcu* k/d (** P = 0.0071). The scale on the y axis reflects % of complex I activity compared to wt controls. B) Dopaminergic (DA) neuronal cell count in wt, wt MCU (wt microinjected with morpholino (MO) against *mcu*), *pink1^{-/-}*, *pink1^{-/-}* MCU (*pink1^{-/-}* microinjected with MO against *mcu*) zebrafish larvae at 3 dpf. DA neuronal cell count is reduced in *pink1^{-/-}* (* P = 0.012) but completely rescued after MCU inactivation (** P = 0.0085). The scale on the y axis reflects % of DA neurons compared to wt controls [Soman et al., 2016].

PINK1 deficiency is also linked to dysfunction of mitochondrial $\text{Na}^+/\text{Ca}^{2+}$ exchanger which leads to mitochondrial Ca^{2+} accumulation and increased ROS production [Gandhi et al., 2009]. In our paper, we reported specific transcriptional upregulation of *micu1* in *pink1^{-/-}* zebrafish larvae. MICU1 is a subunit of MCU complex which has stimulatory effect on the MCU activity. At the large cytosolic Ca^{2+} concentration, MICU1 is activated and leads to rapid mitochondrial Ca^{2+} accumulation [Patron et al., 2014]. We experimentally showed that PINK1 deficiency leads to a marked decrease in the activity of complex I in the mitochondria and also reduce the Dopaminergic (DA) neuronal cell count in the zebrafish larvae [Soman et al., 2016]. We further showed that down regulation of MCU leads to restoring the activity of mitochondrial complex I and increase the number of DA neuronal cell (see Figure 4.18)

To simulate the PINK1 deficiency effect by our described Ca^{2+} - mitochondrial metabolism model, we increased the flux through the MCU by 10% and decreased the flux rate of the $\text{Na}^+/\text{Ca}^{2+}$ exchanger by 10% as well as the glucose uptake rate by 30%. These values were estimated by scanning the model parameters in the physiological range in order to reproduce the experimental results. While the resulting cytosolic Ca^{2+} dynamic is hardly modified compared to *wt* condition (upper panel Figure 4.19B), the mitochondrial Ca^{2+} concentration (Ca_m) and oxygen flux (J_o) exhibit a significant difference (middle panel Figure 4.19B). In particular, the amplitude of J_o that describes the oxygen consumption rate and is therefore a measure of respiration activity, decreases dramatically due to mitochondrial Ca^{2+} overload. This effect can be compensated in the model by decreasing MCU activity by 14% preventing mitochondrial Ca^{2+} overload and restoring respiration (lower panel Figure 4.19B).

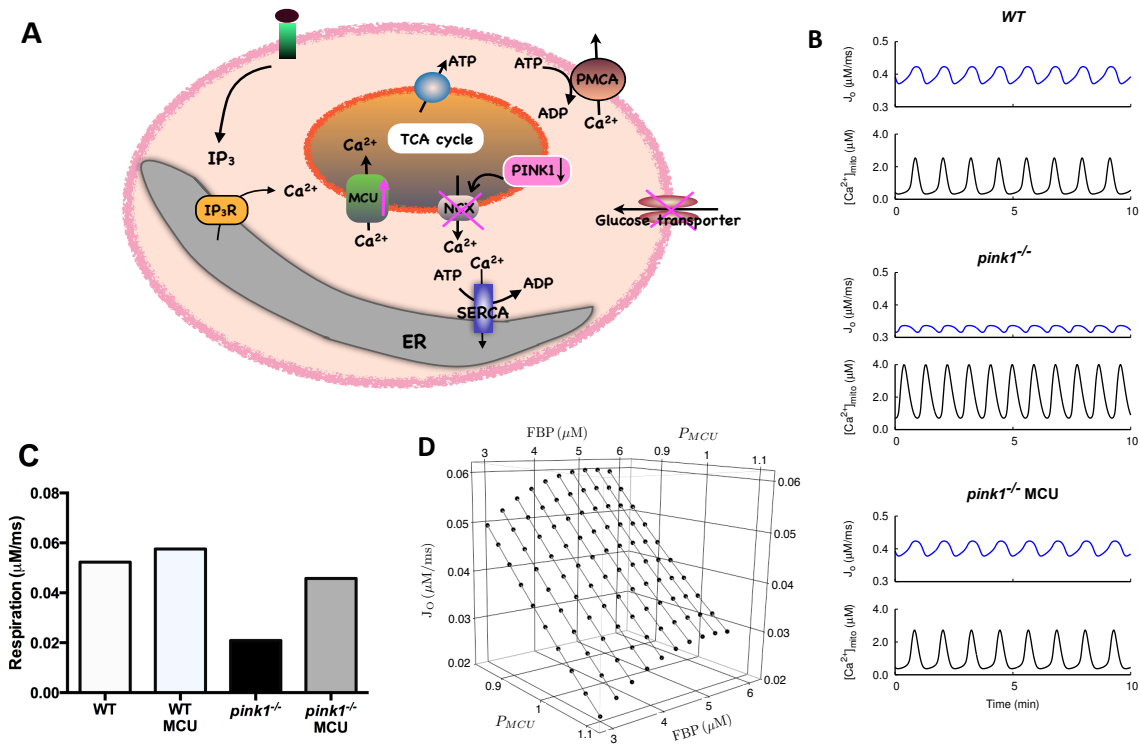


Figure 4.19. A) Scheme of the rate equation model and the considered effect of PINK1 deletion. The effect of PINK1 deficiency on glucose uptake and mitochondrial Ca²⁺ handling is indicated in pink color. B) Dynamic modeling results of mitochondrial Ca²⁺ concentrations and resulting oxygen flux (J_o) for *wt*, *pink1^{-/-}* and *pink1^{-/-} + MCU* down regulation conditions. Compared to the *wt* scenario (top panel), *pink1^{-/-}* leads to mitochondrial Ca²⁺ overload and subsequently to smaller J_o amplitudes indicating decreased respiration (middle panel). This effect could be compensated by down regulation of MCU reestablishing mitochondrial Ca²⁺ homeostasis and mitochondrial activity (bottom panel). C) Respiration activity for the different conditions. The oxygen consumption rate as an indicator for respiratory activity exhibit a similar pattern to the dopaminergic neuronal survival and complex I activity (see Figure 4.18) D) Intensive parameter scans have shown the stability of the compensatory effect of MCU down regulation compared to *wt* conditions ($P_{\text{MCU}} = 1$) on respiration measured by oxygen consumption.

The different scenarios are summarized in Figure 4.19 C with respect to the oxygen consumption rate corresponding to respiratory activity. The described flux modifications lead to a very similar picture as in the experimentally determined neuronal survival. Since neuronal survival will not depend linearly on respiration activity, we performed comprehensive model parameter scans to test the stability of our results. Figure 4.19 D exhibits a parameter scan with respect to MCU activity (P_{MCU}) and fructose-bisphosphate (FBP) concentration that indicates the glucose uptake rate. The obtained dependency of respiration on P_{MCU} and FBP as well as similar results from additional parameter scans demonstrate that the mechanistic modeling supporting the experimental findings do not depend on specific parameter combinations but are robust for a wide physiological parameter range.

4.4 CaSiAn: Calcium Signaling Analysis Software

Discriminating Ca^{2+} signals requires quantifying the kinetics of calcium ions on the basis of spike descriptors such as amplitude, spike width and frequency of Ca^{2+} spikes. Measurement of spike descriptors in the first step requires finding peaks/nadirs of each Ca^{2+} spike. However, accurate detection of peaks/nadirs of Ca^{2+} signals is a challenging task. First because of the variability of spikes in terms of amplitude and interspike intervals in the Ca^{2+} signals. Second, because of the noisy observations that happen due to the imaging method such as photon shot noise, background fluorescence and typically low temporal resolution. Third, because of the possible existing artifacts in the signals like signal baseline variations or unwanted peaks in the signal occurring by floating particles that are created during imaging. The Ca^{2+} signal artifacts are mainly created due to the issues of imaging method like fluorophore leaking, photobleaching and phototoxicity [Grienberger and Konnerth, 2012].

To address these issues, we developed the CaSiAn (**C**alcium **S**ignaling **A**nalysis) tool, an open source software implemented with java language that provides a full-fledged user interface allowing biologists to easily analyze a large amount of Ca^{2+} signals, tune peak detection parameters for each signal, examine detected peaks/nadirs of Ca^{2+} signals and access the quantified descriptors of Ca^{2+} spikes in the form of an excel or text file. Figure 4.20 shows the graphical user interface of CaSiAn software.

Figure 4.21 shows the steps which users should perform in CaSiAn in order to analyze the Ca^{2+} signals. Ca^{2+} signals are determined by averaging or getting the median of pixel intensities in the regions of interest from a sequence of fluorescence images captured during a period of time. After performing Ca^{2+} imaging, Ca^{2+} signals should be extracted from regions of interest and then be loaded in CaSiAn software. In CaSiAn, user can determine the part of signal that is interesting to analyze. The user can define the signal peaks/nadirs by setting just one parameter namely the Peak threshold parameter. This parameter defines

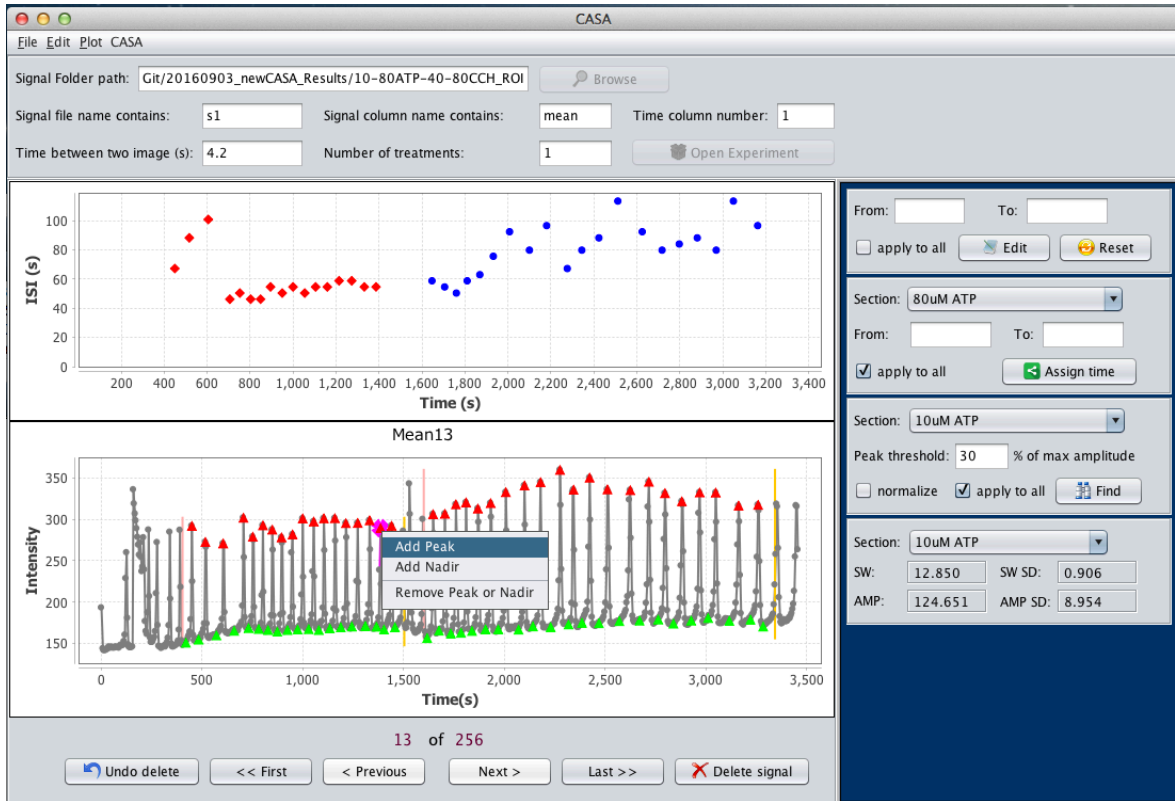


Figure 4.20. Graphical user interface of CaSiAn software

as the percentage of maximum amplitude that occurs in the signal. The complete algorithm for finding peak/nadir of signals is described in appendix Section A.1. The user can also remove the signal baseline and normalize the signal intensities by fitting different curves to the signal baseline (see appendix Section A.2).

By finding the signal peak/nadir, CaSiAn extracts the features of Ca^{2+} signals automatically (algorithms are described in the appendix Section A.3). These features are (see Figure 4.21 D):

- Interspike intervals (ISI): the time between two consecutive peaks.
- Average of ISIs (T_{av}) and standard deviation of ISIs (σ).
- Spike amplitude (AMP): the magnitude of the difference between spike's extreme intensities.
- Spike width (SW): the duration of the spike when the Ca^{2+} channels are highly activated and the intracellular Ca^{2+} concentration is higher than the base level of cellular Ca^{2+} concentration. CaSiAn identifies the Ca^{2+} spike width as the duration of spike at 20% of the spike amplitude.
- Time to peak (TTP): the time difference between the peak time and the nadir time of the spike.

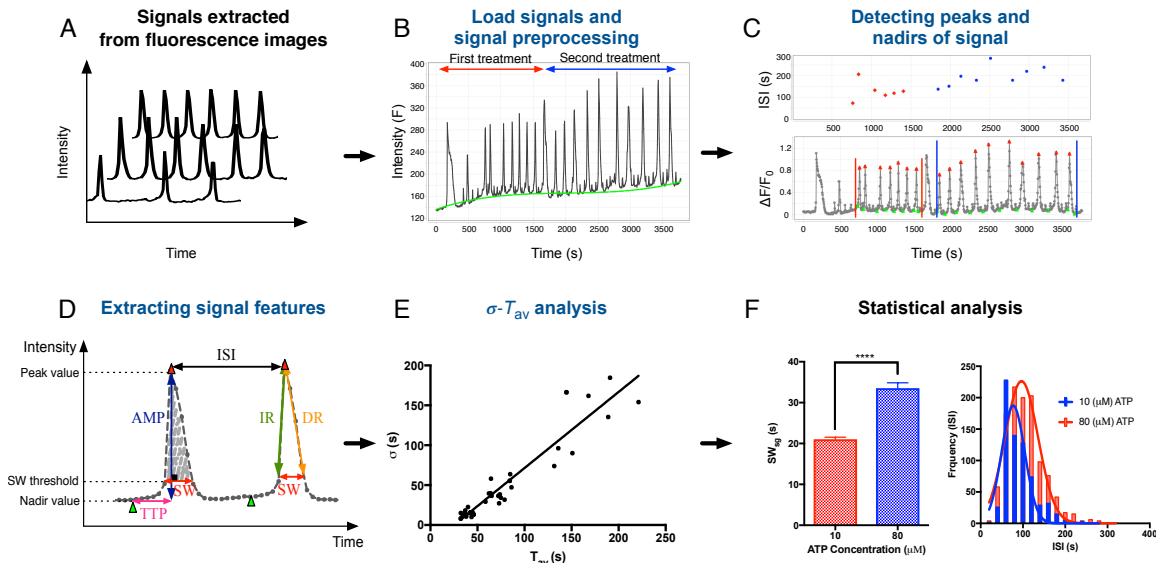


Figure 4.21. Workflow of CaSiAn. A) Time course data extracted from fluorescence images are loaded into CaSiAn. B) Preprocessing allows for defining different analysis periods, normalisation and background removal by several non-linear fitting methods for each individual signal. C) In the resulting data, peaks and nadirs are automatically detected by threshold parameters interactively adjustable in the GUI. Misclassified peaks and nadirs can be interactively added or removed leading to identification of individual ISIs. D) Based on the processed time courses, CaSiAn determines signal properties like ISI, amplitude, spike width and more. E) After automated processing of all signals, CaSiAn offers to plot the $\sigma - T_{av}$ relation where each dot correspond to an individual signal. This relation can be further analyzed in an interactive manner. F) Finally, all processed signals including ISI detection can be saved in a single pdf file and determined signal characteristics can be exported as csv or excel files for further analysis.

- Effective area under spike (AUS): the surface above the horizontal line $Intensity = TH_{SW}$ and the spike function, where TH_{SW} is the threshold of spike width. CaSiAn estimates AUS using trapezoidal method.
- Ca^{2+} increasing rate (IR) and Ca^{2+} decreasing rate (DR): the slope of upward edge of each spike defines the IR and the slope of downward edge of each spike defines the DR. CaSiAn also measures the increasing rate and the decreasing rate of the whole Ca^{2+} signal by averaging the IRs and the DRs of all spikes in the Ca^{2+} signal, respectively.
- CaSiAn also measures: mean of intensities, standard deviation of intensities, signal-to-noise ratio, average of the peak values and average of the nadir values of each Ca^{2+} signal.

After extracting the features of Ca^{2+} signals, the user is able to see the $\sigma-T_{av}$ plot for the all signals and filter for signals with specific number of peaks. CaSiAn fits a linear line to the points in the $\sigma-T_{av}$ plot and shows the slope (α) of the fitted line to the user. The α indicates the signal coefficient of variation and were shown to be cell type and pathway specific [Skupin and Falcke, 2010, Thurley et al., 2014]. Smaller slope shows the higher

signal-to-noise ratio and longer recovery periods in the Ca^{2+} signals.

In this thesis, we analyzed the Ca^{2+} signals of all experiments using CaSiAn software and compared the T_{av} of Ca^{2+} signals in different experiments. CaSiAn is an open source or, more specifically, free software. It is implemented by object-oriented approach with java language in the Netbeans IDE. It contains 25 classes and roughly 13K lines. CaSiAn uses Jfreechart library (<http://www.jfree.org/jfreechart/>) to display different plots. The functionalities of CaSiAn have been tested with around 100 case studies. Running CaSiAn requires installing Java Runtime Environment (JRE) version 1.8.0. We have tested CaSiAn on Mac, Windows XP, 7 and Server 64-bit version. CaSiAn is available for download at (<http://r3lab.uni.lu/web/casa/>).

CaSiAn is a user-friendly tool that quantifies Ca^{2+} signal descriptors fast and precisely. The tool enables biologists to easily visualize and explore a large amount of signals, remove the background intensities and normalize signals, detect and examine signal peaks and nadirs, look into the ISIs distributions and access the quantified descriptors of Ca^{2+} signals. Quantifying Ca^{2+} spike features helps biologist to asses the effect of a treatment on the shape of Ca^{2+} signals and more importantly, helps them to highlight the potential pathways and intracellular processes that may cause to a typical signal profile.

4.5 Summary

This chapter presented the main results of the thesis where we started from computational model predictions and subsequently validated them by experiments. Careful analysis of the experimental data has then led to new experimental finding on a potential metabolic control mechanism.

First, we showed that the ATP-dependent model is more robust compare to ATP-independent model in case of cellular ATP perturbation. We showed by model that decreasing the mitochondrial substrate leads to decreasing average cellular ATP level and increasing frequency of Ca^{2+} signals. The model predictions were approved experimentally since cells in the no glucose medium exhibit higher ADP/ATP ratio and higher frequency of Ca^{2+} signals. We showed that high frequency of Ca^{2+} signals in the cells with no access to glucose is a mechanism for compensating reduced ATP production by refilling TCA cycle with glutamine. Measuring the glucose and glutamine uptake rates while stimulating GPCRs showed a well-defined relation between stimulus intensity and metabolite uptake rate. We could show a sigmoidal relation between glucose uptake rate and periods of Ca^{2+} signals which indicates the metabolic decoding relation of cytosolic Ca^{2+} signals. We also showed the application of our developed Ca^{2+} - mitochondrial model in simulating PINK1 deficiency. At the end,

we described our developed software for analyzing intracellular Ca^{2+} signals.

Chapter 5

Discussion

The present thesis applied a systems biology approach to the crosstalk between Ca^{2+} signaling and mitochondrial metabolism. We started from literature based knowledge and developed a usable model for the crosstalk between IP_3 - mediated Ca^{2+} signaling and mitochondrial metabolism. The goal was to integrate the model of mitochondria established by Bertram and coworkers with a well-established model of IP_3 - mediated Ca^{2+} signaling in order to investigate the interaction between Ca^{2+} signaling and mitochondrial metabolism [Bertram et al., 2006]. With the combined model we could show: 1) mitochondrial Ca^{2+} oscillation follow the same pattern as cytosolic Ca^{2+} oscillation, 2) increasing mitochondrial Ca^{2+} concentration following elevating cytosolic Ca^{2+} concentration leads to increasing mitochondrial ATP production and 3) decreasing mitochondrial substrates change the profile of Ca^{2+} signals and results in increasing frequency of Ca^{2+} spikes which is in agreement with experiments.

Our developed Ca^{2+} - mitochondrial model is a periodic, complex and highly non-linear system. It is possible to simulate periodic behaviors by linear ODE models of order 2, but they are fragile or non-robust to small perturbations in the model and also their oscillation characteristics depend on the initial condition. Thus, biological systems which exhibit periodic behavior are modeled by non-linear ODEs, which create limit cycles. In our model, the Ca^{2+} oscillation behavior is modeled based on known biological mechanism which is periodic Ca^{2+} releasing from IP_3 Rs and Ca^{2+} removing to ER through the SERCA pumps. Also the corresponding flux equations given in Section 3.1.1 reflect the known molecular mechanisms and include non-linearities. The parameter values of this non-linear model are identified by performing parameter scans in the way that system variables oscillate in physiological range and the results of the model simulations are in agreement with the captured experimental observations.

However, the current model (like every model) is a simplified and abstract model, which

does not consider all details like the stochastic properties of IP₃Rs or the glycolysis pathway. In the presented model, the Ca²⁺ oscillation does not arise from hierarchical structure of IP₃Rs clusters and the random behavior of IP₃Rs, which have been observed experimentally and theoretically as the mechanism of Ca²⁺ spiking in the cells [Skupin and Falcke, 2009]. Our model considers three compartments: ER, cytosol and mitochondria and assumes that all fluxes are averages on the volume of a given intracellular compartment. Therefore our ODE model neglects the spatial scale of the fluxes, which can limit it for solving problems that can be investigated only in models that consider spatial scale. One of the relevant examples is the effect of SERCA expression on the amplitude and spike width of Ca²⁺ signals that we investigated in [Komin et al., 2015]. As we discussed there, the special model could show the exponential decay of amplitude and spike width in dependence of SERCA pump strength, which were in agreement with experiments while the rate equation model failed to show the experimental observations.

However, we showed that our proposed deterministic model can reproduce the experimental results about Ca²⁺ frequency dependency, which shows the same predictive power as the stochastic models [Cao et al., 2014, Fall and Keizer, 2001]. Therefore, to obtain qualitative predictions of how oscillation frequency depends on parameters, the proposed ODE model is sufficient. We also showed that considering the ATP dependency of SERCA and PMCA pumps enhances the coupling of the cytosolic Ca²⁺ signals with the mitochondrial ATP production and also creates more robust ATP signaling profile if a perturbation occurs in the system.

We showed by modeling that decreasing cytosolic ATP levels lead to increasing frequency of Ca²⁺ signals (Figure 4.7) and this result was validated also experimentally (see Figure 4.10). This result may show a frequency encoding mechanism of the intracellular ATP level. Since mitochondria exhibit a similar temporal Ca²⁺ profile as cytosolic Ca²⁺ oscillation, the frequency encoded information can be transferred into mitochondria and be decoded in the mitochondrial matrix through the Ca²⁺-regulated dehydrogenases. It is shown that the activity of mitochondrial dehydrogenases increases in response to increasing mitochondrial Ca²⁺ concentration in the steady state [Denton et al., 1980]. Pyruvate dehydrogenase complex (PDH) is one of the key enzymes in oxidation of pyruvate by the TCA cycle. PDH is activated by a Ca²⁺-stimulated pyruvate dehydrogenase phosphatase (PDP) and inactivated by a Ca²⁺-independent kinase. NAD-isocitrate dehydrogenase (ICDH) and α -ketoglutarate/oxoglutarate dehydrogenase (KGDH) are two other enzymes that are allosterically regulated by Ca²⁺ and their sensitivity to Ca²⁺ is lowered by increasing the ATP/ADP ratio. Activation of dehydrogenases occurs at relatively low calcium concentrations (less than 20 μ M). Calcium, in high concentrations (greater than 100 μ M), however, inhibits α -KGDH [Lai and Cooper, 1986], ICDH [Bulos et al., 1984] and PDH [Rex Sheu et al., 1985].

This effect could significantly contribute to the damaging effects of high calcium concentration in neurons under pathological conditions [Tretter and Adam-Vizi, 2005].

Exposing cells to extracellular stimuli like hormones and neurotransmitters changes the cytosolic Ca^{2+} concentration. Depending on the stimuli lead to involvement of different Ca^{2+} channels and Ca^{2+} binding proteins, a specific Ca^{2+} signal is induced. The process of building up a unique signal that can be associated with a specific stimulus is called information encoding [Smedler and Uhlén, 2014]. We showed by modeling and experimentally that increasing the concentration of extracellular stimuli leads to increasing frequency of Ca^{2+} spikes (Figure 4.13). It has been shown that despite variability in the frequency of Ca^{2+} spikes between cells, changes in extracellular stimulus intensity are encoded by fold changes in the average stochastic period of the interspike intervals ($T_{\text{av}} - T_{\text{min}}$). The following equation shows the relation between stimulus intensity and T_{av} , which indicates an exponential dependence between the stimulus concentration and periods of Ca^{2+} signals [Thurley et al., 2014]:

$$T_{\text{av}} = e^{-\gamma([stm] - [stm_{\text{ref}}])} (T_{\text{av,ref}} - T_{\text{min}}) + T_{\text{min}} \quad (5.1)$$

where $[stm]$ is the concentration of stimulus, T_{av} is the period of Ca^{2+} signals upon stimulation with $[stm]$, T_{min} is the sum of the spike duration and refractory period of T_{av} , $T_{\text{av,ref}}$ reflects the average ISI measured at a reference stimulus concentration $[stm_{\text{ref}}]$ and γ describes the sensitivity of the stochastic period of T_{av} to $[stm]$. Therefore the signal transduction can occur through frequency modulation of Ca^{2+} signals.

The decoding of Ca^{2+} signals is typically performed by enzymes that have multiple Ca^{2+} binding residues and can regulate differentially its total phosphorylation, thereby activating distinct cellular programs [Smedler and Uhlén, 2014]. A study on single hepatocytes has shown that mitochondrial Ca^{2+} oscillations stimulate and controls Ca^{2+} -sensitive mitochondrial enzymes [Hajnóczky et al., 1995]. In this study, hepatocytes were stimulated by vasopressin and then the cytosolic Ca^{2+} , the concentration of NADH and FADH_2 were monitored by fluorescence imaging. Studies in cat brain [Jöbsis et al., 1971], brain slices [Lipton, 1973] and cardiomyocytes [Eng et al., 1989] all showed Ca^{2+} dependent changes in mitochondrial function in response to physiological stimulation.

This thesis showed experimentally that stimulating GPCRs by extracellular agonists leads to increasing glucose and glutamine uptake rates (Figure 4.14). We can explain these observations by two potential mechanisms: 1) released Ca^{2+} from IP_3Rs is taken up by mitochondria leading to activation of PDH and KGDH enzymes and consumption of glucose and glutamine substrates. This may result in more glucose and glutamine uptake from the medium by the cell in order to refill the TCA cycle. 2) It has been shown that the produced ROS as the result of elevated Ca^{2+} concentration in the mitochondrial matrix (which cause

activating TCA enzymes and ETC) leads to up-regulation of GLUT protein expression and increases glucose uptake [Liemburg-Apers et al., 2015]. Thus, it is possible that ROS triggers glucose uptake and couples Ca^{2+} signaling to energy metabolism.

We also showed a sigmoidal relation between the frequency of Ca^{2+} signals and glucose flux in HEK293 and astrocytes (Figure 5.1 B and C). The results obtained in 1980 using rat heart mitochondria [Denton et al., 1980] showed that increasing extramitochondrial calcium ion concentrations in the physiological range increase the activity of both PDH and KGDH within mitochondria (Figure 5.1 A). Since glucose and glutamine are the substrates of PDH and KGDH enzymes and there is correlation between substrate availability and the enzyme activity, based on Figure 5.1, we speculate that the activity of PDH and KGDH are regulated by frequency of Ca^{2+} spikes. The regulation of the Ca^{2+} - sensitive mitochondrial dehydrogenases by the frequency of Ca^{2+} signals also has been shown by the Hajnoczky et al. study [Hajnóczky et al., 1995]. In this study, they conclude that the activity of Ca^{2+} - sensitive mitochondrial enzymes can be regulated over a broad range by the frequency of the oscillating Ca^{2+} signals and by contrast, the maintained high Ca^{2+} concentration cannot sustain the activation of the mitochondrial enzymes. We also simulated the relation between frequency of Ca^{2+} spikes and the average flux of PDH enzyme with our Ca^{2+} - mitochondrial model (Figure 5.1 E). This figure shows that the found sigmoidal decoding relation is a promising result that should be followed up to establish a new integrator of Ca^{2+} spikes.

Regulation of rate limiting enzymes of the TCA cycle by the frequency of Ca^{2+} signals reveals that Ca^{2+} acts like a mediator which first reliably encodes information content of extracellular stimuli and second transfer this information into mitochondria, which are then decoded by TCA cycle enzymes.

Astrocytes are the most abundant cell type in the brain. They exhibit a large number of GPCRs linked to Ca^{2+} mobilization from internal store which can be activated *in situ* by application of agonists and also by neurotransmitters released from presynaptic terminals [Agulhon et al., 2008]. Increasing astrocytic Ca^{2+} concentration evoked by neurotransmitters demonstrates the existence of neuron-to-astrocyte communication through the Ca^{2+} elevations. Neurons release glutamate and GABA in response to electrical activation and the released neurotransmitters cause increasing Ca^{2+} concentration in astrocytes [Porter and McCarthy, 1996, Kang et al., 1998]. A study on the isolated rat retina showed that neuron-to-glia signaling in the retina is mediated by ATP release from neurons and activation of glial purinergic receptors [Newman, 2005]. Astrocytes to neuron signaling has also been observed. Increasing astrocytic Ca^{2+} concentration results in the release of gliotransmitters, primarily glutamate, and modulation of the electrical excitability of neighboring neurons [Newman, 2003a, Fellin and Carmignoto, 2004]. In both culture and brain-slice

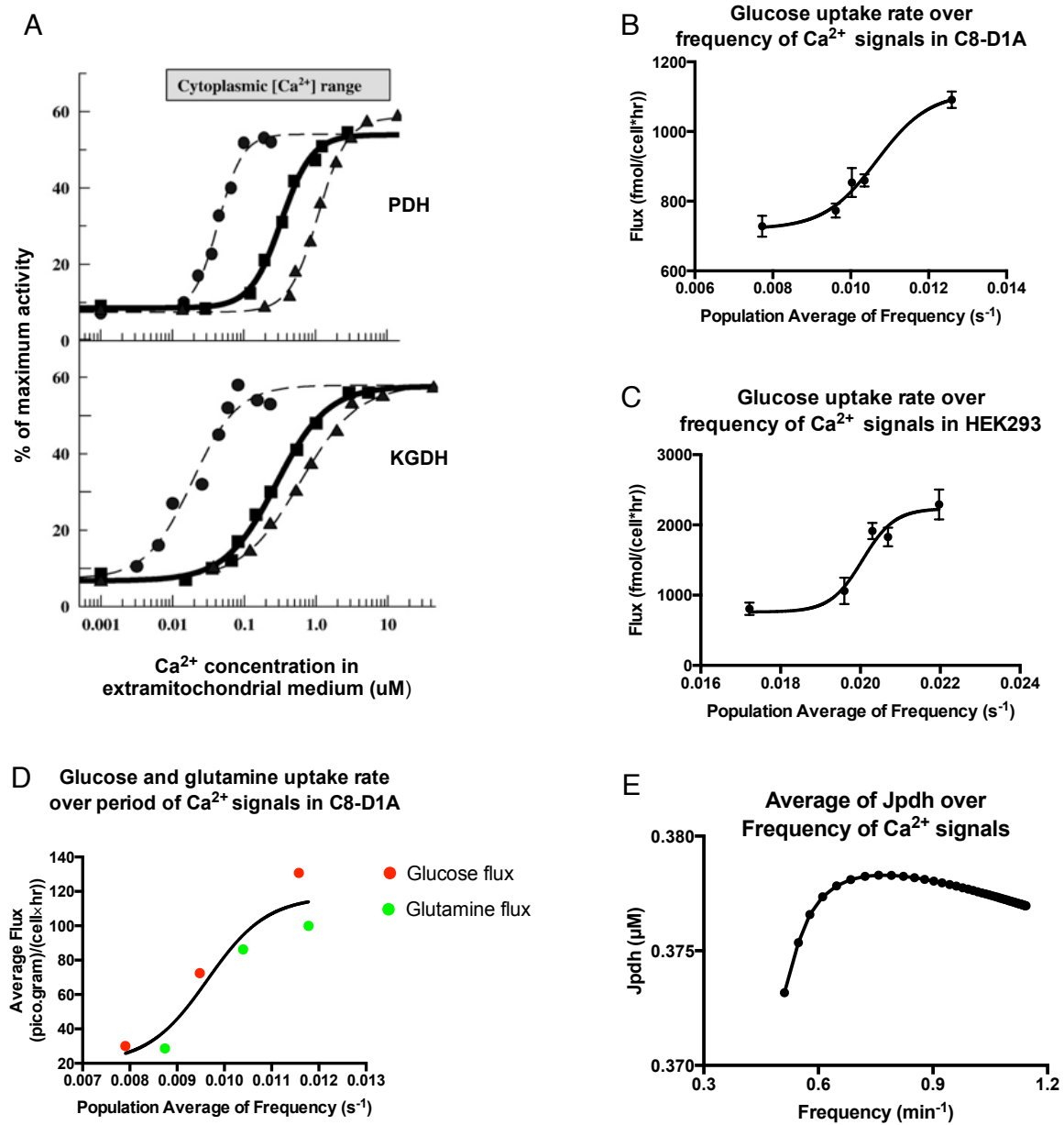


Figure 5.1. Metabolic decoding of Ca^{2+} signals. (A) The activity of PDH and KGDH increases in the coupled rat heart mitochondria in response to increasing mitochondrial Ca^{2+} concentration. The results of these experiments are fully described in [Denton et al., 1980, Denton, 2009]. (B, C) The glucose flux increases by increasing frequency of Ca^{2+} signals in C8-D1A and HEK293 cells. There is a sigmoidal relation between the glucose uptake rate and frequency of Ca^{2+} signals. (D) The glucose and glutamine flux over frequency of Ca^{2+} signals are combined in one graph. This graph also reveals a sigmoidal relation between glucose and glutamine fluxes and frequency of Ca^{2+} signals. (E) The model simulation of the relation between frequency of Ca^{2+} spikes and the average flux of PDH enzyme. Although the model cannot exhibit the complete shape of sigmoidal relation, but we can see increasing the activity of PDH enzyme for the frequencies higher than 0.5 min^{-1} .

preparations, increases in Ca^{2+} concentration result in a release of glutamate from astrocytes [Newman, 2003b]. Ca^{2+} excitability in astrocytes is a key element in the information exchange between astrocytes and neurons.

In relevance to astrocyte-to-neuron communication, the observed metabolic decoding of Ca^{2+} spikes in our experiments may be a way for transferring information between astrocytes and neurons. We showed that glucose and glutamine uptake rate increases in response to exposing astrocytes to extracellular stimuli. Neurons can stimulate Ca^{2+} signaling in astrocytes by releasing neurotransmitters. Thus neurons can increase glucose and glutamine uptake rates by releasing neurotransmitters and stimulating Ca^{2+} signals in neighboring astrocytes. The up taken glucose or glutamine may be converted to lactate and deliver back to neurons as energy substrates or may be metabolized in the TCA cycle of astrocytes.

Astrocytes take up glucose while they take up released glutamate at the synapse together with 3 Na^+ ions. Extruding Na^+ by the action of the Na^+/K^+ ATPase, consumes ATP, that triggers glucose uptake from the circulation through the glucose transporter [Anderson and Swanson, 2000]. Released glutamate from neurons at the synapse also stimulate Ca^{2+} signaling in astrocytes and from our experiments, stimulating Ca^{2+} signaling may be additional reason for increasing glucose uptake while astrocytes are exposed to large concentration of glutamate.

In our experiments, we observed that stimulation of C8-D1A astrocytic cells with extracellular ATP evokes an intercellular Ca^{2+} wave which propagates between glial cells. These waves could occur by diffusion of IP_3 through gap junctions between astrocytes which are close to each other or could happen by release of ATP and results in Ca^{2+} wave among distant cells.

As an another application of the systems biology approach in solving biological problems we showed the efficiency of our developed *in silico* model in predicting experimental results of PINK1 deficiency (see Section 4.3). In the model, we decreased the parameter values of the mitochondrial $\text{Na}^+/\text{Ca}^{2+}$ exchanger flux (J_{NCX}) and the mitochondrial carbon input (FBP concentration) and increased the flux of mitochondrial Ca^{2+} uniporter (J_{MCU}) as the result of PINK1 deficiency. Then the model simulation showed decreased mitochondrial respiration which was in agreement with experiments on the zebrafish larvae DA neural cells. We could also show by modeling that down regulation of MCU channel restore mitochondrial respiration which was again in agreement with experiments.

This dissertation showed that compromised cellular metabolism modifies the profile of Ca^{2+} signals and Ca^{2+} spikes, which in turn can change the metabolic profile in electrically non-excitable cells, HEK293 and astrocytes. Thus, the stability of the crosstalk between

Ca^{2+} signaling and energy metabolism is essential for the proper cellular function. Disturbance of this interplay causes Ca^{2+} dyshomeostasis and energy metabolism dysregulation which may lead to cell death.

Chapter 6

Conclusion and Future Perspectives

6.1 Conclusion

Cells communicate with each other and to the environment through sending and receiving signals. Cells receive messages through the receptors on the cellular plasma membrane which then are transferred to the cellular processes through the second messengers. Ca^{2+} is a versatile second messenger that regulate many diverse cellular processes. On the other hand, signaling and information processing consume energy. This energy is mostly provided by the mitochondria. Thus, Ca^{2+} signaling and energy metabolism interact in order to orchestrate the chemical reactions sustaining life. Since Ca^{2+} signaling and mitochondrial metabolism are itself a complex system, their combination is even a bigger and more complex system, therefore its understanding needs a mechanistic approach that can tackle this complexity. In this thesis, we studied the crosstalk between Ca^{2+} signaling and mitochondrial metabolism using a systems biology approach. For this purpose, we combined mathematical modeling with Ca^{2+} imaging and metabolic flux analysis. The developed *in silico* model integrated a well-established model of IP_3 -mediated Ca^{2+} signaling with a simplified model of mitochondrial Ca^{2+} handling and metabolic function. The incorporation of mitochondria in the Ca^{2+} signaling model results in more robust system in case of perturbation of the intracellular ATP level. This model showed that decreasing mitochondrial substrates leads to decrease the intracellular ATP level and mitochondrial Ca^{2+} overload as well as increasing frequency of intracellular Ca^{2+} spikes. These results were confirmed experimentally by performing Ca^{2+} imaging and measuring the frequency of Ca^{2+} signals in the starved cells. Further, we quantified glucose and glutamine uptake rates for distinct stimulated Ca^{2+} signals. The analysis showed a well defined relation between the frequency of Ca^{2+} spikes and glucose/glutamine uptake rate. These results indicate that the information content of intracellular ATP level as well as the extracellular agonist are encoded in the frequency of Ca^{2+} spikes which then are transferred into energy metabolism system. These data are decoded

by the energy metabolism through increasing glucose/glutamine uptake rate or may be transferred into mitochondria leading to activating Ca^{2+} -sensitive mitochondrial enzymes and increasing ATP production. We also showed that exposing astrocytes to extracellular stimuli leads to an increase in the frequency of Ca^{2+} signals and a corresponding increase in the intracellular ATP level. Thus, dysregulation of the crosstalk between Ca^{2+} signaling and energy metabolism may disturb the information transferring mechanism and lead to dysregulation of Ca^{2+} signaling, energy metabolism and cellular ATP level. We also showed that Ca^{2+} dyshomeostasis and decreasing glucose uptake rate resulted from PINK1 deficiency disturb mitochondrial respiration and ATP production in the DA neurons in zebrafish larvae and lead to loss of DA neurons. We could explain with our Ca^{2+} -mitochondrial model that down regulation of MCU channel restores Ca^{2+} regulation and mitochondrial respiration which was in agreement with experiments. Further, to quantify Ca^{2+} signals, we developed a user-friendly software for analyzing and extracting features of Ca^{2+} signals which could measure the characteristics of many diverse Ca^{2+} signals fast and precisely.

6.2 Future Perspectives

The successful application of our developed Ca^{2+} -mitochondrial model in the simulating PINK1 deficiency shows that we are able to generate new knowledge from *in silico* studies. Therefore, the current model can be used in simulating the cellular behavior in diseases that there is impairment of the crosstalk between Ca^{2+} signaling and mitochondrial metabolism. For example in the Leigh syndrome, defective ATP production and abnormally high mitochondrial membrane potential plus altered Ca^{2+} homeostasis have been observed. But the mechanisms responsible for the disruption of mitochondrial calcium homeostasis is not discovered [Lorenz et al., 2017]. Our model can be used for simulating the cellular behavior and understanding the underling mechanism of these experimental observations.

Future work is needed to develop a new model for the crosstalk between Ca^{2+} signaling and mitochondrial metabolism in electrically excitable cells. In electrically excitable cells, Ca^{2+} oscillations occur by changing the voltage of the cell membrane and opening voltage-gated Ca^{2+} channels. Hence excitable cells often have a cytosolic Ca^{2+} oscillator linked to a plasma membrane potential oscillator, potentially giving rise to highly complex behaviors. Then the question would be how mitochondrial dynamics change with fast Ca^{2+} transients in the excitable cells?

The model can also be extended to include the spatial scale in addition to the time scale. It is shown that spatial models exhibit more accurate predictions about amplitude and spike width of Ca^{2+} signals. We also can answer questions related to the spatial scale. For example, how the close contact of ER and mitochondria affect Ca^{2+} and ATP dynamics in the

cytosol as well as mitochondria.

A main finding of this thesis is metabolic decoding relation of intracellular Ca^{2+} signals (Section 4.2.7). We showed experimentally that there is a sigmoidal relation between frequency of Ca^{2+} signal and glucose/glutamine uptake rate. From the published papers [Denton et al., 1980, Denton, 2009], we speculate the activity of PDH and KGDH enzymes might be modulated by frequency of Ca^{2+} spikes. Since glucose and glutamine are precursor substrates of PDH and KGDH enzymes, this modulation lead to increasing glucose and glutamine uptake rates. To prove this dependency, there is need to perform more metabolomic experiments. This experiment should measure the metabolite level of the PDH and KGDH products (Acetyl-CoA and Succinyl CoA, respectively) while exposing cells with different concentration of extracellular stimuli in order to change the frequency of Ca^{2+} signals. Furthermore this dependency can be analyzed in the context of relation between information flow and energy demand.

This work has used a minimal model to investigate the crosstalk and discovered the dynamic metabolic decoding relation. While the model is a simple one, it has some limitations. One limitation is its assumption that Ca^{2+} oscillations are deterministic and based on a Hopf bifurcation. This leads to a fixed parameter regime for an oscillatory behavior and limits the period range of oscillations. As a consequence this model is not able to simulate the full sigmoidal metabolic decoding relation (Figure 5.1 E). An essential extension would be a stochastic model [Skupin et al., 2010] that exhibits stochastic spiking with larger periods. Therefore it might exhibit the whole sigmoidal decoding relation. This would further indicate the essential role of stochasticity in Ca^{2+} signaling. Another extension of model would be the inclusion of the glucose and glutamine uptake rate based on the enzymes activity.

The developed CaSiAn software is a flexible and general tool that allow studying Ca^{2+} signaling in a wide range applications. For example the software has been used for analyzing Ca^{2+} signals in the mouse hippocampal neural cell line, namely HT22. By analyzing and comparing Ca^{2+} signals in the HT22 control and PIMT (L-isoaspartyl methyltransferase) gene knockout cells, we could observe lower Ca^{2+} concentration, wider spike width and lower amplitude in the PIMT knockout. These results highlighted the possible low level of cytosolic ATP in the PIMT knockout cells. The protein PIMT is a repair enzyme that initiate the conversion of the isoaspartyl residue (isoAsp), which is a major product of protein damage via asparagine deamidation and aspartate (Asp) isomerization, to normal Asp residues. PIMT is expressed in almost all cells and tissues, and is particularly highly expressed in brain. PIMT knockout mice show retardation of growth, perturbed glutamate metabolism, and usually die at less than 2 months of age from fatal seizures [Yang et al., 2013].

The CaSiAn software can also be used as a java library and be coupled to other tools for creating a pipeline in analyzing Ca^{2+} signals. For example, it can be coupled to the software which analyze Ca^{2+} images, segment cells and extract Ca^{2+} signals from fluorescent Ca^{2+} images. The extracted signals from Ca^{2+} images then can be fed to the functions of CaSiAn as the input for performing the other analyzing steps.

Appendix A

CaSiAn: Calcium Signal Analysis Software

Ca^{2+} signals are determined by averaging or getting the median of pixel intensities in the regions of interest from a sequence of fluorescence images captured during a period of time. Therefore each signal is a discrete-time function that can be represented as a set of paired values $sg = \{(t_k, f_k), k = 1, \dots, N\}$ where f is the intensity at time point t , k is the frame number and N is the total number of successive Ca^{2+} images. In this section, first we explain the algorithm that CaSiAn implements for finding peaks and nadirs of Ca^{2+} signals. Second, we describe the CaSiAn methods for removing signal baseline and signal normalization. In the end, we delineate the signal features and the algorithms that CaSiAn implements for measuring features.

A.1 Peak and Nadir Detection

The fact of existing noise in the fluorescence Ca^{2+} images makes the peak detection process difficult. Although applying smoothing techniques like signal or image filtration may increase signal to noise ratio, but they substantially change the shape and features of Ca^{2+} spikes [Balkenius et al., 2015, Janicek et al., 2013] that can distort the experimental results. A common practice for enhancing the performance of the peak detection algorithms in the noisy data is defining a sliding window with the length of signal period and identifying global maximum values within the window as signal peaks. But this technique is not applicable to Ca^{2+} signals since they are non-periodic signals made of interspike intervals with different lengths.

In CaSiAn tool, we have introduced a new promising constraint-based method for finding peaks and nadirs of Ca^{2+} signals that simply needs one parameter setting by user. This

algorithm contains the following steps: (1) Find the local maxima (local peaks) and local minima (local nadirs) in the signal. (2) Identify the initial list of global peaks by selecting local peaks that have mean edge magnitude higher than the Peak threshold parameter. The magnitude of a peak edge is defined as the intensity difference between peak value and its prior/next nadir. The Peak threshold parameter is determined by the user, as the percentage of maximum amplitude that occurs in the signal. The maximum amplitude in a signal is the maximum intensity difference between two consecutive local nadir and local peak. In summary, the two edges of each local peak are averaged and then the peaks which have the mean peak edge magnitudes higher than the amplitude threshold are selected as the initial list of global peaks. (3) Find the final list of signal peaks by filtering the initial list of global peaks. If two consecutive local peaks specified in step 1 are also identified as two global peaks in the step 2, then there is the possibility that one of these two peaks be false positive (see Figure A.1, A', B', D', E'). Because detecting two consecutive local peaks as two global peaks of the signal is not expected since there are usually some local peaks as noise between global peaks in the signal. In order to decide about the detection correctness, another constraint is applied to these peaks which is based on the expected shape of the peak. This constraint checks whether the height of the shorter edge of the peak is more than fifty percent of the longer edge height. If even one of the peaks does not meet this condition (see Figure A.1, B' and D'), then just one peak should be selected as global peak that is the one with higher intensity value (see Figure A.1, A' and E'). (4) At the end, identify one nadir for each peak. Let $t_p = (t_{p_1}, t_{p_2}, \dots, t_{p_n})$, $t_{p_k} < t_{p_{k+1}}$ be the vector of peak times, where n is the total number of detected peaks. The nadir of k -th peak is identified as minimum intensity detected in the $[t_{p_k} - (t_{p_k} - t_{p_{k-1}})/2, t_{p_k}]$ interval.

Applying the peak and nadir detection algorithm to the Ca^{2+} signals results in a peak vector $p = (p_1, p_2, \dots, p_n)$ indicating the intensity of peaks, a nadir vector $d = (d_1, d_2, \dots, d_n)$ showing the intensity of nadirs and a time vector $t_{dp} = (t_{d_1}, t_{p_1}, t_{d_2}, t_{p_2}, \dots, t_{d_n}, t_{p_n})$ representing the time points that each element of p and d vector happens there, where $t_{d_k} < t_{p_k} < t_{d_{k+1}}$. CaSiAn uses the data of detected peaks and nadirs as the input to the other implemented signal analysis methods. So the accuracy of this data is important, since they may affect the results of the rest analysis steps. Although applying this algorithm to the Ca^{2+} signals result in quite low rate of false positives and true negatives, but still CaSiAn provides an interactive interface that user can manually remove peaks or nadirs that are wrongly detected or add peaks or nadirs that are not detected by the proposed algorithm.

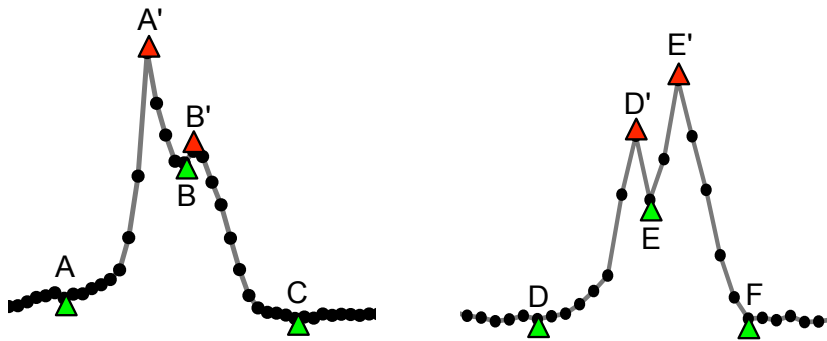


Figure A.1. Detecting and removing false positive peaks. In the step (2) of peak detection algorithm, points A', B', D', E' are detected as potential signal peaks. In the step (3) of algorithm, points B', D' are identified as false positives and just points A' and E' are detected as signal peaks. Points A, B, C, D, E and F are local minima. In the step (4) of algorithm, points A and D are identified as nadirs.

A.2 Background Removal and Normalization

CaSiAn can represent the intensities of Ca^{2+} signals in two common ways: (1) the ratio of the relative fluorescence change and the baseline fluorescence (I) and (2) the ratio of fluorescence intensity and the baseline fluorescence (I').

$$I(k) = \frac{f(k) - F_0(k)}{F_0(k)}, \quad (\text{A.1})$$

$$I'(k) = \frac{f(k)}{F_0(k)}, \quad (\text{A.2})$$

where $f(k)$ is the intensity of region of interest at frame k and $F_0(k)$ is the background intensity at frame k [Waters, 2009]. Function I subtracts the background intensities from the signal intensities and then normalize the results by dividing them to the background intensities. Since finding the real background function F_0 is not a trivial task, CaSiAn infers the background fluorescence \hat{F}_0 using following methods:

Constant Baseline. One simple way for estimating baseline is considering constant background. In this method, \hat{F}_0 is determined by averaging signal intensities during resting state of the cell:

$$\hat{F}_0 = \frac{1}{n} \sum_{k=1}^n f(k), \quad (\text{A.3})$$

where k is the index of image frame and n is the frame number of the first response of cell.

Curve Fitting. Curve fitting method provides more precise approximation of the signal background since it considers fluorophore leaking and photobleaching, i.e., fading the emitted fluorescence during observation [Diaspro et al., 2006]. In the curve fitting method,

CaSiAn omits the trends from signal baseline by fitting a curve to the data set $po_{min} = \{(t_{m_k}, f_{m_k}), k = 1, \dots, n\}$ ($t_{m_k} < t_{m_{k+1}}$), where f_m is the minimum intensity happening in the area between two consecutive peaks, t_m is the time of occurring minimum intensity and n is the number of signal ISIs [Mikhailyuk and Razzhivin, 2003, Balkenius et al., 2015]. CaSiAn implements the following curve fitting techniques for estimating \hat{F}_0 function:

Linear Regression (LR). Regression techniques are able to estimate the parameters of a best-fit curve to the signal baseline set by minimizing the sum squared error of the signal baseline and estimated curve. Linear regression infers the signal baseline \hat{F}_0 as a linear function:

$$\hat{F}_0(t, f) = \beta_0 + \beta_1 t \quad (\text{A.4})$$

Polynomial Regression (PR). Polynomial regression assumes that F_0 is a nonlinear function. The inferred function \hat{F}_0 takes the form of an m th-degree polynomial:

$$\hat{F}_0(t, f) = \beta_0 + \sum_{i=1}^m \beta_i t^i, \quad (\text{A.5})$$

CaSiAn implements PR($m = 2, 3, 4$) because based on our experiments they can predict the background curve of the majority of signals while by increasing m the goodness of fit decreases. The parameters β_i have to be estimated using po_{min} data set.

Spike Base Line. This method infers one \hat{F}_0 for each spike using the line that connects two consecutive points of po_{min} data set. Let (t_{m_k}, f_{m_k}) and $(t_{m_{k+1}}, f_{m_{k+1}})$ be two consecutive points in the po_{min} data set, \hat{F}_{0k} is inferred as:

$$\hat{F}_{0k}(t, f) = \beta_{0k} + \beta_{1k} t \quad (\text{A.6})$$

where the slope of \hat{F}_{0k} is:

$$\beta_{1k} = (f_{m_{k+1}} - f_{m_k}) / (t_{m_{k+1}} - t_{m_k}) \quad (\text{A.7})$$

Background correction by the curve fitting method lead to the zero value for the minimum signal intensity. In some signals, subtracting estimated background from the signal intensities may cause negative values. In this case, CaSiAn computes the minimum of the negative values and offset all signal intensities by the absolute value of this minimum that result in zero value for the minimum intensity of signal.

A.3 Feature Extraction

Extracting descriptors of Ca^{2+} spikes are essential for understanding kinetics of calcium ions and downstream analysis. CaSiAn measures a set of features that characterize distinguishable signal shapes that helps biologist to have more accurate interpretation of the

experimental results. CaSiAn is able to measure these features for a large amount of Ca^{2+} signals fast and precisely. This makes a new door from simple Ca^{2+} signal analysis methods, like comparing average intensities, to the wide spectrum of sophisticated data analysis techniques that are more effective and meaningful if they are performed on the signal features instead of large, noisy and redundant signal intensities.

ISI, T_{av} and σ . The Interspike interval (ISI) is the period of Ca^{2+} spikes that is equal to the time difference between two consecutive peaks in a Ca^{2+} signal. For a signal containing n peaks, $\text{ISI-time} = \{(isi_k, t_{isi_k}), k = 1, \dots, (n-1)\}$ is a set of paired values where $isi_k = (t_{p_{k+1}} - t_{p_k})$, $t_{isi_k} = t_{p_k}$ and t_{p_k} is the time that k -th peak occurs. Modeling and experimental studies have shown that Ca^{2+} signals are made from random sequences of ISIs with not predictable length. Each ISI has a large stochastic period that leads to forming distribution of ISI values [Skupin et al., 2008, Thurley et al., 2011]. CaSiAn plots isi values versus t_{isi} values for each signal indicating the distribution of ISIs over time. It also writes isi values of all signals in an output file. So user is able to plot the histogram of all isi values for a cell population that reveals the distribution of spike periods in the experiment. Since different cellular pathways may exhibit different distribution of ISIs, this plot is a useful diagram for downstream analysis [Skupin et al., 2010].

For each Ca^{2+} signal, the average of ISI values is called average period (T_{av}) and the standard deviation of ISI values is called sigma (σ). Assume a vector of signals $(sg_1, sg_2, \dots, sg_l)$ with $(t_{av1}, t_{av2}, \dots, t_{avl})$ and $(\sigma_1, \sigma_2, \dots, \sigma_l)$, where l is the total number of signals extracted from a cell population. Statistical analysis of ISIs has shown the linear relation between t_{avj} and σ_j ($j = 1, \dots, l$) where t_{avj} and σ_j values are in the same range indicating the stochastic dynamic of Ca^{2+} signals [Skupin and Falcke, 2010]. CaSiAn plots the σ_j values versus t_{avj} values for a cell population and then fit a linear function $\Lambda = \alpha T_{av} + \beta$ to the t_{avj} and σ_j points using linear regression method. The period of Ca^{2+} spikes (ISIs) is one the information encoding mechanism of Ca^{2+} signals. Therefore the slope α that shows the ratio of ISI mean (T_{av}) and ISI standard deviation (σ) for a cell population indicates the signal-to-noise ratio or information content of the period of Ca^{2+} signals. Several studies have shown that this slope is pathway specific, robust against cell to cell variability of Ca^{2+} signals and is sensitive to the global negative feedback inhibitions in the cellular Ca^{2+} signaling pathway [Skupin et al., 2010, Thurley et al., 2014].

Amplitude (AMP). The spike amplitude (AMP_{sp}) is the magnitude of the difference between spike's extreme intensities. While the peak value shows the highest intensity of a spike, the nadir value may not indicate the lowest intensity of spike (see Figure A.3). Our goal is to find the spike base level while considering the possible asymmetric shape of the spike. For this purpose, we define the lowest point of a spike $po_{base} = (t_{base}, I_{base})$ as the intersection point

resulting from crossing two lines, the line L_m that connects the two minimum points located on the spike edges and the vertical line $V_p = t_p$ that goes through peak point of the spike. The equation of L_m line is identified using nadir point (t_d, d) of the spike and the minimum point $(t_{d'}, d')$ occurring after the spike peak.

Let (t_{p_k}, p_k) be the peak point and (t_{d_k}, d_k) be the nadir point of the k -th spike and $(t_{d_{k+1}}, d_{k+1})$ is the nadir of $(k+1)$ -th spike. The minimum point occurring after k -th peak, $po_{d_{l_k}} = (t_{d'_k}, d'_k)$ is the solution of the following objective function:

$$O(po_{d_{l_k}}) = \min_{t_{p_k} < t \leq t_{d_{k+1}}} \{f(t) - d_k\} \quad (\text{A.8})$$

subject to: $po_{d_{l_k}} \neq \text{local maximum}$

Function $O(po_{d_{l_k}})$ finds the minimum intensity difference between each point located in the $(t_{p_k}, t_{d_{k+1}}]$ window and the intensity of k -th nadir point (see Figure A.3). The constraint of $O_{d_{l_k}}$ function indicates that the solution cannot be a local maximum because the local maximums located between two peaks are considered as noise. After detecting $po_{d_{l_k}}$ point, the equation of the L_{m_k} line is determined as $L_{m_k} = a_k t + b_k$, where the slope a_k takes the following value:

$$a_k = \frac{d'_k - d_k}{t_{d'_k} - t_{d_k}} \quad (\text{A.9})$$

Therefore the lowest extreme point $po_{base_k} = (t_{base_k}, I_{base_k})$ of the k -th spike results from crossing of L_{m_k} line and $V_{p_k} = t_{p_k}$ vertical line is equal to $(t_{p_k}, a_k t_{p_k} + b_k)$, and the amplitude of k -th spike is measured as $AMP_{sp_k} = p_k - I_{base_k}$.

Let $\{AMP_{sp_1}, AMP_{sp_2}, \dots, AMP_{sp_n}\}$ be the set of spike amplitudes of a signal. Then the average of spike amplitudes AMP_{sg} identifies the signal amplitude:

$$AMP_{sg} = \frac{1}{n} \sum_{k=1}^n AMP_{sp_k}, \quad (\text{A.10})$$

where n is the total number of spikes in the signal.

Spike Width (SW). The width of a Ca^{2+} spike is the duration of the spike when the Ca^{2+} channels are highly activated and the intracellular Ca^{2+} concentration is higher than the base level of cellular Ca^{2+} concentration. CaSiAn identifies the Ca^{2+} spike width (SW_{sp}) as the duration of spike at 20% of the spike amplitude. Let AMP_{sp} be the amplitude, and I_{base} be the base level of a spike, then the spike width threshold TH_{SW} is:

$$TH_{SW} = 0.2AMP_{sp} + I_{base} \quad (\text{A.11})$$

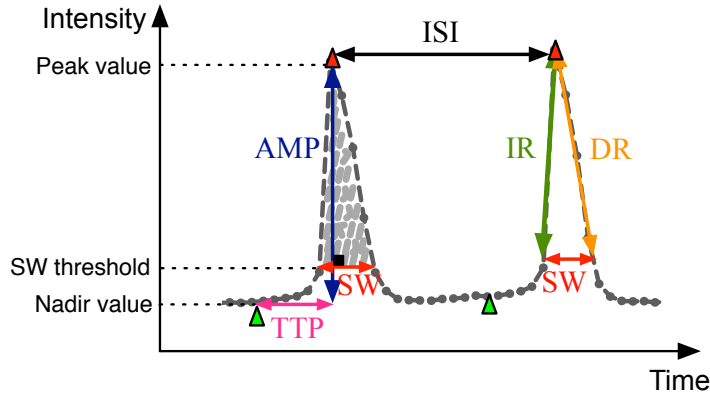


Figure A.2. Overview of Ca^{2+} spike descriptors. CaSiAn quantifies Ca^{2+} spikes by computing following features as illustrated: interspike intervals (ISI), spike amplitude (AMP), spike width (SW), effective area under spike (AUS), increasing rate (IR), decreasing rate (DR), time to peak (TTP), peak intensity, nadir intensity and spike width threshold (TH_{SW}). The red triangles are peaks and the green triangles are the nadirs.

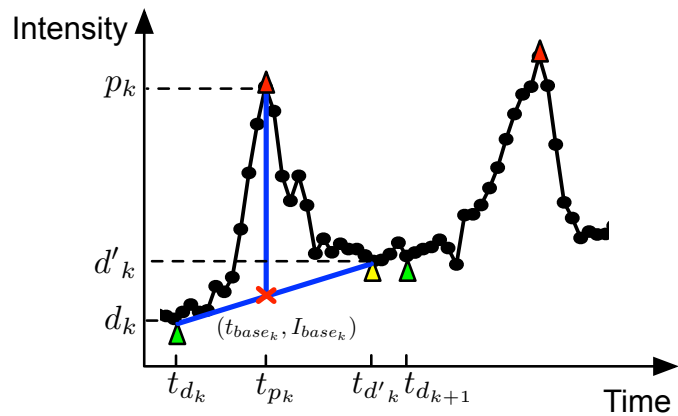


Figure A.3. Spike amplitude (AMP). The spike amplitude is equivalent to the difference between the spike peak intensity and the po_{base} intensity. The red triangles are the peaks and the green triangles are the nadirs. The yellow triangle is the minimum point detected after the spike peak. The $po_{base} = (t_{base}, I_{base})$ is resulted from the intersection of the vertical line that pass through spike peak and the line that connects the spike nadir and the minimum point detected after the spike peak.

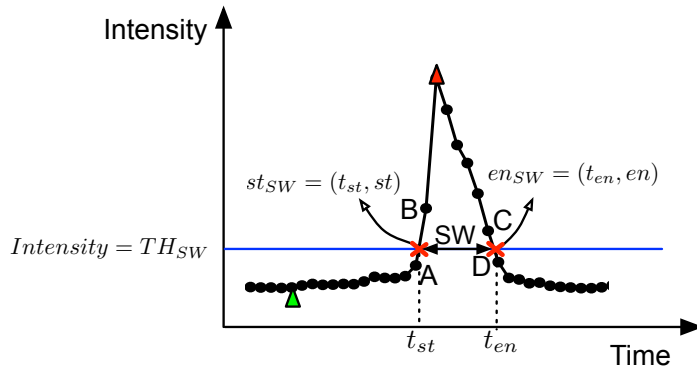


Figure A.4. Spike width (SW). The spike width of a Ca^{2+} spike is computed as spike duration at 20% of spike amplitude.

The intensity values that are higher than TH_{SW} value occur in the effective duration of the spike (see Figure A.4). In order to measure the width of a spike, we compute the time difference between two points of the spike that have the intensity values equivalent to the spike width threshold. Let $st_{SW} = (t_{st}, st)$ be the point where the effective duration of the spike starts and $en_{SW} = (t_{en}, en)$ be the point where the effective duration of the spike ends. The spike width value is equal to the difference between t_{st} and t_{en} . The coordinates of the st_{SW} and en_{SW} points are identified from the intersection of $intensity = TH_{SW}$ line and the spike function. But Ca^{2+} spikes are discrete-time functions that may not contain sample points with the TH_{SW} intensity value. Therefore, for finding the width of a spike, we perform upsampling, i.e., constructing new data points. For this purpose, we find $A = (t_A, f(t_A))$ and $B = (t_B, f(t_B))$, the two neighbor points on the upward edge, and $C = (t_C, f(t_C))$ and $D = (t_D, f(t_D))$, the two neighbor points on the downward edge of the k -th spike, where $t_A < t_B < t_C < t_D$, $f(t_A) \leq TH_{SW_k} < f(t_B)$ and $f(t_D) \leq TH_{SW_k} < f(t_C)$. The search algorithm explores the $[t_{d_k}, t_{p_k}]$ interval for finding B point, the first sample with the intensity higher than TH_{SW_k} value, and explores $[t_{p_k}, t_{d_{k+1}}]$ interval for finding D point, the first sample point with the intensity lower than the TH_{SW_k} value, where t_{d_k} is the nadir time, and t_{p_k} is the peak time of k -th peak and $t_{d_{k+1}}$ is the nadir time of $(k+1)$ -th peak. The point A and point C are identified as the prior samples of point B and point D , respectively. Then we find the intersection points, st_{SW} and en_{SW} , resulting from meeting the AB and CD lines with the $Intensity = TH_{SW}$ horizontal line, respectively. Finally, the spike width is computed as: $SW = t_{en} - t_{st}$ (see Figure A.4).

Let $\{SW_{sp_1}, SW_{sp_2}, \dots, SW_{sp_n}\}$ be the set of spike widths of a signal, then the average of spike widths of the signal SW_{sg} specifies the signal spike width:

$$SW_{sg} = \frac{1}{n} \sum_{k=1}^n SW_{sp_k}, \quad (\text{A.12})$$

where n is the total number of signal spikes.

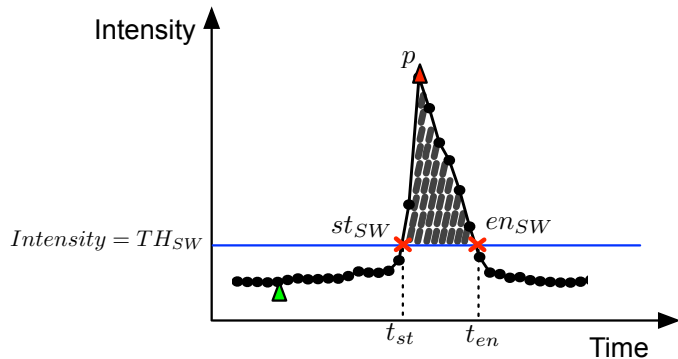


Figure A.5. Effective area under spike (AUS). Effective area under spike is equivalent to the surface between spike function and the spike width threshold line. CaSiAn estimates AUS using trapezoidal method.

Time To Peak (TTP). Time to peak of a spike (TTP_{sp}) is the time difference between the peak time and the nadir time of the spike (see Figure A.2). The time to peak of one Ca^{2+} signal (TTP_{sg}) is computed by averaging the TTP_{sp} of all spikes in the Ca^{2+} signal.

Effective Area Under Spike (AUS). The effective area under a spike (AUS_{sp}) is the surface above the horizontal line $Intensity = TH_{SW}$ and the spike function, where TH_{SW} is the threshold of spike width (see Figure A.5). This area can quantify the cellular calcium concentration for the effective duration of spike where Ca^{2+} channels are highly activated [Charlton and Vauquelin, 2010]. The effective area under the spike is a more precise measurement for quantifying the cellular Ca^{2+} concentration compare to the spike amplitude. Because it involves information of the period that Ca^{2+} concentration is higher than resting level. We approximate the AUS_{sp} feature by the trapezoidal rule. Let $P(t, I) = \{(t_{st}, st), (t_1, f_1), \dots, (t_m, f_m), (t_{en}, en)\}$ be the set of samples that occur in effective duration of spike, where $st_{SW} = (t_{st}, st)$ and $en_{SW} = (t_{en}, en)$ are the start and end points of the effective duration of a spike, respectively and $t_{st} < t_1 < t_m < t_{en}$. The effective area under the spike (AUS_{sp}) is approximated as:

$$AUS_{sp} = \frac{1}{2} \sum_{k=1}^n (t_{k+1} - t_k)(I_{k+1} - I_k) \quad (\text{A.13})$$

where $n = m + 2$ shows the number of points in the P data set.

If $\{AUS_{sp_1}, AUS_{sp_2}, \dots, AUS_{sp_n}\}$ be the set of effective spike areas of a Ca^{2+} signal, then the average of spike areas AUS_{sg} is computed as follow:

$$AUS_{sg} = \frac{1}{n} \sum_{k=1}^n AUS_{sp_k}, \quad (\text{A.14})$$

where n is the total number of signal spikes.

Ca²⁺ Increasing Rate (IR) and Ca²⁺ Decreasing Rate (DR). During the course of a spike, the fluxes that introduce Ca²⁺ to the cytoplasm (J_{in}) are counteracted by the fluxes that remove Ca²⁺ from cytoplasm (J_{out}). The resulted net flux leads to increasing or decreasing Ca²⁺ concentration in the cytoplasm. Therefore the cellular Ca²⁺ concentration ([Ca²⁺]) at time point ($t + 1$) is equivalent to: $[Ca^{2+}]_{t+1} = [Ca^{2+}]_t + J_{in_{t+1}} - J_{out_{t+1}}$. The upward edge of a Ca²⁺ spike shows the period that the net of Ca²⁺ influx is higher than the net of Ca²⁺ efflux that results in increasing cellular Ca²⁺ concentration. The downward edge of a Ca²⁺ spike indicates the period that the rate of Ca²⁺ removal fluxes is higher than the rate of Ca²⁺ releasing fluxes that lead to dropping cellular Ca²⁺ concentration to the resting level. Increasing cytosolic Ca²⁺ concentration happens as a result of releasing Ca²⁺ from internal and external sources. Ca²⁺ release from the internal stores ER/SR through the IP₃ receptors and ryanodine receptors. Ca²⁺ also enters the cell from extracellular space through the Ca²⁺- permeant channels like voltage-gated Ca²⁺ channels, Stim/Orai channels and ligand gated channels [Clapham, 2007]. Cytosolic Ca²⁺ removing happens by four different mechanisms: the PMCA and SERCA pumps, the plasma membrane Na⁺/Ca²⁺exchanger and the mitochondrial uniporter [Berridge et al., 2003].

CaSiAn estimates the rate of increasing cytosolic Ca²⁺ concentration (IR) by computing the slope of upward edge of each spike. It also approximates the rate of decreasing cytosolic Ca²⁺ concentration (DR) by computing the slope of downward edge of spike. Let $p = (t_p, p)$ be the peak point and $st_{SW} = (t_{st}, st)$ be the start point and $en_{SW} = (t_{en}, en)$ be the end point of the effective duration of a spike (see Figure A.6). The increasing rate IR_{sp} and the decreasing rate DR_{sp} of Ca²⁺ concentration during one spike is computed as follow:

$$IR_{sp} = \frac{p - st}{t_p - t_{st}}, \quad (A.15)$$

$$DR_{sp} = \left| \frac{p - en}{t_p - t_{en}} \right|, \quad (A.16)$$

since DR_{sp} takes the negative value, we compute its absolute value.

CaSiAn also measures the increasing rate and the decreasing rate of a Ca²⁺ signal by averaging the increasing rates and the decreasing rates of all spikes in the Ca²⁺ signal, respectively.

Other Features. CaSiAn also measures the following features for each Ca²⁺ signal: mean of intensities, standard deviation of intensities, signal-to-noise ratio, average of the peak values and average of the nadir values.

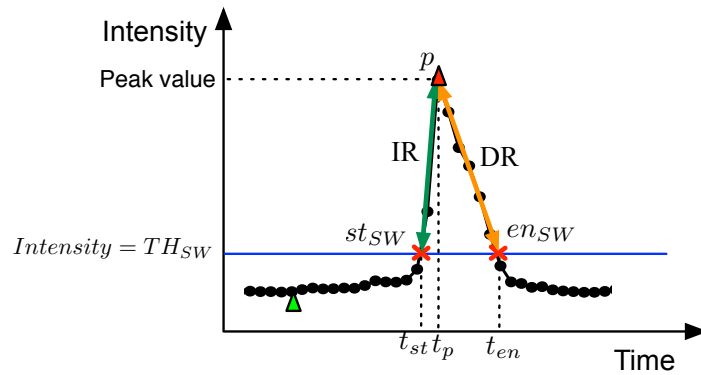


Figure A.6. Increasing rate (IR) and Decreasing rate (DR). The rate of rising cytosolic Ca^{2+} concentration is equivalent to the slope of upward edge of the spike. The rate of decreasing cytosolic Ca^{2+} concentration is equivalent to the slope of downward edge of the spike.

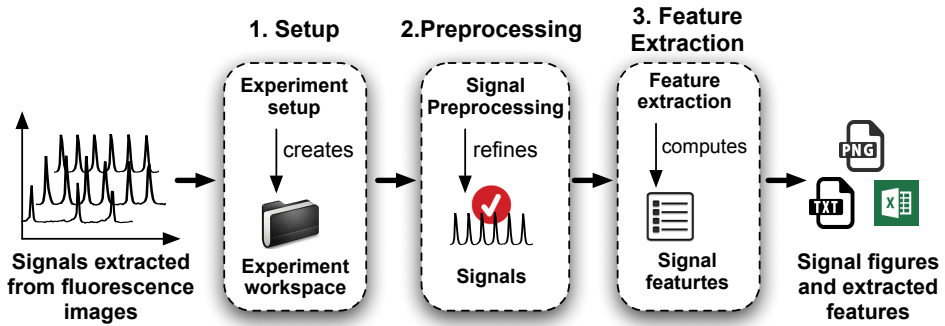


Figure A.7. An overview of CaSiAn. The three steps of CaSiAn, from loading data to exporting the quantified signal descriptors are described.

A.4 Tool Overview

Figure A.7 shows an overview of CaSiAn that consists of three steps: (1) Creating and initializing an experiment workspace, i.e., a container for the Ca^{2+} signal inputs and configuration data (setup), (2) refining the input signals (manipulation), and (3) Computing the characteristics of Ca^{2+} signals (feature extraction). Below, we discuss the three steps of the process in Figure A.7.

A.4.1 Setup

In the Setup step, the user creates an experiment workspace, which is a structure used to store the input data, experiment configurations, and store the analysis results. User creates a workspace for an experiment by doing the following steps: (1) Browse the directory of signal files (*.xls, *.txt, *.csv, *.dat) of one experiment. (2) Enter the common string among input file names. (3) Enter the common string among the column header names that contain the

intensities of Ca^{2+} signals. (4) Enter the number of column that contains the time of Ca^{2+} signals. If the time column contains the frame number of the observed intensities instead of the real acquisition times, user can enter the time difference between two consecutive images in the specified input field of CaSiAn. Then CaSiAn computes the time of each sample by multiplying the frame number and the time difference between two consecutive images. (5) Identify the names of treatments during the imaging, if there is any one. (6) Load signals in the CaSiAn by clicking on the "open experiment" button.

A.4.2 Preprocessing

In the Preprocessing step, user identifies the signal regions that aims to analyze, remove the background from the signal intensities and normalize the signal amplitudes. After the setup step, CaSiAn visualizes the loaded Ca^{2+} signals and user can go through each signal and edit the signal length. If there was any treatment during observations, user can divide signals into the sections and analyze the data of each treatment separately. For the background removal and signal normalization, user should select the appropriate curve for estimating the background intensities. The proper curve is the one with the best goodness of fit. CaSiAn provides different curves for fitting to the signal baseline namely, Constant, Linear, Polynomial degree 2, 3, 4 and Spikeline. Figure A.8 shows different curves that are fitted to the signal baselines as discussed in Section A.2. After choosing the proper curve, user can subtract the background intensities from the signal intensities by clicking on "Subtract background" button and also normalize signal intensities by clicking on "Normalize" button.

A.4.3 Feature Extraction

During the Feature Extraction step, CaSiAn finds the peaks and nadirs of Ca^{2+} signals using the Peak threshold parameter as discussed in section A.1. The user identifies the Peak threshold parameter either for all signals or for each signal separately. Then CaSiAn visualizes the result of peak and nadir detection process and user is able to examine them. If any peak or nadir point is not detected or is detected wrongly, user can easily right click on it and add it to the list of peaks or nadirs or remove it from the list of peaks or nadirs. After finding peak and nadir of signals, CaSiAn computes all other signal characteristics as described in section A.3. The user can access to the all computed features in the form of text or excel file by clicking on the "Export Data and Figures" button.

A.5 Case Study

To show the application of CaSiAn tool for analyzing Ca^{2+} signals, we performed Ca^{2+} imaging of individual astrocytic cells called C8-D1A while exposing them twice with differ-

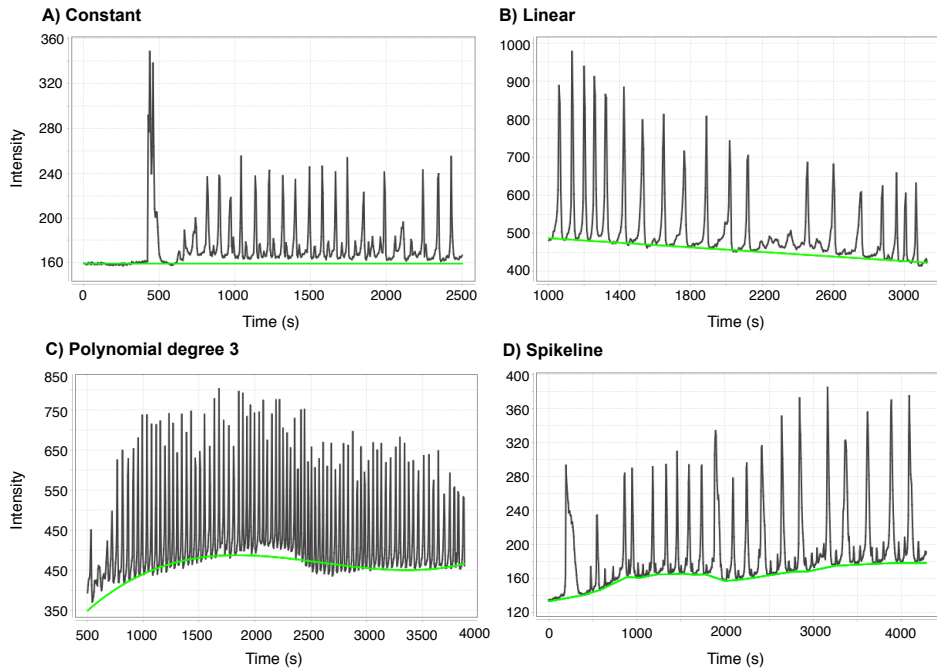


Figure A.8. CaSiAn fits different curves to the signal baseline. The user is able to select a curve type from a list and CaSiAn finds the best fit-curve to the signal baseline. Then user can remove the estimated baseline from signal or normalize signal.

ent concentrations of adenosine triphosphate (ATP) molecules. ATP molecules induce Ca^{2+} releasing from ER by binding to purinergic receptors on the cell membrane, stimulating production of IP_3 molecules and opening IP_3 receptors (IP_3Rs) located on the ER membrane. The main mechanism of Ca^{2+} oscillation in the astrocytes is releasing Ca^{2+} from ER through IP_3Rs and removing back into the ER through SERCA pumps that result in propagating Ca^{2+} signals regeneratively. The goal of this experiment is answering the question, how successive stimulations of purinergic receptors change the profile of Ca^{2+} signals in the astrocytes? To do so, we treated cells twice while imaging: first by $10 \mu\text{M}$ ATP at image number 30 and second, by $80 \mu\text{M}$ ATP at image number 350. After imaging, we extracted Ca^{2+} signals of 250 individual cells by ImageJ software and then analyzed them by CaSiAn tool. In CaSiAn, we first segmented all signals based on the treatment duration. Then CaSiAn measured the signal features of each section separately. Figure A.9 shows a snapshot of an analyzed Ca^{2+} signal in CaSiAn, where the red and blue regions show the duration of $10 \mu\text{M}$ and $80 \mu\text{M}$ ATP treatments, respectively. In order to have sufficient statistical power, we filtered signals with less than 6 peaks by CaSiAn. As a result, the averages and standard deviations make more precise inferences about population from samples.

After computing and exporting signal features, we compared the features of $10 \mu\text{M}$ to the $80 \mu\text{M}$ ATP treatment by performing statistical analysis on the cell population. The results

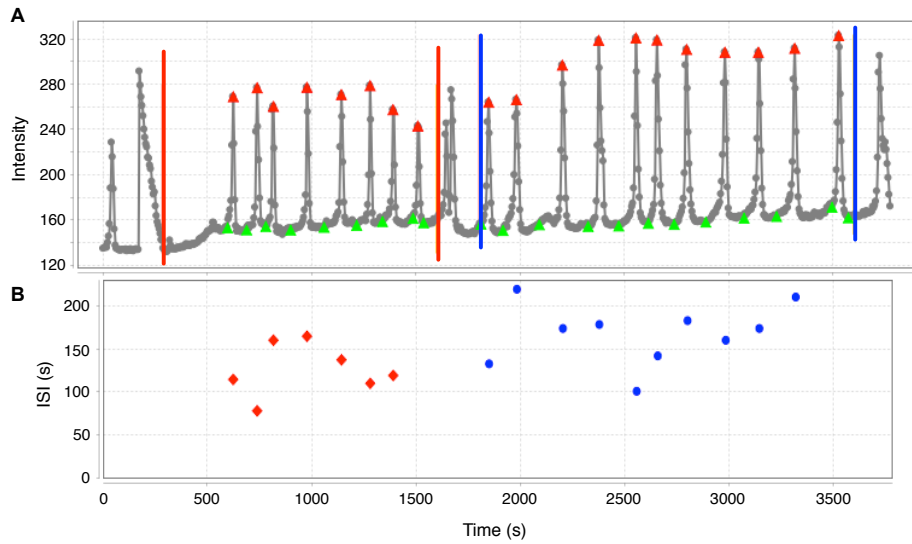


Figure A.9. An analyzed Ca^{2+} signal in CaSiAn. The signal is divided into two sections in CaSiAn, based on the treatment duration. The red region shows the duration of $10 \mu\text{M}$ ATP treatment and the blue region shows the duration of $80 \mu\text{M}$ ATP treatment. We discarded the first responses of cell to the stimulation by excluding them from identified regions. The bottom plot shows the variations of ISIs by time. The x value of each point is equal to the peak time and the y value is equivalent to the successive interspike interval.

show the second stimulation with $80 \mu\text{M}$ ATP leads to increasing the average period (T_{av}) (Figure A.10A), the average amplitude (AMP_{sg}) (Figure A.10B) and the average spike width (SW_{sg}) (Figure A.10C) significantly.

The wider Ca^{2+} spikes in $80 \mu\text{M}$ ATP treatment is resulted from slower increasing rate (IR_{sg}) and slower decreasing rate (DR_{sg}) (see Figure A.10 D, E). Comparing the average area under the spikes (AUS_{sg}) indicates more transferred Ca^{2+} into the cytosol during $80 \mu\text{M}$ ATP treatment (see Figure A.10 F).

Plotting the histogram of individual ISIs of each treatment shows that $80 \mu\text{M}$ ATP stimulation shifts the ISI distribution curve to the right and increases the mean of distribution (Figure A.10 G). higher T_{av} plus the smaller slope (α) of $\sigma-T_{av}$ (Figure A.10H, I) during $80 \mu\text{M}$ ATP treatment indicates the slower recovery from negative feedback inhibition processes in the Ca^{2+} pathway and also less variations in the interspike intervals (ISI). The stronger negative feedback inhibition lead to larger stochastic interval due to the slower recovery and decrease the slope of $\sigma-T_{av}$ line. Considering the information is encoded in the frequency of Ca^{2+} signals, then α^{-1} shows signal-to-noise ratio or signal reliability. It is shown that α does not depend on the IP_3Rs cluster properties, but it is determined by the global feedback inhibition processes in the Ca^{2+} signaling pathway like, sensitivity of IP_3Rs to IP_3 and Ca^{2+} , IP_3 metabolism or ER depletion [Skupin and Falcke, 2010, Skupin et al., 2008, Thurley and

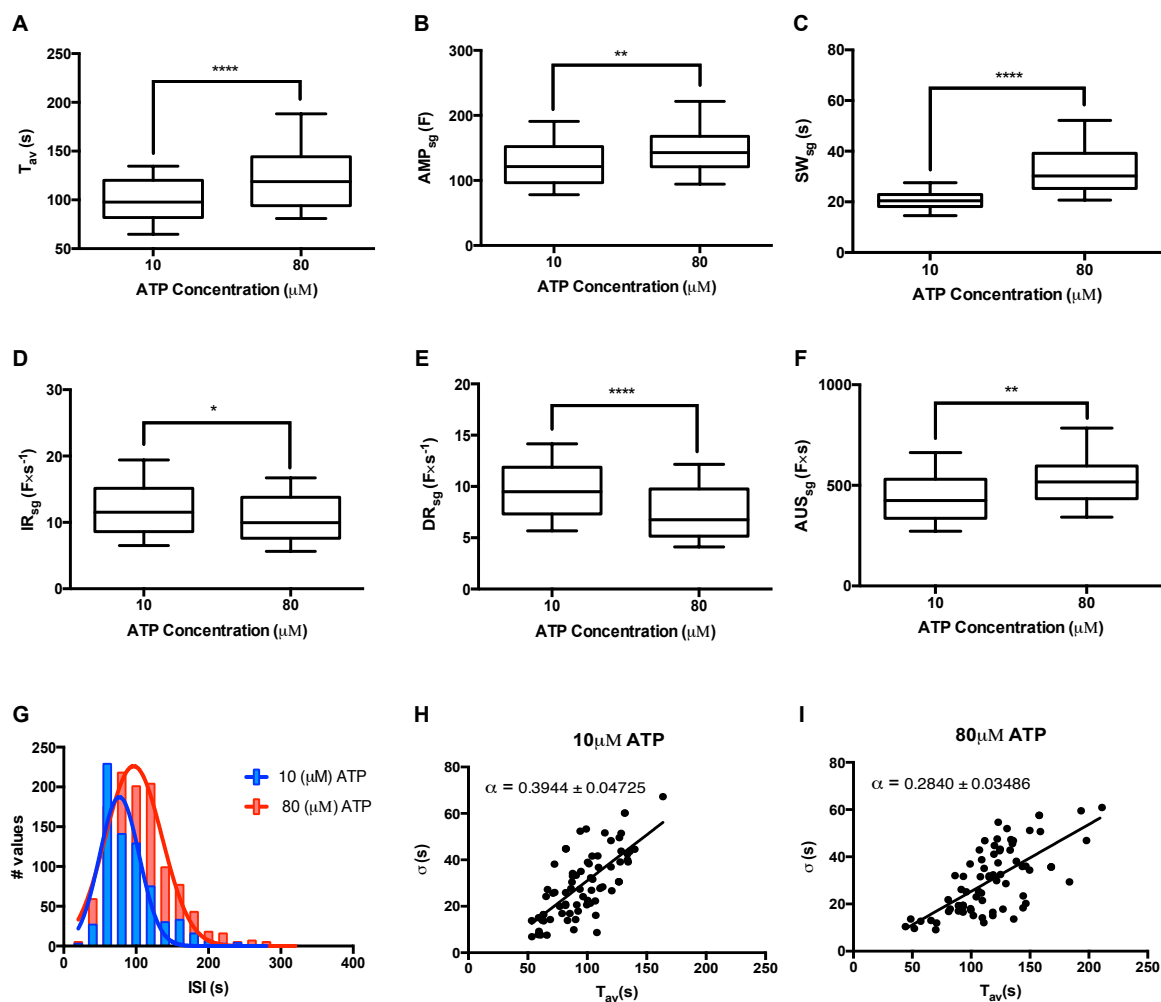


Figure A.10. Statistical analysis of Ca^{2+} signal descriptors. In all plots the statistical tests are done with unpaired t test in Prism (version 6, GraphPad Software) where $P \leq 0.05 = ^*$, $P \leq 0.01 = ^{**}$, $P \leq 0.001 = ^{***}$ and $P \leq 0.0001 = ^{****}$.

Falcke, 2011].

Publications in peer-reviewed journals

- Soman, S., Keatinge, M., **Moein, M.**, DaCosta, M., Mortiboys, H., Skupin, A., ... and Bandmann, O. Inhibition of the mitochondrial calcium uniporter (MCU) rescues dopaminergic neurons in *pink1^{-/-}* zebrafish. " Movement Disorders 31 (2016): S209.
- Komin, N., **Moein, M.**, Ellisman, M. H., Skupin, A. Multiscale Modeling Indicates That Temperature Dependent $[Ca^{2+}]$ Spiking in Astrocytes Is Quantitatively Consistent with Modulated SERCA Activity, Neural plasticity, 2015.

Manuscripts planned to be submitted for publication in peer-reviewed journals

- **Moein, M.**, Skupin, A. CaSiAn: A tool for Analyzing Ca^{2+} Signals. To be submitted to *Bioinformatics*.
- **Moein, M.**, Skupin, A. Dissecting the Crosstalk Between Ca^{2+} Signaling and Mitochondrial Metabolism.

Project presentations

- Dissecting the crosstalk between intracellular Ca^{2+} signaling and mitochondrial metabolism. In the Max Delbrueck Center for Molecular Medicine (MDC), Berlin, Germany.

Poster presentation

- **Moein, M.**, Skupin, A. Metabolic Decoding of Calcium Signaling in Astrocytes. The 3rd International Parkinson Disease Symposium, 2016, Luxembourg.
- **Moein, M.**, Fouquier d'Herouel, A., Skupin, A. A systematic approach to the crosstalk between calcium signaling and mitochondrial dynamics. The 5th edition of Targeting Mitochondria, 2014, Berlin.
- **Moein, M.**, Fouquier d'Herouel, A., Skupin, A. A systematic approach to the crosstalk between calcium signaling and mitochondrial dynamics. The 2nd International Parkinson Disease Symposium, 2014, Luxembourg.

Poster contributions

- Komin, N., **Moein, M.**, Ellisman, M., Skupin, A. Multiscalse astrocyte-neuron interaction in brain energy metabolism. The 2nd International Parkinson Disease Symposium, 2014, Luxembourg.
- Komin, N., **Moein, M.**, Ellisman, M., Skupin, A. Multiscalse astrocyte-neuron interaction in brain energy metabolism. The 8th Annual Salk Institute, Foundation IPSEN and Nature Symposium on Biological Complexity- Genes and Physiology, 2014, San Diego, USA.

- Komin, N., **Moein, M.**, Ellisman, M., Skupin, A. Multiscale astrocyte-neuron interaction in brain energy metabolism. The 2nd International Systems Biomedicine symposium, 2013, Luxembourg.

Bibliography

[Abraham and Bear, 1996] Abraham, W. C. and Bear, M. F. (1996). Metaplasticity: the plasticity of synaptic plasticity. *Trends in neurosciences*, 19(4):126–130.

[Agulhon et al., 2008] Agulhon, C., Petracic, J., McMullen, A. B., Sweger, E. J., Minton, S. K., Taves, S. R., Casper, K. B., Fiacco, T. A., and McCarthy, K. D. (2008). What is the role of astrocyte calcium in neurophysiology? *Neuron*, 59(6):932–946.

[Ahlqvist et al., 1975] Ahlqvist, G., Landin, S., and Wroblewski, R. (1975). Ultrastructure of skeletal muscle in patients with Parkinson's disease and upper motor lesions. *Laboratory investigation; a journal of technical methods and pathology*, 32(5):673–679.

[Alliot and Pessac, 1984] Alliot, F. and Pessac, B. (1984). Astrocytic cell clones derived from established cultures of 8-day postnatal mouse cerebella. *Brain research*, 306(1):283–291.

[Anandatheerthavarada et al., 2003] Anandatheerthavarada, H. K., Biswas, G., Robin, M.-A., and Avadhani, N. G. (2003). Mitochondrial targeting and a novel transmembrane arrest of Alzheimer's amyloid precursor protein impairs mitochondrial function in neuronal cells. *The Journal of cell biology*, 161(1):41–54.

[Anderson and Swanson, 2000] Anderson, C. M. and Swanson, R. A. (2000). Astrocyte glutamate transport: review of properties, regulation, and physiological functions. *Glia*, 32(1):1–14.

[Anglade et al., 1997] Anglade, P., Vyas, S., Javoy-Agid, F., Herrero, M., Michel, P., Marquez, J., Mouatt-Prigent, A., Ruberg, M., Hirsch, E., and Agid, Y. (1997). Apoptosis and autophagy in nigral neurons of patients with Parkinson's disease. *Histology and histopathology*, 12(1):25–32.

[Area-Gomez and Schon, 2016] Area-Gomez, E. and Schon, E. A. (2016). Mitochondria-associated ER membranes and Alzheimer's disease. *Current opinion in genetics & development*, 38:90–96.

Bibliography

[Babcock et al., 1997] Babcock, D. F., Herrington, J., Goodwin, P. C., Park, Y. B., and Hille, B. (1997). Mitochondrial participation in the intracellular Ca^{+2} network. *The Journal of cell biology*, 136(4):833–844.

[Balaban, 2002] Balaban, R. S. (2002). Cardiac energy metabolism homeostasis: role of cytosolic calcium. *Journal of molecular and cellular cardiology*, 34(10):1259–1271.

[Balkenius et al., 2015] Balkenius, A., Johansson, A. J., and Balkenius, C. (2015). Comparing analysis methods in functional calcium imaging of the insect brain. *PloS one*, 10(6):e0129614.

[Bazargani and Attwell, 2016] Bazargani, N. and Attwell, D. (2016). Astrocyte calcium signaling: the third wave. *Nature neuroscience*, 19(2):182–189.

[Bélanger et al., 2011] Bélanger, M., Allaman, I., and Magistretti, P. J. (2011). Brain energy metabolism: focus on astrocyte-neuron metabolic cooperation. *Cell metabolism*, 14(6):724–738.

[Berg et al., 2002] Berg, J. M., Tymoczko, J. L., and Stryer, L. (2002). Glycolysis is an energy-conversion pathway in many organisms.

[Berridge, 1997] Berridge, M. J. (1997). Elementary and global aspects of calcium signalling. *The Journal of physiology*, 499(2):291–306.

[Berridge, 2002] Berridge, M. J. (2002). The endoplasmic reticulum: a multifunctional signaling organelle. *Cell calcium*, 32(5):235–249.

[Berridge, 2010] Berridge, M. J. (2010). Calcium hypothesis of Alzheimer’s disease. *Pflügers Archiv-European Journal of Physiology*, 459(3):441–449.

[Berridge, 2013] Berridge, M. J. (2013). Dysregulation of neural calcium signaling in Alzheimer disease, bipolar disorder and schizophrenia. *Prion*, 7(1):2–13.

[Berridge et al., 1998] Berridge, M. J., Bootman, M. D., and Lipp, P. (1998). Calcium-a life and death signal. *Nature*, 395(6703):645–648.

[Berridge et al., 2003] Berridge, M. J., Bootman, M. D., and Roderick, H. L. (2003). Calcium signalling: dynamics, homeostasis and remodelling. *Nature reviews Molecular cell biology*, 4(7):517–529.

[Bertram and Arceo II, 2008] Bertram, R. and Arceo II, R. C. (2008). A mathematical study of the differential effects of two SERCA isoforms on Ca^{2+} oscillations in pancreatic islets. *Bulletin of mathematical biology*, 70(5):1251–1271.

[Bertram et al., 2006] Bertram, R., Pedersen, M. G., Luciani, D. S., and Sherman, A. (2006). A simplified model for mitochondrial ATP production. *Journal of theoretical biology*, 243(4):575–586.

[Bertram et al., 2007] Bertram, R., Satin, L. S., Pedersen, M. G., Luciani, D. S., and Sherman, A. (2007). Interaction of glycolysis and mitochondrial respiration in metabolic oscillations of pancreatic islets. *Biophysical journal*, 92(5):1544–1555.

[Billington and Hall, 2012] Billington, C. K. and Hall, I. P. (2012). Novel cAMP signalling paradigms: therapeutic implications for airway disease. *British journal of pharmacology*, 166(2):401–410.

[Blaustein and Lederer, 1999] Blaustein, M. P. and Lederer, W. J. (1999). Sodium/calcium exchange: its physiological implications. *Physiological reviews*, 79(3):763–854.

[Bosetti et al., 2002] Bosetti, F., Brizzi, F., Barogi, S., Mancuso, M., Siciliano, G., Tendi, E. A., Murri, L., Rapoport, S. I., and Solaini, G. (2002). Cytochrome c oxidase and mitochondrial F₁F₀-ATPase (ATP synthase) activities in platelets and brain from patients with AlzheimerâŽs disease. *Neurobiology of aging*, 23(3):371–376.

[Bratic and Trifunovic, 2010] Bratic, I. and Trifunovic, A. (2010). Mitochondrial energy metabolism and ageing. *Biochimica et Biophysica Acta (BBA)-Bioenergetics*, 1797(6):961–967.

[Brini et al., 2013] Brini, M., Calì, T., Ottolini, D., and Carafoli, E. (2013). The plasma membrane calcium pump in health and disease. *FEBS Journal*, 280(21):5385–5397.

[Brini and Carafoli, 2009] Brini, M. and Carafoli, E. (2009). Calcium pumps in health and disease. *Physiological reviews*, 89(4):1341–1378.

[Bubber et al., 2005] Bubber, P., Haroutunian, V., Fisch, G., Blass, J. P., and Gibson, G. E. (2005). Mitochondrial abnormalities in Alzheimer brain: mechanistic implications. *Annals of neurology*, 57(5):695–703.

[Bulos et al., 1984] Bulos, B. A., Thomas, B. J., and Sacktor, B. (1984). Calcium inhibition of the NAD⁺-linked isocitrate dehydrogenase from blowfly flight muscle mitochondria. *Journal of Biological Chemistry*, 259(16):10232–10237.

[Burnstock and Williams, 2000] Burnstock, G. and Williams, M. (2000). P2 purinergic receptors: modulation of cell function and therapeutic potential. *Journal of Pharmacology and Experimental Therapeutics*, 295(3):862–869.

Bibliography

[Cao et al., 2014] Cao, P., Tan, X., Donovan, G., Sanderson, M. J., and Sneyd, J. (2014). A deterministic model predicts the properties of stochastic calcium oscillations in airway smooth muscle cells. *PLoS Comput Biol*, 10(8):e1003783.

[Carafoli, 2012] Carafoli, E. (2012). The interplay of mitochondria with calcium: an historical appraisal. *Cell Calcium*, 52(1):1–8.

[Cardoso et al., 2004] Cardoso, S. M., Proen  a, M. T., Santos, S., Santana, I., and Oliveira, C. R. (2004). Cytochrome c oxidase is decreased in Alzheimer's disease platelets. *Neurobiology of aging*, 25(1):105–110.

[Catterall, 2011] Catterall, W. A. (2011). Voltage-gated calcium channels. *Cold Spring Harbor perspectives in biology*, 3(8):a003947.

[Chan et al., 2009] Chan, C. S., Gertler, T. S., and Surmeier, D. J. (2009). Calcium homeostasis, selective vulnerability and Parkinson's disease. *Trends in neurosciences*, 32(5):249–256.

[Charlton and Vauquelin, 2010] Charlton, S. J. and Vauquelin, G. (2010). Elusive equilibrium: the challenge of interpreting receptor pharmacology using calcium assays. *British journal of pharmacology*, 161(6):1250–1265.

[Cieri et al., 2016] Cieri, D., Brini, M., and Cal  , T. (2016). Emerging (and converging) pathways in Parkinson's disease: keeping mitochondrial wellness. *Biochemical and Biophysical Research Communications*.

[Clapham, 1995] Clapham, D. E. (1995). Calcium signaling. *Cell*, 80(2):259–268.

[Clapham, 2007] Clapham, D. E. (2007). Calcium signaling. *Cell*, 131(6):1047–1058.

[Colbran and Brown, 2004] Colbran, R. J. and Brown, A. M. (2004). Calcium/calmodulin-dependent protein kinase ii and synaptic plasticity. *Current opinion in neurobiology*, 14(3):318–327.

[Cole et al., 1988] Cole, G., Dobkins, K. R., Hansen, L. A., Terry, R. D., and Saitoh, T. (1988). Decreased levels of protein kinase C in Alzheimer brain. *Brain research*, 452(1):165–174.

[Dani et al., 1992] Dani, J. W., Chernjavsky, A., and Smith, S. J. (1992). Neuronal activity triggers calcium waves in hippocampal astrocyte networks. *Neuron*, 8(3):429–440.

[De Koninck and Schulman, 1998] De Koninck, P. and Schulman, H. (1998). Sensitivity of CaM kinase ii to the frequency of Ca^{+2} oscillations. *Science*, 279(5348):227–230.

[De Young and Keizer, 1992] De Young, G. W. and Keizer, J. (1992). A single-pool inositol 1, 4, 5-trisphosphate-receptor-based model for agonist-stimulated oscillations in Ca^{2+} concentration. *Proceedings of the National Academy of Sciences*, 89(20):9895–9899.

[DeLuca and Engstrom, 1961] DeLuca, H. F. and Engstrom, G. (1961). Calcium uptake by rat kidney mitochondria. *Proceedings of the National Academy of Sciences*, 47(11):1744–1750.

[Demaurex et al., 2009] Demaurex, N., Poburko, D., and Frieden, M. (2009). Regulation of plasma membrane calcium fluxes by mitochondria. *Biochimica et Biophysica Acta (BBA)-Bioenergetics*, 1787(11):1383–1394.

[Dempsey et al., 2000] Dempsey, E. C., Newton, A. C., Mochly-Rosen, D., Fields, A. P., Reyland, M. E., Insel, P. A., and Messing, R. O. (2000). Protein kinase C isozymes and the regulation of diverse cell responses. *American Journal of Physiology-Lung Cellular and Molecular Physiology*, 279(3):L429–L438.

[Demuro et al., 2010] Demuro, A., Parker, I., and Stutzmann, G. E. (2010). Calcium signaling and amyloid toxicity in Alzheimer disease. *Journal of Biological Chemistry*, 285(17):12463–12468.

[Denton et al., 1980] Denton, R., McCormack, J., and Edgell, N. (1980). Role of calcium ions in the regulation of intramitochondrial metabolism. effects of Na^+ , Mg^{2+} and ruthenium red on the Ca^{2+} -stimulated oxidation of oxoglutarate and on pyruvate dehydrogenase activity in intact rat heart mitochondria. *Biochemical Journal*, 190(1):107–117.

[Denton, 2009] Denton, R. M. (2009). Regulation of mitochondrial dehydrogenases by calcium ions. *Biochimica et Biophysica Acta (BBA)-Bioenergetics*, 1787(11):1309–1316.

[Denton et al., 1978] Denton, R. M., Richards, D. A., and Chin, J. G. (1978). Calcium ions and the regulation of NAD^+ -linked isocitrate dehydrogenase from the mitochondria of rat heart and other tissues. *Biochemical Journal*, 176(3):899–906.

[Diaspro et al., 2006] Diaspro, A., Chirico, G., Usai, C., Ramoino, P., and Dobrucki, J. (2006). Photobleaching. In *Handbook of biological confocal microscopy*, pages 690–702. Springer.

[Dolmetsch et al., 1998] Dolmetsch, R. E., Xu, K., and Lewis, R. S. (1998). Calcium oscillations increase the efficiency and specificity of gene expression. *Nature*, 392(6679):933–936.

[Dupont and Combettes, 2016] Dupont, G. and Combettes, L. (2016). Fine tuning of cytosolic Ca^{2+} oscillations. *F1000Research*, 5.

Bibliography

[Dupont et al., 2016] Dupont, G., Falcke, M., Kirk, V., and Sneyd, J. (2016). *Models of Calcium Signaling*, volume 43. Springer.

[Dupont and Goldbeter, 1998] Dupont, G. and Goldbeter, A. (1998). CaM kinase ii as frequency decoder of Ca^{2+} oscillations. *Bioessays*, 20(8):607–610.

[Durante et al., 2004] Durante, P., Cardenas, C. G., Whittaker, J. A., Kitai, S. T., and Scroggs, R. S. (2004). Low-threshold L-type calcium channels in rat dopamine neurons. *Journal of neurophysiology*, 91(3):1450–1454.

[Eng et al., 1989] Eng, J., Lynch, R. M., and Balaban, R. S. (1989). Nicotinamide adenine dinucleotide fluorescence spectroscopy and imaging of isolated cardiac myocytes. *Biophysical Journal*, 55(4):621–630.

[Erecińska and Wilson, 1982] Erecińska, M. and Wilson, D. F. (1982). Regulation of cellular energy metabolism. *Journal of Membrane Biology*, 70(1):1–14.

[Exner et al., 2012] Exner, N., Lutz, A. K., Haass, C., and Winklhofer, K. F. (2012). Mitochondrial dysfunction in Parkinson’s disease: molecular mechanisms and pathophysiological consequences. *The EMBO journal*, 31(14):3038–3062.

[Falcke et al., 2003] Falcke, M., Li, Y., Lechleiter, J. D., and Camacho, P. (2003). Modeling the dependence of the period of intracellular Ca^{2+} waves on SERCA expression. *Biophysical journal*, 85(3):1474–1481.

[Fall and Keizer, 2001] Fall, C. P. and Keizer, J. E. (2001). Mitochondrial modulation of intracellular Ca^{2+} signaling. *Journal of theoretical biology*, 210(2):151–165.

[Fellin and Carmignoto, 2004] Fellin, T. and Carmignoto, G. (2004). Neurone-to-astrocyte signalling in the brain represents a distinct multifunctional unit. *The Journal of physiology*, 559(1):3–15.

[Fenster et al., 1999] Fenster, C. P., Beckman, M. L., Parker, J. C., Sheffield, E. B., Whitworth, T. L., Quick, M. W., and Lester, R. A. (1999). Regulation of $\alpha 4\beta 2$ nicotinic receptor desensitization by calcium and protein kinase c. *Molecular pharmacology*, 55(3):432–443.

[Fontanesi, 2001] Fontanesi, F. (2001). Mitochondria: Structure and role in respiration. *eLS*.

[Frantz et al., 1994] Frantz, B., Nordby, E. C., Bren, G., Steffan, N., Paya, C. V., Kincaid, R. L., Tocci, M. J., O’keefe, S., and O’neill, E. (1994). Calcineurin acts in synergy with PMA to inactivate I kappa B/MAD3, an inhibitor of NF- κ B. *The EMBO journal*, 13(4):861.

[Gandhi et al., 2009] Gandhi, S., Wood-Kaczmar, A., Yao, Z., Plun-Favreau, H., Deas, E., Klupsch, K., Downward, J., Latchman, D. S., Tabrizi, S. J., Wood, N. W., et al. (2009). PINK1-associated Parkinson's disease is caused by neuronal vulnerability to calcium-induced cell death. *Molecular cell*, 33(5):627–638.

[Gatenby and Gillies, 2004] Gatenby, R. A. and Gillies, R. J. (2004). Why do cancers have high aerobic glycolysis? *Nature Reviews Cancer*, 4(11):891–899.

[Giaume and Venance, 1998] Giaume, C. and Venance, L. (1998). Intercellular calcium signaling and gap junctional communication in astrocytes. *Glia*, 24(1):50–64.

[Gibbs, 2015] Gibbs, M. E. (2015). Role of glycogenolysis in memory and learning: Regulation by noradrenaline, serotonin and ATP. *Frontiers in integrative neuroscience*, 9.

[Goldbeter et al., 1990] Goldbeter, A., Dupont, G., and Berridge, M. J. (1990). Minimal model for signal-induced Ca^{2+} oscillations and for their frequency encoding through protein phosphorylation. *Proceedings of the National Academy of Sciences*, 87(4):1461–1465.

[Grienberger and Konnerth, 2012] Grienberger, C. and Konnerth, A. (2012). Imaging calcium in neurons. *Neuron*, 73(5):862–885.

[Griffiths and Rutter, 2009] Griffiths, E. J. and Rutter, G. A. (2009). Mitochondrial calcium as a key regulator of mitochondrial ATP production in mammalian cells. *Biochimica et Biophysica Acta (BBA)-Bioenergetics*, 1787(11):1324–1333.

[Gunter et al., 2000] Gunter, T., Buntinas, L., Sparagna, G., Eliseev, R., and Gunter, K. (2000). Mitochondrial calcium transport: mechanisms and functions. *Cell calcium*, 28(5):285–296.

[Gunter et al., 1994] Gunter, T. E., Gunter, K. K., Sheu, S.-S., and Gavin, C. E. (1994). Mitochondrial calcium transport: physiological and pathological relevance. *American Journal of Physiology-Cell Physiology*, 267(2):C313–C339.

[Gunter and Pfeiffer, 1990] Gunter, T. E. and Pfeiffer, D. R. (1990). Mechanisms by which mitochondria transport calcium. *American Journal of Physiology-Cell Physiology*, 258(5):C755–C786.

[Gunter et al., 2004] Gunter, T. E., Yule, D. I., Gunter, K. K., Eliseev, R. A., and Salter, J. D. (2004). Calcium and mitochondria. *FEBS letters*, 567(1):96–102.

[Guthrie et al., 1999] Guthrie, P. B., Knappenberger, J., Segal, M., Bennett, M. V., Charles, A. C., and Kater, S. B. (1999). ATP released from astrocytes mediates glial calcium waves. *Journal of Neuroscience*, 19(2):520–528.

Bibliography

[Hajnóczky et al., 2006] Hajnóczky, G., Csordás, G., Das, S., Garcia-Perez, C., Saotome, M., Roy, S. S., and Yi, M. (2006). Mitochondrial calcium signalling and cell death: approaches for assessing the role of mitochondrial Ca^{2+} uptake in apoptosis. *Cell calcium*, 40(5):553–560.

[Hajnóczky et al., 1995] Hajnóczky, G., Robb-Gaspers, L. D., Seitz, M. B., and Thomas, A. P. (1995). Decoding of cytosolic calcium oscillations in the mitochondria. *Cell*, 82(3):415–424.

[Hala et al., 1983] Hala, K., Vilhelmová, M., Hartmanová, I., and Pink, W. (1983). Chronic parkinsonism in humans due to product of meperidine-analog synthesis.

[Halestrap, 2009] Halestrap, A. P. (2009). What is the mitochondrial permeability transition pore? *Journal of molecular and cellular cardiology*, 46(6):821–831.

[Hall and Guyton, 2006] Hall, J. E. and Guyton, A. C. (2006). *Textbook of medical physiology*. Elsevier Inc.

[Hell et al., 1993] Hell, J. W., Westenbroek, R. E., Warner, C., Ahlijanian, M. K., Prystay, W., Gilbert, M. M., Snutch, T. P., and Catterall, W. A. (1993). Identification and differential subcellular localization of the neuronal class C and class D L-type calcium channel alpha 1 subunits. *The Journal of cell biology*, 123(4):949–962.

[Helton et al., 2005] Helton, T. D., Xu, W., and Lipscombe, D. (2005). Neuronal L-type calcium channels open quickly and are inhibited slowly. *The Journal of neuroscience*, 25(44):10247–10251.

[Hiraoka et al., 1980] Hiraoka, T., DeBuysere, M., and Olson, M. (1980). Studies of the effects of beta-adrenergic agonists on the regulation of pyruvate dehydrogenase in the perfused rat heart. *Journal of Biological Chemistry*, 255(16):7604–7609.

[Hirase et al., 2004] Hirase, H., Qian, L., Barthó, P., and Buzsáki, G. (2004). Calcium dynamics of cortical astrocytic networks in vivo. *PLoS Biol*, 2(4):e96.

[Hisatsune and Mikoshiba, 2012] Hisatsune, C. and Mikoshiba, K. (2012). Molecular biology of the InsP_3 Rs: focus on brain function in health and disease. *Wiley Interdisciplinary Reviews: Membrane Transport and Signaling*, 1(5):589–604.

[Hogan et al., 2003] Hogan, P. G., Chen, L., Nardone, J., and Rao, A. (2003). Transcriptional regulation by calcium, calcineurin, and NFAT. *Genes & development*, 17(18):2205–2232.

[Hölscher et al., 1999] Hölscher, C., Gigg, J., and O’Mara, S. M. (1999). Metabotropic glutamate receptor activation and blockade: their role in long-term potentiation, learning and neurotoxicity. *Neuroscience & Biobehavioral Reviews*, 23(3):399–410.

[Hoth et al., 2000] Hoth, M., Button, D. C., and Lewis, R. S. (2000). Mitochondrial control of calcium-channel gating: a mechanism for sustained signaling and transcriptional activation in t lymphocytes. *Proceedings of the National Academy of Sciences*, 97(19):10607–10612.

[Hu et al., 1999] Hu, Q., Deshpande, S., Irani, K., and Ziegelstein, R. C. (1999). $[Ca^{+2}]_i$ oscillation frequency regulates agonist-stimulated NF- κ b transcriptional activity. *Journal of Biological Chemistry*, 274(48):33995–33998.

[Innocenti et al., 2000] Innocenti, B., Parpura, V., and Haydon, P. G. (2000). Imaging extracellular waves of glutamate during calcium signaling in cultured astrocytes. *The Journal of Neuroscience*, 20(5):1800–1808.

[Ishii et al., 2006] Ishii, K., Hirose, K., and Iino, M. (2006). Ca^{2+} shuttling between endoplasmic reticulum and mitochondria underlying Ca^{2+} oscillations. *EMBO reports*, 7(4):390–396.

[Jacobson and Duchen, 2004] Jacobson, J. and Duchen, M. R. (2004). Interplay between mitochondria and cellular calcium signalling. *Molecular and cellular biochemistry*, 256(1):209–218.

[Janicek et al., 2013] Janicek, R., Hotka, M., Zahradníková Jr, A., Zahradníková, A., and Zahradník, I. (2013). Quantitative analysis of calcium spikes in noisy fluorescent background. *PLoS one*, 8(5):e64394.

[Jin et al., 2015] Jin, L., Alesi, G., and Kang, S. (2015). Glutaminolysis as a target for cancer therapy. *Oncogene*.

[Jöbsis et al., 1971] Jöbsis, F., O’Connor, M., Vitale, A., and Vreman, H. (1971). Intracellular redox changes in functioning cerebral cortex. i. metabolic effects of epileptiform activity. *Journal of neurophysiology*, 34(5):735–749.

[Kang et al., 1998] Kang, J., Jiang, L., Goldman, S. A., and Nedergaard, M. (1998). Astrocyte-mediated potentiation of inhibitory synaptic transmission. *Nature neuroscience*, 1(8):683–692.

[Kim et al., 2005] Kim, E., Cho, S., Jeong, Y., Park, K., Kang, S., Kang, E., Kim, S., Lee, K., and Na, D. (2005). Glucose metabolism in early onset versus late onset Alzheimer’s disease: an SPM analysis of 120 patients. *Brain*, 128(8):1790–1801.

Bibliography

[Klipp et al., 2016] Klipp, E., Liebermeister, W., Wierling, C., Kowald, A., and Herwig, R. (2016). *Systems biology: a textbook*. John Wiley & Sons.

[Komin et al., 2015] Komin, N., Moein, M., Ellisman, M. H., and Skupin, A. (2015). Multiscale modeling indicates that temperature dependent $[Ca^{2+}]$. *Neural plasticity*, 2015.

[Krebs et al., 1959] Krebs, E. G., Graves, D. J., and Fischer, E. H. (1959). Factors affecting the activity of muscle phosphorylase b kinase. *Journal of Biological Chemistry*, 234(11):2867–2873.

[Kuo et al., 1998] Kuo, T. H., Kim, H.-R. C., Zhu, L., Yu, Y., Lin, H.-M., and Tsang, W. (1998). Modulation of endoplasmic reticulum calcium pump by Bcl-2. *Oncogene*, 17(15):1903–1910.

[Kupzig et al., 2005] Kupzig, S., Walker, S. A., and Cullen, P. J. (2005). The frequencies of calcium oscillations are optimized for efficient calcium-mediated activation of ras and the ERK/MAPK cascade. *Proceedings of the National Academy of Sciences of the United States of America*, 102(21):7577–7582.

[L Ferreira et al., 2010] L Ferreira, I., Resende, R., Ferreiro, E., C Rego, A., and F Pereira, C. (2010). Multiple defects in energy metabolism in Alzheimer’s disease. *Current drug targets*, 11(10):1193–1206.

[LaFerla, 2002] LaFerla, F. M. (2002). Calcium dyshomeostasis and intracellular signalling in Alzheimer’s disease. *Nature Reviews Neuroscience*, 3(11):862–872.

[Lai and Cooper, 1986] Lai, J. C. and Cooper, A. J. (1986). Brain α -ketoglutarate dehydrogenase complex: Kinetic properties, regional distribution, and effects of inhibitors. *Journal of neurochemistry*, 47(5):1376–1386.

[Li et al., 1994] Li, Y.-X., Rinzel, J., Keizer, J., and Stojilković, S. S. (1994). Calcium oscillations in pituitary gonadotrophs: comparison of experiment and theory. *Proceedings of the National Academy of Sciences*, 91(1):58–62.

[Liemburg-Apers et al., 2015] Liemburg-Apers, D. C., Willems, P. H., Koopman, W. J., and Grefte, S. (2015). Interactions between mitochondrial reactive oxygen species and cellular glucose metabolism. *Archives of toxicology*, 89(8):1209–1226.

[Lin et al., 2003] Lin, A. P., Shic, F., Enriquez, C., and Ross, B. D. (2003). Reduced glutamate neurotransmission in patients with Alzheimer’s disease—an in vivo ^{13}C magnetic resonance spectroscopy study. *Magnetic Resonance Materials in Physics, Biology and Medicine*, 16(1):29–42.

[Lipp et al., 1997] Lipp, P., Thomas, D., Berridge, M. J., and Bootman, M. D. (1997). Nuclear calcium signalling by individual cytoplasmic calcium puffs. *The EMBO journal*, 16(23):7166–7173.

[Lipton, 1973] Lipton, P. (1973). Effects of membrane depolarization on nicotinamide nucleotide fluorescence in brain slices. *Biochemical Journal*, 136(4):999–1009.

[Lorenz et al., 2017] Lorenz, C., Lesimple, P., Bukowiecki, R., Zink, A., Inak, G., Mlody, B., Singh, M., Semtner, M., Mah, N., Auré, K., et al. (2017). Human iPSC-derived neural progenitors are an effective drug discovery model for neurological mtDNA disorders. *Cell Stem Cell*.

[Magnus and Keizer, 1997] Magnus, G. and Keizer, J. (1997). Minimal model of beta-cell mitochondrial Ca^{2+} handling. *American Journal of Physiology-Cell Physiology*, 273(2):C717–C733.

[Magnus and Keizer, 1998] Magnus, G. and Keizer, J. (1998). Model of β -cell mitochondrial calcium handling and electrical activity. i. cytoplasmic variables. *American Journal of Physiology-Cell Physiology*, 274(4):C1158–C1173.

[Marhl et al., 2000] Marhl, M., Haberichter, T., Brumen, M., and Heinrich, R. (2000). Complex calcium oscillations and the role of mitochondria and cytosolic proteins. *Biosystems*, 57(2):75–86.

[Marinissen and Gutkind, 2001] Marinissen, M. J. and Gutkind, J. S. (2001). G-protein-coupled receptors and signaling networks: emerging paradigms. *Trends in pharmacological sciences*, 22(7):368–376.

[McCormack and Denton, 1979] McCormack, J. G. and Denton, R. M. (1979). The effects of calcium ions and adenine nucleotides on the activity of pig heart 2-oxoglutarate dehydrogenase complex. *Biochemical Journal*, 180(3):533–544.

[McCormack and Denton, 1981] McCormack, J. G. and Denton, R. M. (1981). The activation of pyruvate dehydrogenase in the perfused rat heart by adrenaline and other inotropic agents. *Biochemical Journal*, 194(2):639–643.

[McCormack and England, 1983] McCormack, J. G. and England, P. (1983). Ruthenium red inhibits the activation of pyruvate dehydrogenase caused by positive inotropic agents in the perfused rat heart. *Biochemical Journal*, 214(2):581–585.

[McCormack and Denton, 1984] McCormack, J. G. and Denton, R. M. (1984). Role of Ca^{2+} ions in the regulation of intramitochondrial metabolism in rat heart. evidence from studies with isolated mitochondria that adrenaline activates the pyruvate dehydrogenase and

Bibliography

2-oxoglutarate dehydrogenase complexes by increasing the intramitochondrial concentration of Ca^{2+} . *Biochemical Journal*, 218(1):235–247.

[Metallo and Vander Heiden, 2013] Metallo, C. M. and Vander Heiden, M. G. (2013). Understanding metabolic regulation and its influence on cell physiology. *Molecular cell*, 49(3):388–398.

[Michikawa and Yanagisawa, 1999] Michikawa, M. and Yanagisawa, K. (1999). Inhibition of cholesterol production but not of nonsterol isoprenoid products induces neuronal cell death. *Journal of neurochemistry*, 72(6):2278–2285.

[Mikhailyuk and Razzhivin, 2003] Mikhailyuk, I. and Razzhivin, A. (2003). Background subtraction in experimental data arrays illustrated by the example of raman spectra and fluorescent gel electrophoresis patterns. *Instruments and Experimental Techniques*, 46(6):765–769.

[Missiaen et al., 1991] Missiaen, L., Taylor, C. W., and Berridge, M. J. (1991). Spontaneous calcium release from inositol trisphosphate-sensitive calcium stores. *Nature*, 352(6332):241–244.

[Moenke et al., 2012] Moenke, G., Falcke, M., and Thurley, K. (2012). Hierarchic stochastic modelling applied to intracellular Ca^{2+} signals. *PloS one*, 7(12):e51178.

[Moreira et al., 2007] Moreira, P. I., Santos, M. S., Seiça, R., and Oliveira, C. R. (2007). Brain mitochondrial dysfunction as a link between Alzheimer’s disease and diabetes. *Journal of the neurological sciences*, 257(1):206–214.

[Nedergaard et al., 2003] Nedergaard, M., Ransom, B., and Goldman, S. A. (2003). New roles for astrocytes: redefining the functional architecture of the brain. *Trends in neurosciences*, 26(10):523–530.

[Newman, 2003a] Newman, E. A. (2003a). Glial cell inhibition of neurons by release of ATP. *Journal of Neuroscience*, 23(5):1659–1666.

[Newman, 2003b] Newman, E. A. (2003b). New roles for astrocytes: regulation of synaptic transmission. *Trends in neurosciences*, 26(10):536–542.

[Newman, 2005] Newman, E. A. (2005). Calcium increases in retinal glial cells evoked by light-induced neuronal activity. *Journal of Neuroscience*, 25(23):5502–5510.

[Newman and Zahs, 1997] Newman, E. A. and Zahs, K. R. (1997). Calcium waves in retinal glial cells. *Science*, 275(5301):844–847.

[Nunn and Taylor, 1992] Nunn, D. L. and Taylor, C. W. (1992). Luminal Ca^{2+} increases the sensitivity of Ca^{2+} stores to inositol 1, 4, 5-trisphosphate. *Molecular Pharmacology*, 41(1):115–119.

[Osłowski and Urano, 2011] Osłowski, C. M. and Urano, F. (2011). Measuring er stress and the unfolded protein response using mammalian tissue culture system. *Methods in enzymology*, 490:71.

[Parekh, 2003] Parekh, A. B. (2003). Store-operated Ca^{2+} entry: dynamic interplay between endoplasmic reticulum, mitochondria and plasma membrane. *The Journal of Physiology*, 547(2):333–348.

[Parpura et al., 1994] Parpura, V., Basarsky, T. A., Liu, F., Jeftinija, K., Jeftinija, S., and Haydon, P. G. (1994). Glutamate-mediated astrocyte–neuron signalling.

[Patron et al., 2014] Patron, M., Checchetto, V., Raffaello, A., Teardo, E., Reane, D. V., Mantoan, M., Granatiero, V., Szabò, I., De Stefani, D., and Rizzuto, R. (2014). MICU1 and mICU2 finely tune the mitochondrial Ca^{2+} uniporter by exerting opposite effects on MCU activity. *Molecular cell*, 53(5):726–737.

[Pattni and Banting, 2004] Pattni, K. and Banting, G. (2004). Ins (1, 4, 5) p 3 metabolism and the family of ip 3-3kinases. *Cellular signalling*, 16(6):643–654.

[Pellerin and Magistretti, 1994] Pellerin, L. and Magistretti, P. J. (1994). Glutamate uptake into astrocytes stimulates aerobic glycolysis: a mechanism coupling neuronal activity to glucose utilization. *Proceedings of the National Academy of Sciences*, 91(22):10625–10629.

[Perez and Sanderson, 2005] Perez, J. F. and Sanderson, M. J. (2005). The frequency of calcium oscillations induced by 5-HT, ACH, and KCl determine the contraction of smooth muscle cells of intrapulmonary bronchioles. *The Journal of general physiology*, 125(6):535–553.

[Periasamy and Huke, 2001] Periasamy, M. and Huke, S. (2001). SERCA pump level is a critical determinant of Ca^{2+} homeostasis and cardiac contractility. *Journal of molecular and cellular cardiology*, 33(6):1053–1063.

[Peterson et al., 1999] Peterson, B. Z., DeMaria, C. D., and Yue, D. T. (1999). Calmodulin is the Ca^{2+} sensor for Ca^{2+} -dependent inactivation of L-type calcium channels. *Neuron*, 22(3):549–558.

[Petravic et al., 2008] Petracic, J., Fiacco, T. A., and McCarthy, K. D. (2008). Loss of IP₃ receptor-dependent Ca^{2+} increases in hippocampal astrocytes does not affect baseline ca1 pyramidal neuron synaptic activity. *The Journal of Neuroscience*, 28(19):4967–4973.

Bibliography

[Porter and McCarthy, 1996] Porter, J. T. and McCarthy, K. D. (1996). Hippocampal astrocytes in situ respond to glutamate released from synaptic terminals. *The Journal of Neuroscience*, 16(16):5073–5081.

[Prakriya et al., 2006] Prakriya, M., Feske, S., Gwack, Y., Srikanth, S., Rao, A., and Hogan, P. G. (2006). Orai1 is an essential pore subunit of the CRAC channel. *Nature*, 443(7108):230–233.

[Qi and Shuai, 2016] Qi, H. and Shuai, J. (2016). Alzheimer’s disease via enhanced calcium signaling caused by the decrease of endoplasmic reticulum–mitochondrial distance. *Medical hypotheses*, 89:28–31.

[Rex Sheu et al., 1985] Rex Sheu, K.-F., Kim, Y.-T., Blass, J. P., and Weksler, M. E. (1985). An immunochemical study of the pyruvate dehydrogenase deficit in Alzheimer’s disease brain. *Annals of neurology*, 17(5):444–449.

[Rickard and Ng, 1995] Rickard, N. and Ng, K. (1995). Blockade of metabotropic glutamate receptors prevents long-term memory consolidation. *Brain research bulletin*, 36(4):355–359.

[Ritz et al., 2010] Ritz, B., Rhodes, S. L., Qian, L., Schernhammer, E., Olsen, J. H., and Friis, S. (2010). L-type calcium channel blockers and Parkinson disease in Denmark. *Annals of neurology*, 67(5):600–606.

[Rizzuto et al., 2012] Rizzuto, R., De Stefani, D., Raffaello, A., and Mammucari, C. (2012). Mitochondria as sensors and regulators of calcium signalling. *Nature reviews Molecular cell biology*, 13(9):566–578.

[Rizzuto et al., 1998] Rizzuto, R., Pinton, P., Carrington, W., Fay, F. S., Fogarty, K. E., Lifshitz, L. M., Tuft, R. A., and Pozzan, T. (1998). Close contacts with the endoplasmic reticulum as determinants of mitochondrial Ca^{2+} responses. *Science*, 280(5370):1763–1766.

[Rizzuto et al., 1992] Rizzuto, R., Simpson, A., Brini, M., and Pozzan, T. (1992). Rapid changes of mitochondrial Ca^{2+} revealed by specifically targeted recombinant aequorin. *Nature*, 358(6384):325–327.

[Robb-Gaspers et al., 1998] Robb-Gaspers, L. D., Burnett, P., Rutter, G. A., Denton, R. M., Rizzuto, R., and Thomas, A. P. (1998). Integrating cytosolic calcium signals into mitochondrial metabolic responses. *The EMBO journal*, 17(17):4987–5000.

[Rossi et al., 2007] Rossi, D. J., Brady, J. D., and Mohr, C. (2007). Astrocyte metabolism and signaling during brain ischemia. *Nature neuroscience*, 10(11):1377–1386.

[Santella et al., 2004] Santella, L., Lim, D., and Moccia, F. (2004). Calcium and fertilization: the beginning of life. *Trends in biochemical sciences*, 29(8):400–408.

[Skupin and Falcke, 2009] Skupin, A. and Falcke, M. (2009). From puffs to global Ca^{2+} signals: how molecular properties shape global signals. *Chaos: An Interdisciplinary Journal of Nonlinear Science*, 19(3):037111.

[Skupin and Falcke, 2010] Skupin, A. and Falcke, M. (2010). Statistical analysis of calcium oscillations. *The European Physical Journal Special Topics*, 187(1):231–240.

[Skupin et al., 2010] Skupin, A., Kettenmann, H., and Falcke, M. (2010). Calcium signals driven by single channel noise. *PLoS Comput Biol*, 6(8):e1000870.

[Skupin et al., 2008] Skupin, A., Kettenmann, H., Winkler, U., Wartenberg, M., Sauer, H., Tovey, S. C., Taylor, C. W., and Falcke, M. (2008). How does intracellular Ca^{2+} oscillate: by chance or by the clock? *Biophysical journal*, 94(6):2404–2411.

[Slater et al., 1973] Slater, E., Rosing, J., and Mol, A. (1973). The phosphorylation potential generated by respiring mitochondria. *Biochimica et Biophysica Acta (BBA)-Bioenergetics*, 292(3):534–553.

[Smedler and Uhlén, 2014] Smedler, E. and Uhlén, P. (2014). Frequency decoding of calcium oscillations. *Biochimica Et Biophysica Acta (BBA)-General Subjects*, 1840(3):964–969.

[Soderling et al., 2001] Soderling, T. R., Chang, B., and Brickey, D. (2001). Cellular signaling through multifunctional Ca^{2+} /calmodulin-dependent protein kinase ii. *Journal of Biological Chemistry*, 276(6):3719–3722.

[Sofroniew and Vinters, 2010] Sofroniew, M. V. and Vinters, H. V. (2010). Astrocytes: biology and pathology. *Acta neuropathologica*, 119(1):7–35.

[Soman et al., 2016] Soman, S., Keatinge, M., Moein, M., DaCosta, M., Mortiboys, H., Skupin, A., Sugunan, S., Bazala, M., Kuznicki, J., and Bandmann, O. (2016). Inhibition of the mitochondrial calcium uniporter (MCU) rescues dopaminergic neurons in pink1-/- zebrafish. *European Journal of Neuroscience*.

[Stathopoulos et al., 2008] Stathopoulos, P. B., Zheng, L., Li, G.-Y., Plevin, M. J., and Ikura, M. (2008). Structural and mechanistic insights into STIM1-mediated initiation of store-operated calcium entry. *Cell*, 135(1):110–122.

[Strehler et al., 2007] Strehler, E. E., Caride, A. J., Filoteo, A. G., Xiong, Y., Penniston, J. T., and Enyedi, A. (2007). Plasma membrane Ca^{2+} ATPases as dynamic regulators of

Bibliography

cellular calcium handling. *Annals of the New York Academy of Sciences*, 1099(1):226–236.

[Supnet and Bezprozvanny, 2010] Supnet, C. and Bezprozvanny, I. (2010). The dysregulation of intracellular calcium in Alzheimer disease. *Cell calcium*, 47(2):183–189.

[Surmeier et al., 2010] Surmeier, D. J., Guzman, J. N., and Sanchez-Padilla, J. (2010). Calcium, cellular aging, and selective neuronal vulnerability in Parkinson’s disease. *Cell calcium*, 47(2):175–182.

[Surmeier et al., 2016] Surmeier, D. J., Schumacker, P. T., Guzman, J. D., Ilijic, E., Yang, B., and Zampese, E. (2016). Calcium and Parkinson’s disease. *Biochemical and Biophysical Research Communications*.

[Swulius and Waxham, 2008] Swulius, M. and Waxham, M. (2008). Ca^{2+} /calmodulin-dependent protein kinases. *Cellular and molecular life sciences*, 65(17):2637–2657.

[Taylor and Laude, 2002] Taylor, C. and Laude, A. (2002). IP_3 receptors and their regulation by calmodulin and cytosolic Ca^{2+} . *Cell calcium*, 32(5):321–334.

[Territo et al., 2001] Territo, P. R., French, S. A., Dunleavy, M. C., Evans, F. J., and Balaban, R. S. (2001). Calcium activation of heart mitochondrial oxidative phosphorylation rapid kinetics of mvO_2 , nadh, and light scattering. *Journal of Biological Chemistry*, 276(4):2586–2599.

[Thomas and Gustafsson, 2013] Thomas, R. L. and Gustafsson, Å. B. (2013). Mitochondrial autophagy: An essential quality control mechanism for myocardial homeostasis. *Circulation journal: official journal of the Japanese Circulation Society*, 77(10):2449.

[Thurley and Falcke, 2011] Thurley, K. and Falcke, M. (2011). Derivation of Ca^{2+} signals from puff properties reveals that pathway function is robust against cell variability but sensitive for control. *Proceedings of the National Academy of Sciences*, 108(1):427–432.

[Thurley et al., 2011] Thurley, K., Smith, I. F., Tovey, S. C., Taylor, C. W., Parker, I., and Falcke, M. (2011). Timescales of IP_3 -evoked Ca^{2+} spikes emerge from Ca^{2+} puffs only at the cellular level. *Biophysical journal*, 101(11):2638–2644.

[Thurley et al., 2014] Thurley, K., Tovey, S. C., Moenke, G., Prince, V. L., Meena, A., Thomas, A. P., Skupin, A., Taylor, C. W., and Falcke, M. (2014). Reliable encoding of stimulus intensities within random sequences of intracellular Ca^{2+} spikes. *Science signaling*, 7(331):ra59.

[Tomida et al., 2003] Tomida, T., Hirose, K., Takizawa, A., Shibasaki, F., and Iino, M. (2003). NFAT functions as a working memory of Ca^{2+} signals in decoding Ca^{2+} oscillation. *The EMBO Journal*, 22(15):3825–3832.

[Tompa et al., 2001] Tompa, P., Töth-Boconádi, R., and Friedrich, P. (2001). Frequency decoding of fast calcium oscillations by calpain. *Cell calcium*, 29(3):161–170.

[Tretter and Adam-Vizi, 2005] Tretter, L. and Adam-Vizi, V. (2005). Alpha-ketoglutarate dehydrogenase: a target and generator of oxidative stress. *Philosophical Transactions of the Royal Society of London B: Biological Sciences*, 360(1464):2335–2345.

[Vasington and Murphy, 1961] Vasington, F. and Murphy, J. (1961). Active binding of calcium by mitochondria. In *Fed. Proc*, volume 20, pages 2670–2677.

[Venkatachalam et al., 2002] Venkatachalam, K., van Rossum, D. B., Patterson, R. L., Ma, H.-T., and Gill, D. L. (2002). The cellular and molecular basis of store-operated calcium entry. *Nature Cell Biology*, 4(11):E263–E272.

[Volterra and Meldolesi, 2005] Volterra, A. and Meldolesi, J. (2005). Astrocytes, from brain glue to communication elements: the revolution continues. *Nature Reviews Neuroscience*, 6(8):626–640.

[Wacquier et al., 2016] Wacquier, B., Combettes, L., Van Nhieu, G. T., and Dupont, G. (2016). Interplay between intracellular Ca^{2+} oscillations and Ca^{2+} -stimulated mitochondrial metabolism. *Scientific reports*, 6.

[Wang et al., 2006] Wang, X., Lou, N., Xu, Q., Tian, G.-F., Peng, W. G., Han, X., Kang, J., Takano, T., and Nedergaard, M. (2006). Astrocytic Ca^{2+} signaling evoked by sensory stimulation in vivo. *Nature neuroscience*, 9(6):816–823.

[Waters, 2009] Waters, J. C. (2009). Accuracy and precision in quantitative fluorescence microscopy. *The Journal of cell biology*, 185(7):1135–1148.

[Watras et al., 1991] Watras, J., Ehrlich, B. E., et al. (1991). Bell-shaped calcium-response curves of Ins (1, 4, 5)P₃-and calcium-gated channels from endoplasmic reticulum of cerebellum.

[Wegner et al., 2015] Wegner, A., Meiser, J., Weindl, D., and Hiller, K. (2015). How metabolites modulate metabolic flux. *Current opinion in biotechnology*, 34:16–22.

[Yang et al., 2013] Yang, H., Lowenson, J. D., Clarke, S., and Zubarev, R. A. (2013). Brain proteomics supports the role of glutamate metabolism and suggests other metabolic alterations in protein l-isoaspartyl methyltransferase (pimt)-knockout mice. *Journal of proteome research*, 12(10):4566–4576.

Bibliography

[Zhu and Chu, 2010] Zhu, J. and Chu, C. T. (2010). Mitochondrial dysfunction in Parkinson's disease. *Journal of Alzheimer's Disease*, 20(S2):325–334.

[Zucker and Regehr, 2002] Zucker, R. S. and Regehr, W. G. (2002). Short-term synaptic plasticity. *Annual review of physiology*, 64(1):355–405.

[Zuehlke et al., 1999] Zuehlke, R. D., Pitt, G. S., Deisseroth, K., Tsien, R. W., and Reuter, H. (1999). Calmodulin supports both inactivation and facilitation of L-type calcium channels. *Nature*, 399(6732):159–162.